UNIVERSIDAD AUTÓNOMA DE MADRID
FACULTAD DE CIENCIAS
Sección de Ingeniería Química

ESTUDIO DE LA RELACIÓN ENTRE LA ESTRUCTURA Y EL COMPORTAMIENTO DE CATALIZADORES EN REACCIONES DE HIDROTRATAMIENTO DE AGUAS

STUDY OF THE RELATIONSHIP BETWEEN CATALYST STRUCTURE AND PROPERTIES IN WATER HYDROTREATMENT REACTIONS

Tesis Doctoral

JOSÉ ALBERTO BAEZA HERRERA

Madrid, 2014

UNIVERSIDAD AUTÓNOMA DE MADRID
FACULTAD DE CIENCIAS
Sección de Ingeniería Química

ESTUDIO DE LA RELACIÓN ENTRE LA ESTRUCTURA Y EL COMPORTAMIENTO DE CATALIZADORES EN REACCIONES DE HIDROTRATAMIENTO DE AGUAS

STUDY OF THE RELATIONSHIP BETWEEN CATALYST STRUCTURE AND PROPERTIES IN WATER HYDROTREATMENT REACTIONS

MEMORIA

que para optar al grado de

Doctor

Mención Internacional

presenta

José Alberto Baeza Herrera

Directores: Dra. Luisa Calvo Hernández

Dr. Miguel Ángel Gilarranz Redondo

Madrid, 2014

Dña. Luisa Calvo Hernández, Profesora Titular de Universidad, y **D. Miguel Ángel Gilarranz Redondo**, Profesor Titular de Universidad, ambos profesores de la Sección de Ingeniería Química perteneciente al Departamento de Química-Física Aplicada de la Universidad Autónoma de Madrid

HACEN CONSTAR: que el presente trabajo, titulado *"Estudio de la relación entre la estructura y el comportamiento de catalizadores en reacciones de hidrotratamiento de aguas"*, presentado por D. José Alberto Baeza Herrera, ha sido realizado bajo su dirección, en los laboratorios de la Sección de Ingeniería Química, en la Universidad Autónoma de Madrid, y que a su juicio reúne los requisitos de originalidad y rigor científico necesarios para ser presentado como Tesis Doctoral.

Y para que conste a efectos oportunos, firmamos el presente informe en Madrid, a 5 de septiembre de 2014.

Luisa Calvo Hernández Miguel Ángel Gilarranz Redondo

La realización de este trabajo ha sido posible gracias al apoyo económico prestado a través de los proyectos CTQ2009-09983 del Ministerio de Ciencia e Innovación, CTQ2012-32821 del Ministerio de Economía y Competitividad y REMTAVARES S-2009/AMB-1588 de la Comunidad Autónoma de Madrid y a la concesión de una beca de Formación de Personal Investigador (BES-2010-030059) financiada por el Ministerio de Ciencia e Innovación.

INDICE/CONTENTS

RESUMEN / SUMMARY

Resumen

Los hidrotratamientos, procesos de hidrogenación y/o reducción que generalmente se llevan a cabo en presencia de un catalizador, han generado un interés creciente en el ámbito del tratamiento avanzado aguas, dadas sus ventajas frente a otros procesos avanzados. Entre éstas cabe destacar su versatilidad, ya que pueden ser aplicados a un amplio número de compuestos refractarios, desde vertidos de aguas residuales industriales (organohalogenados, percloratos, bromatos, cloratos, nitrosaminas, etc.) hasta la potabilización (nitratos, nitritos). Asimismo, los hidrotratamientos pueden operar en condiciones de temperatura y presión suaves, y conducen a corrientes secundarias de menor toxicidad si la selectividad a productos deseados es adecuada.

Los catalizadores empleados más habitualmente en los hidrotratamientos de aguas son metales nobles soportados sobre diversos materiales tales como alúminas, arcillas, zeolitas o materiales carbonosos. Uno de los retos tradicionales en catálisis es la obtención de catalizadores que permitan alcanzar valores de actividad y selectividad óptimos a través de un diseño racional de los mismos. En concreto, para reacciones sensibles a la estructura, la dificultad para lograr este reto reside en el amplio número de variables que afectan a la actividad y selectividad del catalizador, y en las distintas interacciones entre las mismas. En general, estas variables pueden dividirse en dos grandes grupos: las asociadas al soporte y aquellas asociadas a la fase metálica. Entre las variables asociadas al soporte se encuentran la composición química, la porosidad, la superficie específica o los grupos superficiales, entre otros. En cuanto a la fase metálica, el tamaño de nanopartícula, la forma, el estado de oxidación, la interacción con el soporte o la composición (uno o más elementos) son las variables principales.

Los métodos de preparación de catalizadores convencionales, consistentes generalmente en la impregnación de una disolución de sal metálica sobre un soporte seleccionado y que posteriormente es reducida, no siempre permiten un control adecuado de las variables que afectan a la actividad y selectividad del catalizador en reacciones sensibles a la estructura. En los últimos años, los métodos de síntesis de nanopartículas que permiten el control de tamaño han recibido gran atención, puesto que ofrecen la posibilidad de estudiar las propiedades físicas y químicas dependientes del tamaño de las nanopartículas.

Entre los métodos de síntesis de nanopartículas con control de tamaño (químicos, electroquímicos, sonoquímicos, etc.), el método de reducción química ha sido ampliamente utilizado debido a su sencillez y eficacia. La síntesis de nanopartículas se lleva a cabo poniendo en contacto una disolución de una sal metálica con un agente reductor (alcoholes, hidracina, borohidruro sódico, etc.) en presencia de un agente protector (polivinilpirrolidona, polivinilalcohol, dodecilamina, etc.). Este último evita el crecimiento incontrolado de las nanopartículas, así como su agregación, pero debido a su difícil eliminación de la superficie de las nanopartículas tras la síntesis se introduce una nueva variable con influencia potencial sobre la actividad y selectividad.

Con el fin de generar un conocimiento de utilidad que permita contribuir al diseño racional de catalizadores, en la presente tesis se ha abordado el estudio de determinadas variables que afectan a la actividad y/o selectividad asociadas a la fase activa, como son el tamaño de nanopartícula, el estado de oxidación y la naturaleza del agente protector y reductor. De igual modo, se ha estudiado una de las variables asociadas al soporte, la composición química. Con este fin se han preparado

nanopartículas de metales nobles (Pd, Rh) mediante síntesis con control de tamaño que han sido empleadas como catalizadores modelo en reacciones de hidrodecloración y reducción de nitritos. Asimismo, se ha abordado el análisis cinético como estrategia teórica para estudiar el efecto del tamaño de nanopartícula sobre la actividad. Por lo que se refiere a la influencia de la composición del soporte, se han evaluado materiales carbonosos dopados con nitrógeno.

La estructura de la tesis comprende los capítulos donde se explican en detalle los trabajos realizados (capítulos I – VI), un capítulo de conclusiones generales y un capítulo de previsión de trabajos futuros.

En el Capítulo I se aborda la síntesis y uso como catalizador modelo de nanopartículas de Pd de distintos tamaños, sin soportar, en la hidrodecloración de 4-clorofenol en fase acuosa. La síntesis se lleva a cabo empleando metanol y etanol como agentes reductores y polivinilpirrolidona como agente protector. Se estudia la influencia del tipo y cantidad de agente reductor, así como de la cantidad de agente protector, sobre el tamaño de partícula y el estado de oxidación. La actividad y selectividad de las suspensiones coloidales es discutida en comparación con catalizadores soportados, habiéndose observado una diferencia fundamental en la falta de capacidad para hidrogenar de las nanopartículas sin soportar, cuyo único producto de reacción es el fenol, y los catalizadores soportados descritos en la bibliografía que muestras selectividad a ciclohexanona y ciclohexanol. Las nanopartículas de Pd de menor tamaño mostraron mayor actividad, si bien su actividad por unidad superficie fue menor. Las diferencias en la actividad por unidad de masa y actividad por unidad de

superficie son discutidas, así como las diferencias en la energía de activación aparente entre las nanopartículas sin soportar y los catalizadores soportados.

En el Capítulo II se lleva a cabo la síntesis y uso como catalizador modelo de nanopartículas de Rh de distintos tamaños, sin soportar, en la hidrodecloración de 4-clorofenol en fase acuosa. La síntesis se lleva a cabo empleando metanol como agente reductor y polivinilpirrolidona como agente protector, obteniéndose un intervalo estrecho de tamaños de nanopartícula pero amplio de estados de oxidación (medido en términos de la relación Rh^{n+}/Rh^{0}). La actividad de las nanopartículas de Rh se ve favorecida por una alta proporción de especies metálicas y presenta un máximo para un tamaño de partícula en torno a 2.8 nm. Se discute la actividad de las nanopartículas de Rh en comparación con las de Pd. Se lleva a cabo un modelo de regresión con el fin de relacionar el tamaño de partícula y/o el estado de oxidación y la selectividad a productos de hidrogenación (ciclohexanona y ciclohexanol), observándose un efecto cruzado entre tamaño de partícula y estado de oxidación.

En el Capítulo III se llevan a cabo análisis cinéticos basados en el método de dos etapas y el mecanismo de Langmuir-Hinshelwood aplicado a la hidrodecloración de 4-clorofenol empleando los datos experimentales obtenidos con nanopartículas de Rh sin soportar en el Capítulo III. Se comparan las predicciones teóricas y los resultados experimentales, encontrándose un buen acuerdo en ambos casos y obteniéndose información mecanística. El análisis de los valores obtenidos en los modelos permite ofrecer una explicación a la adsorción preferente del 4-clorofenol sobre las caras (“terraces”) de la nanopartíula frente a los límites (“edges”).

En el Capítulo IV se lleva a cabo la síntesis y uso como catalizador modelo de nanopartículas bimetálicas de Pd-Rh de distintos tamaños, sin soportar, en la hidrodecloración de 4-clorofenol en fase acuosa. Las nanopartículas son sintetizadas empleando metanol como agente reductor y polivinilpirrolidona como agente protector. Para la síntesis se utilizan dos métodos, co-reducción (reducción conjunta de las sales metálicas en la síntesis) y reducción sucesiva (reducción empleando como semillas nanopartículas monometálicas), y tres relaciones molares Pd/Rh. Se estudia cómo el método de síntesis y la relación molar Pd/Rh afecta al tipo de estructura de nanopartícula obtenida (core-shell y cluster-in-cluster). Se discute la actividad en comparación con nanopartículas monometálicas de Pd y Rh, encontrándose fenómenos de antagonismo y sinergia. La actividad se encuentra favorecida por estructuras core-shell con alta concentración de Pd en la superficie, si bien la selectividad a los productos de hidrogenación es mucho mayor para las estructuras cluster-in-cluster.

En el Capítulo V se lleva a cabo la síntesis y uso como catalizadores modelo de nanopartículas de Pd sin soportar en la reducción de nitritos. Las nanopartículas son sintetizadas empleando borohidruro sódico como agente reductor y polivinilpirrolidona y polivinilalcohol como agentes protectores. Se estudian la relación entre el tipo y cantidad de agente protector en el tamaño de partícula, así como la influencia de la cobertura de la superficie de las nanopartículas por el polímero sobre la actividad por sitio activo en función del agente protector. Asimismo, se discuten las diferencias encontradas en la selectividad en función del tipo y concentración del agente protector. La reducción de nitrito puede considerarse sensible a la estructura y la polivinilpirrolidona orienta eficazmente la selectividad a nitrógeno elemental.

En el Capítulo VI se lleva a cabo la preparación de carbones dopados con nitrógeno mediante co-pirólisis de polietileno de baja densidad con distintos precursores de nitrógeno y su uso como soporte de catalizadores de Pd preparados de forma convencional. Los catalizadores son empleados en la hidrodecloración de 4-clorofenol. Se estudia el grado de incorporación del nitrógeno en la matriz carbonosa en función de las condiciones de síntesis de carbón, así como de la fuente de nitrógeno empleada. De igual modo, se estudia cómo el tipo de nitrógeno (cuaternario, piridínico, etc.) y la cantidad incorporada en la matriz carbonosa influyen en la actividad y selectividad de los catalizadores en la reacción. Se discuten los valores de actividad observados en comparación con catalizadores preparadores en condiciones equivalentes cuyo soporte no se encuentra dopado, observándose un efecto sinérgico en el caso de los soportes dopados con nitrógeno.

En el Capítulo Conclusiones se recogen las principales conclusiones extraídas en los capítulos I – VI. En el apartado Trabajos Futuros, se llevan a cabo una serie de previsiones sobre los trabajos necesarios para avanzar en el conocimiento generado por la presente tesis.

Summary

The hydrotreatment processes, hydrogenation and/or reduction reactions usually carried out in the presence of a catalyst, have generated a growing interest in the field of water advanced treatment due to their advantages over other advanced processes. Among such advantages is versatility, since hydrotreatments can be applied to a wide range of refractory compounds in industrial wastewater (organohalogenates, perchlorate, bromate, chlorate, nitrosamines, etc.) and drinking water (nitrates,

nitrites). Likewise, the hydrotreatment processes can be operate under mild conditions of temperature and pressure, and they lead to secondary streams much less toxic if proper selectivity is achieved during the treatment.

The catalysts commonly used in the hydrotreatment of water are noble metals supported on a variety of materials such as alumina, clay, zeolites, or carbon materials. One traditional challenge in catalysis is to obtain catalysts that provide optimum activity and selectivity through rational design. Specifically, for structure sensitive reactions this challenge is difficult to achieve due to the large number of variables that affect the activity and selectivity of the catalyst, and to the potential interaction among variables. In general, these variables can be divided into two groups: those regarding to the support and those regarding to the metallic phase. The most relevant variables associated to the support are the chemical composition, porosity, specific surface area or surface groups, among others. In the case of the metallic phase, nanoparticle size, shape, oxidation state, interaction with the support and the composition (one or more elements) are the most important variables.

The conventional methods for the preparation of catalysts, generally consisting in the impregnation of a metal salt solution on a support and its subsequent reduction, do not always result in an adequate control of the variables that affect the activity and selectivity of the catalyst in sensitive structure reactions. In the last years, the methods for the synthesis of nanoparticles allowing control of size have received remarkable attention in the field of catalysis, since they offer the possibility of studying the physical and chemical properties influenced by the nanoparticle size.
A variety of methods have been reported for the synthesis of nanoparticles with

controlled size: chemical, electrochemical, sonochemical, etc. The chemical reduction method has been widely used because of its simplicity and effectiveness. The synthesis of nanoparticles is carried out by contacting a solution of a metal salt with a reducing agent (alcohol, hydrazine, sodium borohydride, etc.) in the presence of a protective agent (polyvinylpyrrolidone, polyvinyl alcohol, dodecylamine, etc.). The latter prevents the uncontrolled growth of nanoparticles and their aggregation, but as they are difficult to remove from the nanoparticles surface a new variable with potential influence on the activity and selectivity is introduced.

In order to generate valuable knowledge that can be used in the rational design of catalysts, this thesis deals with the study of the influence in hydrotreatment activity and selectivity of some of the variables related to the structure and synthesis of the active phase, namely the nanoparticle size, oxidation state and the nature of the protecting and reducing agent. Likewise, the influence of the chemical composition of the support is evaluated. With this aim, model catalysts consisting in noble metal (Pd, Rh) nanoparticles prepared by size-controlled synthesis have been used in hydrodechlorination and nitrite reduction reactions. A kinetic analysis based on a theoretical mechanistic approach has also been carried out to study the effect of nanoparticle size on the activity. Regarding the influence of the chemical composition of the support, nitrogen doped carbons have been evaluated.

The structure of the thesis comprises chapters that describe in detail the work performed (Chapters I - VI), a chapter of general conclusions and a chapter discussing future work.

In Chapter I the synthesis and use as model catalyst of unsupported Pd nanoparticles of different sizes in the hydrodechlorination of 4-chlorophenol in aqueous phase is studied. The synthesis was carried out using methanol and ethanol as reducing agents and polyvinyl pyrrolidone as a protective agent. The influence of the type and amount of reducing agent and the amount of protective agent on the particle size and the oxidation state is evaluated. The activity and selectivity of Pd colloidal suspensions is discussed in comparison with supported catalysts, showing as the most noticeable difference in the lack of activity of colloids to hydrogenate hydrodechlorination products. Thus, the only reaction product observed was phenol, whereas for supported Pd catalysts some selectivity to cyclohexanone and cyclohexanol has been described in literature. The highest activity was found for the smallest nanoparticles, although they exhibited a lower activity per unit of catalytic surface. The differences in the activity per unit mass and per unit of surface activity are discussed, as well as differences in the apparent activation energy between Pd colloids and supported Pd catalysts.

In Chapter II the synthesis of Rh nanoparticles of different sizes for their use as model catalysts in the hydrodechlorination of 4-chlorophenol in aqueous phase is reported. The synthesis is carried out using methanol as a reducing agent and polyvinyl pyrrolidone as a protective agent, which leads to a rather narrow nanoparticle size range but important differences in oxidation state (measured as Rh^{n+}/Rh^{0} ratio). The activity of the Rh nanoparticles is higher when the proportion of metallic species is high and a maximum is observed for a nanoparticle size around 2.8 nm. A regression model relating the influence of particle size and the oxidation state in the selectivity to

hydrogenation products (cyclohexanone and cyclohexanol) is developed, showing crossed effect between these two variables.

Chapter III describes a kinetic analysis based on the two-step reaction and the Langmuir-Hinshelwood mechanism, applied to the hydrodechlorination of 4-chlorophenol using the experimental data obtained with unsupported Rh nanoparticles in Chapter III. The theoretical predictions and experimental results are compared, showing a good agreement and mechanistic information about the dependence of activity on nanoparticle size. The analysis of the values obtained for the parameters of the models indicates a preferential adsorption of 4-chlorophenol on the terraces of the nanoparticles in contrast to the edges.

In Chapter IV bimetallic Pd-Rh nanoparticles are synthesized and used as unsupported model catalysts in the hydrodechlorination of 4-chlorophenol in aqueous phase. The nanoparticles are synthesized using methanol as a reducing agent and polyvinylpyrrolidone as a protective agent. Two synthesis methods, co-reduction (simultaneous reduction of both metal salts) and successive reduction (reduction using monometallic nanoparticles as seeds) are studied at three Pd/Rh molar ratios. The influence of the synthesis method and the molar Pd/Rh ratio in the type of nanoparticle structure obtained (core-shell, cluster-in-cluster) is reported. The activity of the bimetallic nanoparticles is studied and compared to monometallic Pd and Rh ones, showing synergistic and antagonist effects. The relationship between the selectivity and the type of nanoparticle structure and Pd/Rh ratio is evaluated. The activity is favored by core-shell structures with a high concentration of Pd at the outer

surface, although the highest selectivity to hydrogenation products is achieved for cluster-in-cluster structures.

Chapter V is devoted to the application of unsupported Pd nanoparticles as catalysts models in the reduction of nitrite. The nanoparticles are synthesized using sodium borohydride as a reducing agent and polyvinylpyrrolidone and polyvinyl alcohol as protective agents. The relationship between the type and amount of the protective agent particle size and the influence of the surface coverage of the nanoparticles by the polymer in the activity is studied. Likewise, the differences in selectivity depending on the type and concentration of the protective agent are discussed. The reduction of nitrite ion can be considered as structure sensitive and polyvinylpyrrolidone is effective in promoting the selectivity towards molecular nitrogen.

Chapter VI deals with the preparation of solid carbons doped with nitrogen by co-pyrolysis of low density polyethylene and several nitrogen precursors, and their use as supports for the preparation of Pd catalysts by conventional methods. The catalysts are tested in the hydrodechlorination of 4-chlorophenol. The degree of incorporation of nitrogen into the carbon matrix is discussed in terms of the pyrolysis conditions and the nitrogen precursor used. The influence of the amount of nitrogen incorporated and the nitrogen species created (quaternary, pyridine, etc.) in the activity and selectivity of the catalysts is described. The comparison with Pd catalysts supported on non doped solid carbons, showed a synergistic effect for the nitrogen doped supports.

Conclusions chapter summarizes the main conclusions of the former chapters and the Future Work section provides some ideas about further research to continue research and progress in the knowledge generated by this thesis.

CAPÍTULO I /CHAPTER I

Catalytic behaviour of size-controlled palladium nanoparticles in the hydrodechlorination of 4-chlorophenol in aqueous phase

J.A. Baeza, L. Calvo, M.A. Gilarranz, A.F. Mohedano, J.A. Casas, J.J. Rodriguez,J. Catal. 293 (2012) 85–93.

Abstract

Unsupported Pd nanoparticles of controlled size were tested as catalyst in liquid phase hydrodechlorination (303-323 K, 1 atm) using 4-chlorophenol (4-CP) as target compound. The Pd nanoparticles were synthesized by chemical reduction, using ethanol and methanol as reducing agents and poly(N-vinyl-2-pyrrolidone) (PVP) as capping agent. The size of the nanoparticles and the Pd^{n+}/Pd^{0} ratio decreased with increasing alcohol concentration and PVP/Pd ratio, both being lower for ethanol medium.

High 4-CP conversion values (80-100 %) were achieved at low Pd concentration ($2.45 \cdot 10^{-3} g \cdot L^{-1}$). Phenol was the only reaction by-product detected in contrast to previous results with supported Pd catalysts, where the active phase-support interaction in 4-CP HDC led to obtain also cyclohexanone and cyclohexanol as by-products in equivalent experimental conditions. The smaller nanoparticles showed higher activity due to the higher available surface (m^2/g_{cat}). Thus, the smaller nanoparticles synthesized in ethanol medium ranged between 2.7 and 2.8 nm and yielded activity values between 16.7 and 39.1 $mmol/g_{cat} \cdot min$, whereas the smaller particles obtained in methanol medium were in the 3.1 - 4.2 nm range and exhibited activity values of 20.1 – 25.7 $mmol/g_{cat} \cdot min$. However, the large nanoparticles exhibited higher activity per unit of catalyst surface, e.g. 0.34 – 0.43 $mmol/min \cdot m^2$ in the case of those synthesized in methanol medium. On the other hand, higher activity was observed for the nanoparticles synthesized in methanol medium when equivalent nanoparticle size was compared. Activation energy values around 100 kJ/mol were obtained for Pd nanoparticles of different characteristics, significantly higher than the value reported for supported Pd catalysts.

Keywords: colloidal nanoparticles, palladium, particle size, hydrodechlorination, 4-chlorophenol

1. Introduction

In the last years, catalytic hydrodechlorination (HDC) has received increasing attention for the treatment of wastewaters containing chlorinated organic compounds since it shows some advantages when compared to other techniques of potential application for these hazardous pollutants. HDC can operate at mild conditions [1-3], so that it does not require high temperatures and/or pressures as in the case of incineration or wet oxidation processes. Large amounts of reagents, such as in Fenton oxidation, are not needed and can be applied within a wide range of concentrations of chlorinated compounds, which is not the case of biological methods [4]. Though HDC does not provide the complete destruction of the pollutants, it can lead to a convenient transformation of them into substantially less harmful species [2, 4, 5]. Thus, HDC can be used as a detoxifying stage prior to a biological treatment.

Transition and noble metal-based catalysts have been commonly used in liquid phase HDC [6-14]. Among those metals, Pd has been the most extensively used because of its singular catalytic properties [15] that lead to high dechlorination efficiencies [16-18]. These specific properties are affected by a number of factors such as the metallic particle size, shape, oxidation state and interaction with the support, among others [19-21]. Particularly, metal particle size is crucial for the performance of the catalyst in structure-sensitive reactions. A number of authors have concluded that HDC reaction is structure sensitive [22-28], although there is no general agreement respect to this topic [29] Thus, in order to design efficient catalysts, it is necessary a

previous in-depth knowledge about how this factor affects to the catalytic properties. In general, it is widely accepted that decreasing the particle size of the metallic phase increases the catalytic activity because of a higher surface-to-volume ratio although some limit has been claimed for this effect [30, 31]. Moreover, the nature and the strength of bonding between the molecules adsorbed and the metal particles is affected by the number of particles surrounding a surface metal atom (electronic or ligand effect). Thus, adsorption energies could change with particle size, leading to a poisoning of the catalyst or an activation of the substrate, depending on the nature of the adsorption of the molecule on the particle surface [15]. It is important to remark that the catalysts commonly studied have their metallic phase dispersed at nanometric scale, but there is no precise control on the nanoparticle size upon the synthesis. Therefore, there is a remarkable interest in the literature in designing catalysts with controlled nanoparticle size and size distribution [32-35]. However, it must be emphasized that the influence of nanoparticle size on the catalytic activity is not well defined so far, since decreasing the particle size not always increases the reaction rates evaluated per unit mass of nanoparticle. Thus, when a certain minimum particle size is reached, an additional decrease produces an increase of the ionization energy and, as a result, an increase of the adsorption energy. The resulting stronger adsorption of intermediate species on the particle surface can provoke poisoning of active sites of the catalyst, which diminishes the catalytic activity [15, 36].

Some research efforts have been focused on developing methods of synthesis of nanoparticles with the objective of controlling their size within a narrow distribution in order to investigate chemical and physical size-dependent properties [37-39]. Among the methods of synthesis of noble metals nanoparticles that have been

reported in the literature, chemical [40, 41], electrochemical [42], sonochemical [43] and microbial-based methods [44] are the most relevant. Chemical reduction is considered as a simple method based on the reduction of a metal precursor salt in the presence of a reducing agent (hydrazine, pyrogallol, potassium borohydride, ethanol, methanol, propanol) and a protective or capping agent (poly(N-vinyl-2-pyrrolidone), polivinyl alcohol, dodecylamine). This last inhibits aggregation and is responsible of the controlled growth and shape of the particles. This method has been claimed in some works [45-48] for the design of size-controlled nanoparticles whose catalytic activities have been analyzed in different reactions. For example, Narayanan et al. [36] synthesized size-controlled Pd nanoparticles that were supported on activated carbon and tested them for the Suzuki reaction between phenylboronic acid and iodobenzene for producing biphenyl. In another related work, Joo S.H. et al. [48] studied the effect of particle size on CO oxidation over Ru nanoparticles catalysts. Nevertheless, investigation of size controlled nanoparticles applications in other types of catalytic reactions are scarce and thus, so far there is no still a comprehensive knowledge on how particle size influences the catalytic activity in reactions such as liquid phase HDC.

The aim of this work is to address the effect of the synthesis conditions and the size of Pd nanoparticles on their activity in 4-CP HDC in aqueous phase. The Pd nanoparticles were prepared with poly(N-vinyl-2-pyrrolidone) (PVP) as capping agent and ethanol or methanol as reducing agent.

2. Experimental

2.1 Materials

Sigma-Aldrich $PdCl_2$ (99 %) was used as Pd nanoparticles precursor. Poly(N-vinyl-2-pyrrolidone) (average molecular weight: 40.000, Sigma-Aldrich Co.) was used as capping agent to avoid uncontrolled growing and inhibit aggregation of Pd nanoparticles. Methanol (>99 %) and ethanol (>99 %), used as reducing agents, were purchased from Panreac Quimica S.A.U and Merck KGaA, respectively. Hydrogen (>99 %) was supplied by Praxair. All the reagents were used as received without further purification.

2.2 Synthesis and characterization of Pd nanoparticles

Pd (II) chloride (0.5 mmol), 0.2N HCl (1 mmol) and distilled water (250 mL) were mixed to obtain a H_2PdCl_4 ($2 \cdot 10^{-3}$ M) pale-yellow aqueous solution. An aliquot of 30 mL of the $2 \cdot 10^{-3}$ M H_2PdCl_4 solution was mixed with 70 mL of alcohol/water solution and PVP. The mixture was refluxed in a 250 mL flask connected to a Liebig condenser for 3 hours under atmospheric pressure [37]. The values of PVP/Pd ratio were varied between 5 and 40 (mol/mol) and different mixtures of alcohol/water (10-70%, v/v) were used in order to learn on the effect of these variables on the size and size distribution of Pd nanoparticles. Finally, the colloidal dispersion of nanoparticles (100 mL) was concentrated up to a total volume of approximately 10 mL in a rotary evaporator (Büchi).

The Pd nanoparticles synthesized were characterized by transmission electron microscopy (TEM) at 400kV (JEOL, mod. JEM-4000 EX). Samples were prepared placing a drop of colloidal Pd nanoparticles onto a carbon-coated copper grid and lefting it dry

at room temperature. Software 'ImageJ 1.44i' was used for counting and measuring particles on digital TEM images (more than 200 nanoparticles were measured per image). Surface-area-weighted mean diameters ($d_s = \sum n_i d_i^3 / \sum n_i d_i^2$) and size distribution, characterized by the standard deviation ($\sigma_s = \sqrt{\sum (d_i - d_s)^2 / n}$), were calculated as described elsewhere [49]. Likewise, the catalysts were characterized by XPS (Physical Electronics, mod. ESCA 5701 equipped with a Mg-Kα X-ray excitation source, 1253.6 eV). Software 'Multipak v8.2b' was used for spectrograms deconvolution in order to determine both Pd electrodeficient and zerovalent species in the particle surface. The analysis procedure involved smoothing, a Shirley background subtraction and mixed Gaussian-Lorentzian by a least-square method curve fitting as described in a previous work [50]. C 1s peak (284.6 eV) was used as internal standard for binding energies corrections due to sample charging. Doublet separation for Pd 3d was 5.26 eV as described elsewhere [51]. Deconvoluted peaks showed binding energies in the range of 334.8 - 335.8 eV and 336.2 - 337.1 eV for Pd $3d_{5/2}$ which can be attributed to metallic Pd (Pd^0) and electrodeficient Pd (Pd^{n+}), respectively. All this data values are in good agreement with those reported in NIST X-ray Photoelectron Spectroscopy Database [51]. A probing depth of several nanometres can be assumed; therefore the surface Pd^{n+}/Pd^0 ratio calculated should be essentially the same as the bulk ratio for the particles studied.

2.3 HDC experiments

Catalytic HDC runs were carried out during 4 hours in a three-necked jacketed glass reactor were H_2 was continuously fed at 50 N mL·min^{-1} flow rate under vigorous stirring (600-800 rpm) in order to facilitate hydrogen distribution through the 4-CP

solution (150 mL). The reaction temperature (303-323 K) was controlled by a thermostatic bath connected to the reactor jacket. The system was equipped with a cold trap at the vent to check any possible stripping; no significant stripping was detected. The initial concentration of 4-CP was 100 $mg \cdot L^{-1}$ and the catalyst load was $2.45 \cdot 10^{-3}$ $g \cdot L^{-1}$ of Pd.

A sampling system consisting on a thin tube connected to a syringe allowed taking liquid samples (1 mL), which were collected previous filtering (PTFE filter, pore size 0.45 µm). The samples were analyzed by high performance liquid chromatography (Varian Prostar equipped with a UV-VIS detector) using a C_{18} column as stationary phase and a mixture of acetonitrile and water (1:1, v/v) as mobile phase. Cyclohexanone and cyclohexanol were analyzed by a GC/FID device (GC 3900 Varian) using a 30 m long x 0.25 mm i.d. capillary column (CP-Wax 52 CB, Varian) and nitrogen as carrier gas. The quantification of chloride ion was performed by ion chromatography (Metrohm 790 Personal IC). The carbon and chlorine balances matched always between 90 % and 95 %, respectively, at the least.

3. Results and discussion

3.1 Pd Particle size and size distribution

3.1.1 TEM characterization

Table 1 shows the mean diameters and size distributions of Pd nanoparticles prepared under different conditions. Figure 1 shows, as representative examples, TEM images of four selected series. The nanoparticles appeared mostly spherical although some differences in shape were found in the case of the nanoparticles synthesized in

70 % ethanol (series 4), with polyhedral shapes prevailing over spheres. These nanoparticles showed the largest size with a mean diameter of 22.1 nm.

Table 1. Mean diameter (d_s), size distribution (σ_s), Pd^{n+}/Pd^0 ratio, specific surface area and activity (a) of the Pd nanoparticles prepared under different conditions.

Pd nanoparticles series	Alcohol	Vol Alcohol (%)	PVP/Pd (mol/mol)	d_s (nm)	σ_s (nm)	Pd^{n+}/Pd^0 ratio	Specific surface area (m^2/g_{cat})	a (mmol/g_{cat}·min)
1	Ethanol	10	5	4.7	1.0		106	7.4
2	Ethanol	25	5	3.6	1.2	0.67	138	10.1
3	Ethanol	40	5	4.0	1.9	0.35	125	4.8
4	Ethanol	70	5	22.1	10.4	2.79	23	3.5
5	Ethanol	10	20	3.5	0.9	0.48	143	14.6
6	Ethanol	25	20	2.7	0.7		184	19.4
7	Ethanol	25	35	2.7	0.8	0.54	181	39.1
8	Ethanol	40	20	2.8	0.8		178	16.7
9	Ethanol	55	20	2.8	0.4		178	17.8
10	Methanol	10	5	12.9	7.0	1.46	39	16.8
11	Methanol	10	20	10.9	2.9	1.05	46	17.2
12	Methanol	10	35	3.1	0.6	0.48	161	25.3
13	Methanol	10	40	3.6	0.7	0.51	139	20.1
14	Methanol	25	20	8.5	4.6	1.03	59	19.8
15	Methanol	40	20	3.8	0.8	0.56	131	25.7
16	Methanol	55	20	4.2	1.2	0.39	119	23.7

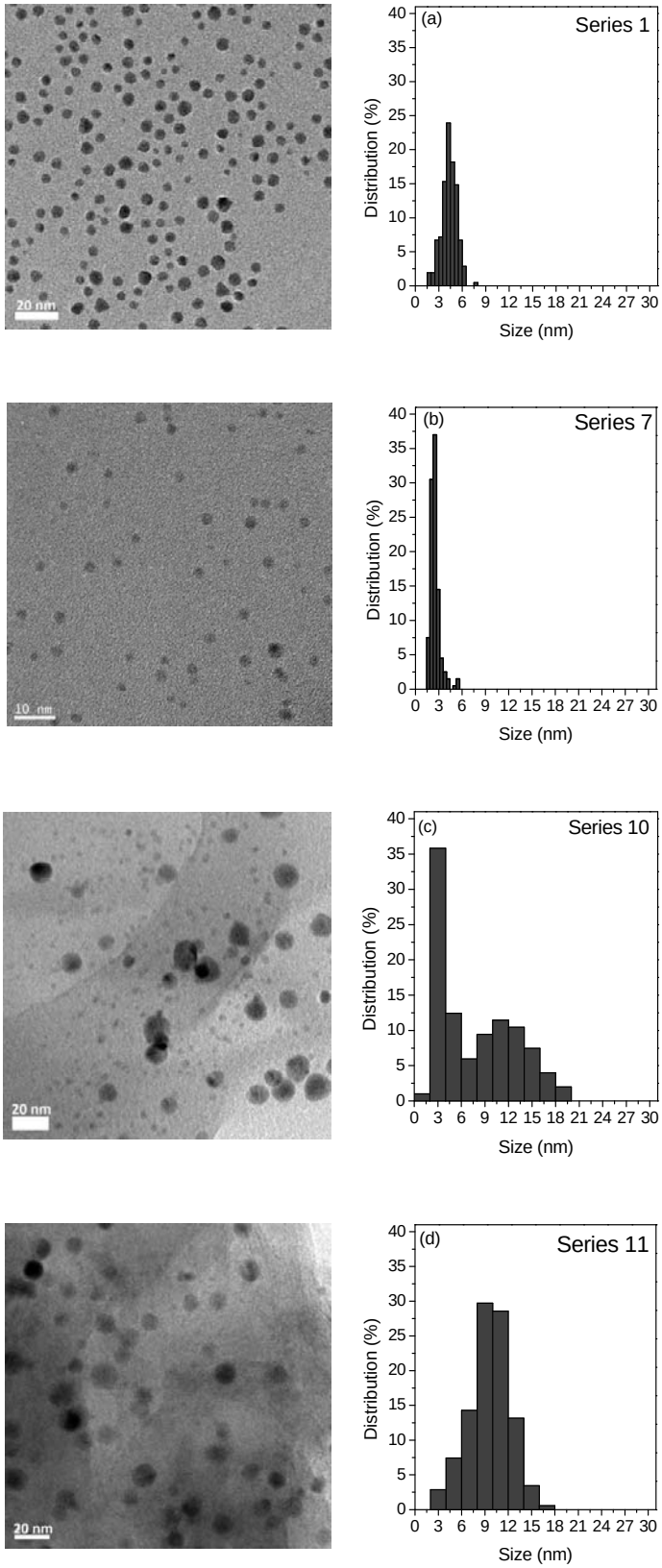

Figure 1. TEM images and size distributions of four samples of Pd nanoparticles prepared in ethanol (a, b) and methanol (c, d) /water media.

3.1.2 Effect of the capping agent on nanoparticles size

The influence of the capping agent on the particle size can be observed in Figure 2. When an intermediate concentration of 25 % ethanol was used, an increase of the PVP/Pd molar ratio from 5 to 20 led to a reduction of both particle size and size distribution. The same trend was observed with a concentration of 10 % methanol but within a wider range of the PVP/Pd molar ratio (5 to 35). At higher PVP/Pd molar ratios, no additional decrease in nanoparticle size and size distribution was found.

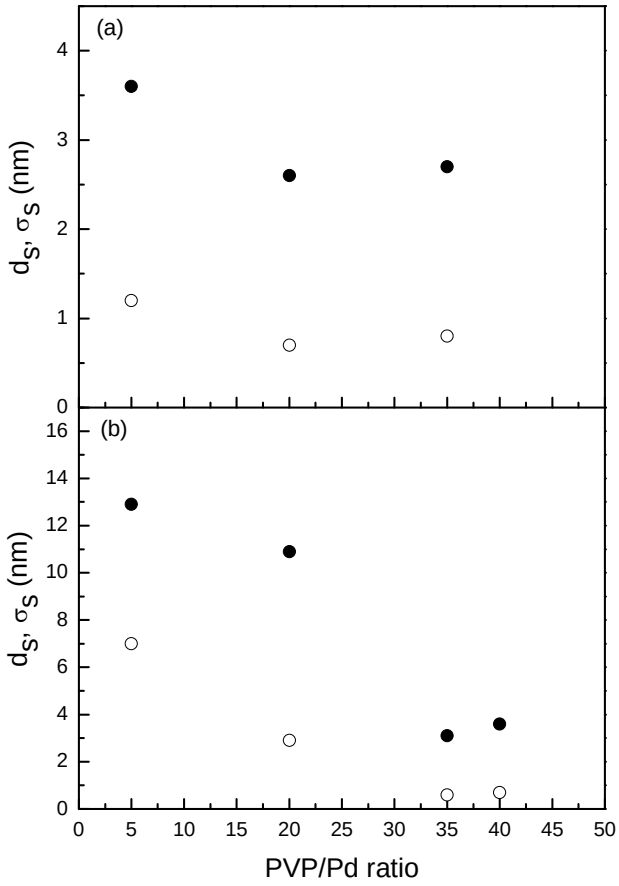

Figure 2. Mean diameter (●) and size distribution (○) of Pd nanoparticles obtained at different PVP/Pd ratios. (a) Ethanol 25 vol % and (b) methanol 10 vol %.

It has been reported that the role of PVP is to act as a protecting agent, allowing controlled particles growth in a reactor of a nano-sized water pool wrapped with PVP, preventing particles aggregation [52, 53]. Increasing the PVP/Pd molar ratios favours the formation of micellar structures that surround the particles and control their growth.

3.1.3 Effect of the reducing agent

The alcohol used as reducing agent showed a crucial effect on the size of the nanoparticles, as can be seen in Table 1. Figure 3 shows that, for a PVP/Pd molar ratio of 5, the ethanol concentration did not show a well defined influence in the range of 10-40 % where mean diameters and size distributions within 3.6 - 4.7 nm and 1.0 - 1.9 nm were respectively observed. However, a significant increase took place in 70 % ethanol medium up to 22 nm mean particle diameter. A different behavior was observed with methanol as reducing agent. For a PVP/Pd molar ratio of 20, the nanoparticle mean diameter decreased when the methanol ratio increased from 10 % to 40 % where a minimum size of 3.8 nm was reached without any further decrease at higher methanol concentration. As reported in the literature [37], two main effects lead to the generation of smaller Pd nanoparticles in relation to the concentration of reducing agent. Firstly, a higher concentration of the reducing agent increases the reduction rate of $[PdCl_4]^{2-}$ to Pd^0, provoking the generation of smaller nanoparticles because of the occurrence of a higher number of Pd nuclei. This effect seems to prevail at ethanol and methanol concentrations within 10-40 % and 10-55 %, respectively. Secondly, while PVP is dissolved in both alcohol and water, H_2PdCl_4 shows decreasing solubility at high alcohol concentration, so it does not disperse homogeneously in a

mixed water-alcohol solution at the highest alcohol ratios tested. Therefore, nanoparticle mean diameter and size distribution become larger and wider, respectively, at high alcohol ratios. This seems to be the prevailing effect at alcohol concentrations beyond 40 %.

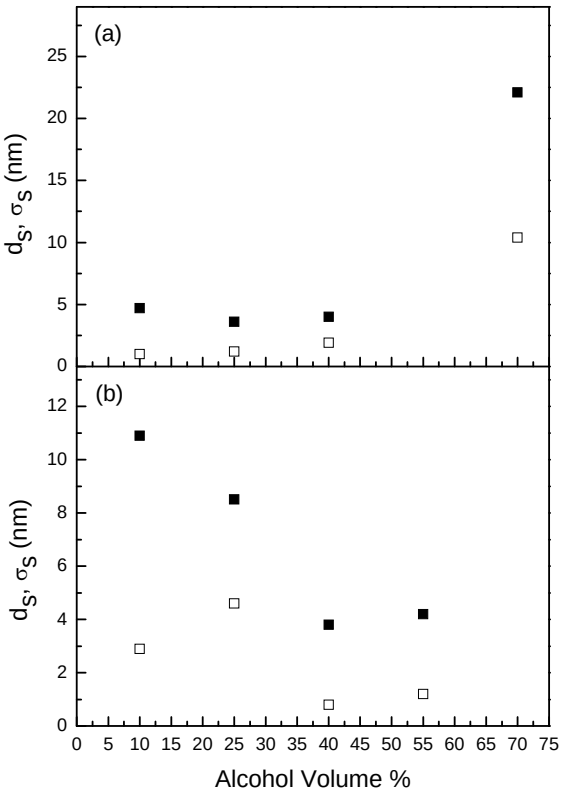

Figure 3. Mean diameter (■) and size distribution (□) of Pd nanoparticles prepared with (a) Ethanol (PVP/Pd ratio = 5 mol/mol) and (b) methanol (PVP/Pd ratio = 20 mol/mol).

The smallest nanoparticles were obtained at different alcohol ratios and PVP/Pd molar ratios for each of the alcohols used. As shown in Table 1, under identical synthesis conditions (alcohol concentration and PVP/Pd ratios), Pd nanoparticles synthesized with ethanol as reducing agent were smaller. The effect of the reducing agent on the particle size has been discussed in the literature. Teranishi et al. [37] suggested a faster reduction of $[PdCl4]^{2-}$ by alcohols with higher boiling point, providing a higher number

of Pd nuclei. Thus, alcohols of higher boiling point lead to Pd nanoparticles of lower size. Likewise, they indicated that ethanol can be oxidized more easily than methanol according to the hydrogenation enthalpies of the corresponding aldehydes. Our results are consistent with this explanation, since all of the nanoparticles synthesized in ethanol medium were of lower size than those synthesized in methanol medium under the same synthesis conditions.

3.2. XPS Characterization

XPS was used to establish the oxidation state of Pd. The Pd^{n+}/ Pd^{0} ratios obtained from the deconvolution of the XPS Pd 3d region spectra are summarized in Table 1. The presence of both Pd^{n+} and Pd^{0} was observed in all the Pd nanoparticles series analyzed. Gómez-Sainero et al. [54] reported that both electrodeficient and zero valent species are required for carbon tetrachloride HDC on Pd/AC in gas phase, whereas catalysts with only one of the species (Pd^{n+} or Pd^{0}) remained inactive. In this sense, they proposed a dual nature of Pd active sites by the association of both species, reaching a maximum of activity at a Pd^{n+}/Pd^{0} ratio close to 1. Other authors were also in agreement with the proposed dual nature of the Pd active sites in HDC in gas phase [50]. Figure 4 shows the Pd 3d deconvolved spectra for the nanoparticles of series 11 and 12. Zerovalent Pd is the prevailing species in series 12 whereas quite similar proportions of electrodeficient and zerovalent Pd were found for series 11.

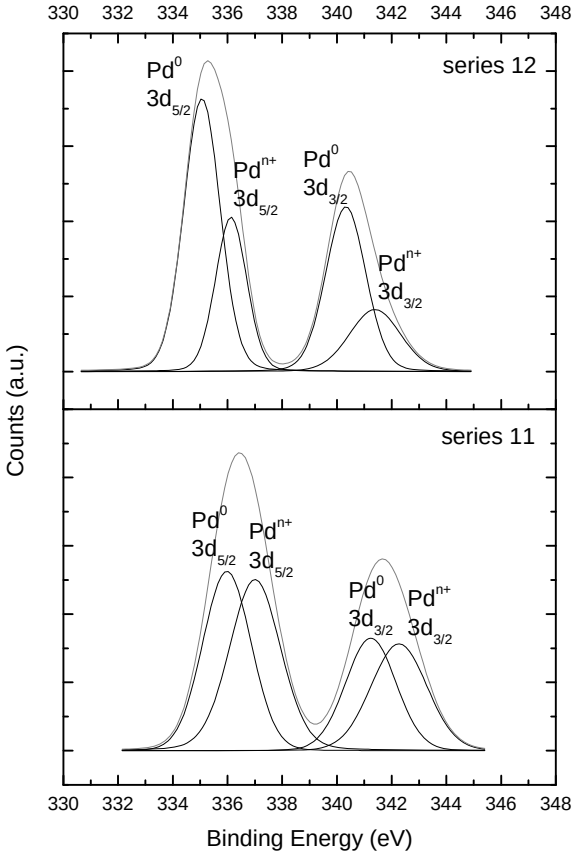

Figure 4. XPS spectra of Pd nanoparticles of series 11 and 12 (Table 1).

As can be seen in Figure 5, there is a relationship between the Pd^{n+}/Pd^{0} ratio values and the mean particle diameter. Three different patterns can be distinguished independently of the alcohol used as reducing agent. The smaller particles (2.7-4.2 nm) show Pd^{n+}/Pd^{0} ratios between 0.35 and 0.67, whereas for larger particles (8.5-12.9 nm) that ratio is between 1.03 and 1.46. Oversized particles (22.1 nm) show Pd^{n+}/Pd^{0} ratio value of 2.79. This observation is consistent with previous results reported in the literature, where small particles had a lower $Pd^{n+/}Pd^{0}$ ratio than large ones [55]. The differences found in Pd^{n+}/Pd^{0} ratios can be related with the higher surface/volume ratio of smaller particles, which provides a higher surface per unit mass of Pd to be reduced by the reducing agent thus leading to a lower Pd^{n+}/Pd^{0} ratio of small particles

compared to larger ones. However, due to the difficulty to address where Pd^{n+} and Pd^0 species are predominantly located in Pd nanoparticles, further research is needed.

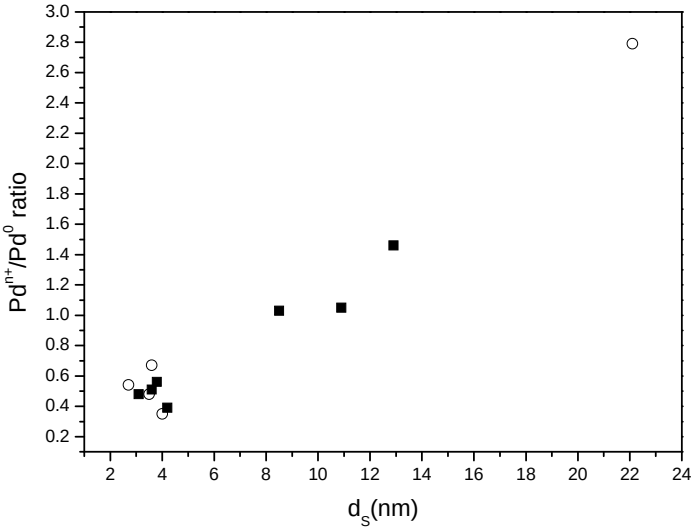

Figure 5. Pd^{n+}/Pd^0 ratio versus nanoparticle mean diameter: methanol (■) and ethanol series (○).

3.3 HDC activity of Pd nanoparticles

The HDC runs were carried out at variable concentrations of PVP in the reactor. Preliminary experiments carried out in the absence of catalyst proved that there was no reaction between PVP, 4-CP and H_2. Moreover, a control experiment was carried out adding to the reaction medium a dose of PVP ten times higher than that needed for the synthesis of the Pd nanoparticles with the aim of addressing the effect of the excess of PVP on the catalytic activity. The results showed no significant differences in activity between the series 10 of Pd nanoparticles (16.8 mmol/gcat·min) and the same particles series in the control experiment (16.5 mmol/gcat·min). Thus no synergistic or inhibitory effect of PVP was observed. These results are in good agreement with those reported by Hirai & Yakura [56] on the study of activity of Pd nanoparticles of different size protected by PVP layers of different thickness. These authors concluded that

activity depends mainly on specific surface area and not in PVP concentration. Chemical control of the reaction has been checked experimentally by using different concentrations of catalyst in 4-CP HDC reaction; no significant differences in the HDC rates per unit mass of catalyst were observed.

Figure 6 shows the evolution of 4-CP conversion upon reaction time with some Pd nanoparticles series. High 4-CP conversion values were achieved (80-100 %) in all cases. Two different behaviors were observed in relation with the reducing agent used. In the case of Pd nanoparticles from the methanol series, changes in particle size were accompanied by small differences in activity. In contrast, in the ethanol series, the activity increased when decreasing the particle size.

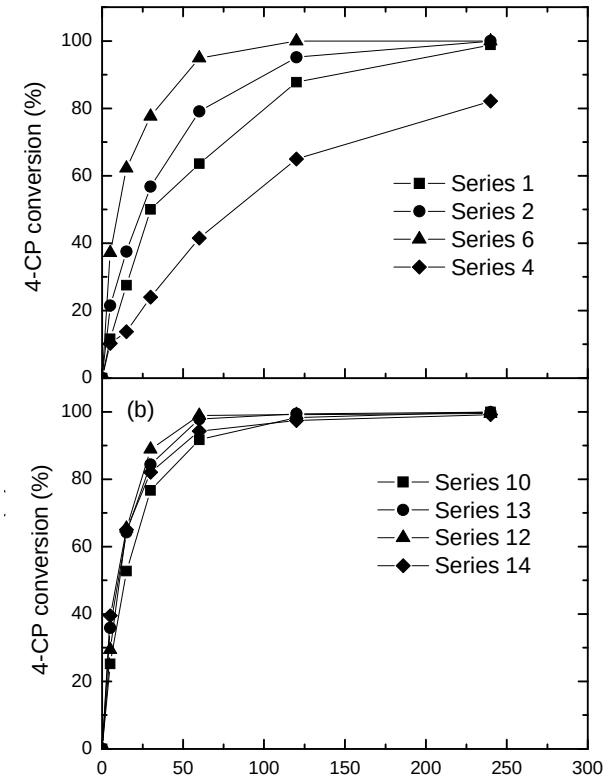

Figure 6. HDC of 4-CP with Pd nanoparticles ($2.45 \cdot 10^{-3}$g/L) of: ethanol (a) and methanol series (b) (Table 1).

The nanoparticle size affects the nature and strength of the interaction of 4-CP with the Pd surface since it determines the number of particles surrounding each surface metal atom. Moreover, the coordination of surface atoms depends on the particle size. Thus, smaller particles contain more surface atoms residing on the edges of the crystallographic planes or on edge junctions, increasing the number of active sites which could be accessible to the 4-CP molecules [15]. Additionally, Diaz et al. [57] indicated that structure sensitive appears as a determining factor on the HDC activity. The results reported suggested that a metal particle size within the 3–4 nm range can be considered as the optimum for Pd-based catalysts. Contradictory results have been found in literature about the most favorable catalyst site (terrace vs. edges/corners) in HDC. A number of works have considered the edges/corners as the most favorable catalyst sites in HDC since a high activity seems to be related with the number of surface Pd atoms of low coordination placed at the edges and corners of Pd particles [58-60], being such atoms more abundant in smaller particles. This interpretation has been also been reported for other catalytic reactions such as Suzuki-Heck reaction [61-62]. Nevertheless, other authors have indicated that large ensembles or single atoms can be considered as the most favorable catalytic sites for HDC [63-64]. Although, studies about the mechanism of liquid phase HDC of 4-CP in the presence of Pd are not available, Orlov et al. [65] reported structure-dependent adsorption of 4-CP on a polycrystalline TiO_2 surface. Likewise, Solomon et al., [66] found differences in phenol adsorption varying from physical adsorption on clean Ag surface to chemisorption on oxygenated Ag surface. Thus the adsorption pattern resulting from the different Pd arrangements may have an important role in catalytic activity.

A relevant result is that phenol was the only HDC product detected. Previous works in the literature showed high catalytic activities for supported Pd catalysts in the HDC of chlorophenols [67]. Previous works on the use of Pd on Al_2O_3 under mild conditions [68, 69] and Pd on activated carbon at higher temperature [4] reported complete conversion of 4-CP, yielding cyclohexanone and cyclohexanol as reaction products in addition to phenol. The concentration of Pd used in those works was several times higher than ours. Thus, it is remarkable that, in the operating conditions tested, the Pd nanoparticles used in the current work did not show activity for phenol hydrogenation in contrast to the behavior reported for supported Pd catalysts. To learn more on this fact some phenol hydrogenation experiments were carried out at the same experimental conditions than for 4-CP HDC, using a 100 $mg \cdot L^{-1}$ phenol aqueous solution, and no detectable phenol hydrogenation was observed after 4 hours reaction time. Thus, the support must play a key role in supported Pd catalysts resulting in phenol hydrogenation to by-products, such as cyclohexanone and/or cyclohexanol. The support can affect to the selectivity of reactions due to its interaction with the metallic active phase, provoking changes in the electronic density of Pd nanoparticles that can affect the strength of adsorption on the metal sites [69].

A simple pseudo-first order kinetic equation was checked to describe the rate of 4-CP disappearance:

$$(-r_{4-cp}) = \frac{-dC_{4-cp}}{dt} = k \times C_{4-cp} \qquad [1]$$

$$t = 0; \quad C_{4-cp} = C_0$$

Table 2 summarizes the results obtained by fitting the experimental 4-CP concentration-time curves. Besides the rate constants values, the Table 2 includes the correlation coefficients and the apparent activation energy as calculated from the Arrhenius equation.

Table 2. Pseudo-first order rate constant and apparent activation energies values (Ea) for 4-CP HDC with Pd nanoparticles

Pd nanoparticles series	Reaction Temperature (K)	Rate constant (min^{-1})	r^2	Ea (kJ/mol)	r^2
2	303	0.026 ± 0.004	0.990	100 ± 15	0.953
	308	0.057 ± 0.007	0.996		
	313	0.090 ± 0.013	0.995		
3	303	0.011 ± 0.002	0.989	105 ± 6	0.994
	310	0.030 ± 0.002	0.997		
	313	0.042 ± 0.004	0.997		
12	303	0.072 ± 0.008	0.995	106 ± 3	0.998
	310	0.181 ± 0.020	0.998		
	313	0.278 ± 0.038	0.998		
11	303	0.026 ± 0.004	0.990	100 ± 1	0.999
	313	0.093 ± 0.010	0.999		
	323	0.310 ± 0.014	0.998		
15	303	0.058 ± 0.013	0.985	118 ± 3	0.999
	308	0.129 ± 0.025	0.992		
	310	0.261 ± 0.020	0.999		

Figure 7 depicts, as representative example, the validation of the rate curves for Pd nanoparticles of series 11. Apparent activation energy values within the range of 100-118 $kJ \cdot mol^{-1}$ were obtained and did not show dependence on nanoparticle size. These activation energy values are significantly higher than those reported in the literature for the HDC of chlorophenols with supported Pd catalysts (21-58 $kJ \cdot mol^{-1}$) [68, 71-73]. This fact was also reported by Schwab [74], who indicated that activation energies for formic acid decomposition were significantly higher for bulk metals than

for supported metals (Cu/MgO, Ag/MgO and Ni/Al_2O_3) due to an effect of metal-support electronic movement, even in supports with low conductivity. Therefore, the supports seem to play an important role in the HDC pathway that not only modifies the selectivity, but also the activation energy.

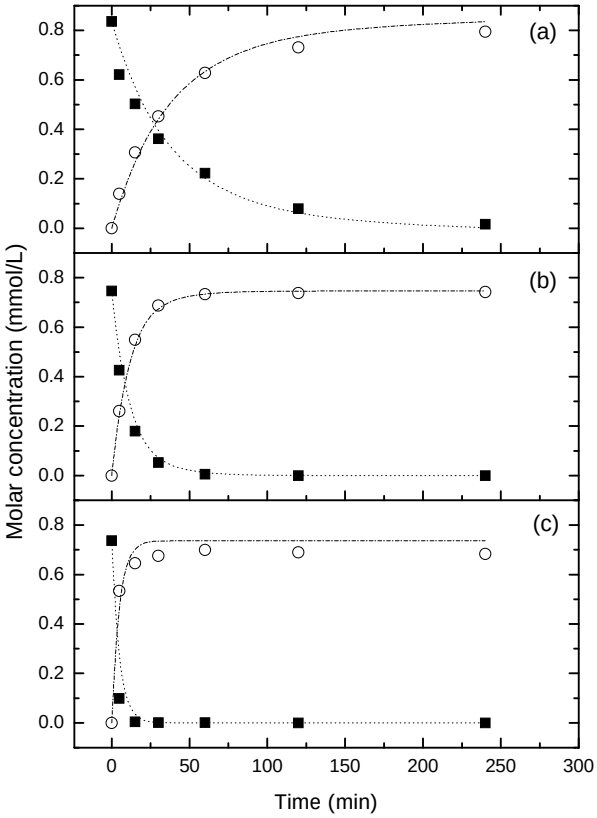

Figure 7. Time evolution of (■) 4-CP and (○) phenol in 4-CP HDC with Pd nanoparticles series 11. Reaction temperature: (a) 303 K, (b) 313 K and (c) 323 K. Predicted curves in dashed lines.

The activity (a) of Pd nanoparticles was evaluated from the pseudo-first order rate constant of 4-CP disappearance and was normalized taking into account the Pd dose used in each experiment:

$$a = k \times \frac{0.150\ L}{m_{Pd}\ (g)} \qquad [2]$$

The available catalytic surface was estimated from the specific surface area and the Pd dose used in each experiment. The specific surface area of Pd nanoparticles was calculated assuming spherical shape from the equation [3].

$$S_a = \frac{6}{d_s \times \rho_{Pd}} \qquad [3]$$

Table 1 shows the specific surface area and catalytic activity values of the Pd nanoparticles tested in the HDC runs. A decrease of nanoparticle size is associated to a higher surface area giving rise to a higher activity. Figure 8 shows this relationship for the two series of nanoparticles prepared in ethanol and methanol media. The particles synthesized in methanol medium showed a higher activity for equivalent particle size and also a less pronounced decrease with increasing size. Therefore, not only the particle size, but also the synthesis conditions are relevant for activity. In this sense the type of reducing agent seems to be an important factor.

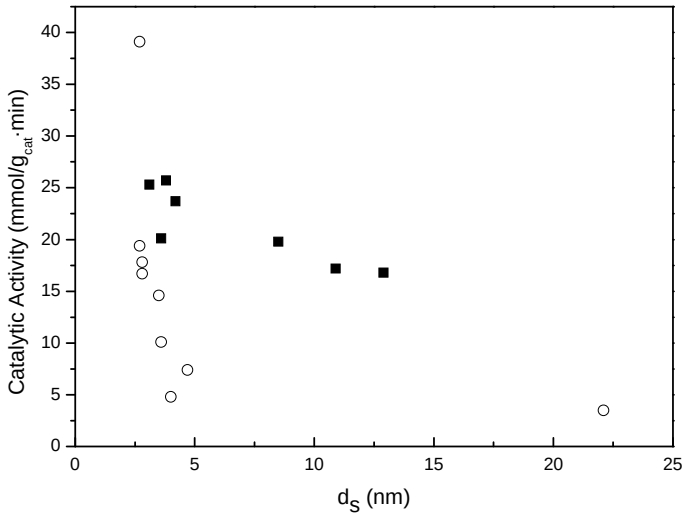

Figure 8. Catalytic activity of Pd nanoparticles versus mean diameter: (■) methanol and (○) ethanol series.

Other additional effects reported in the literature in relation with particle size and catalytic activity are the differences in hydrogen solubility between larger (better solubility) and smaller (worse solubility) particles [75-77], and the better resistance of larger Pd particles to inhibition/poisoning by chlorine [30, 64, 78]. Thus, the higher activity per unit surface area of larger particles found in the present work could be related to a combination of these factors. Changes in coordination number with size should also be taken into account since larger particles could present higher coordination number thus favoring the bonding strength of reactants and products, avoiding the inhibition/poisoning by chlorine of the catalysts and taking advantage of the higher solubility of H_2 as well.

Figure 9 shows that as a general trend the nanoparticles of lower diameter, whose total available surface is higher, exhibit a lower catalytic activity per unit of surface area, the trend being more clear in the case of methanol series. Therefore, the nanoparticles of higher diameter seem to have a more active surface for HDC. The ethanol series did not show significant differences in catalytic activity per unit surface area, besides such activity values were lower than for the methanol series.

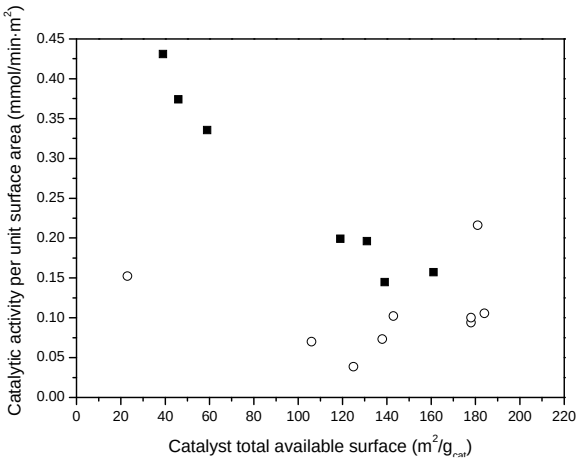

Figure 9. Catalytic activity per unit surface area versus catalysts total available surface: (■) methanol and (○) ethanol series.

Moreover, as can be seen in Figure 10, in the case of the methanol series, a positive effect of the increase of Pd^{n+}/Pd^0 ratio on the catalytic activity per unit surface area can be observed. The values of Pd^{n+}/Pd^0 ratio of the particles with a higher activity per unit surface area were close to the optimum reported in the literature [5, 54, 79, 80]. In the ethanol series, the synthesis method used provided Pd^{n+}/Pd^0 ratios far from that optimum. Thus, Pd nanoparticles with extreme values of Pd^{n+}/Pd^0 ratio within the range studied presented a low activity per unit surface area. Although activity should peak in Figure 10 according to the literature [54], the synthesis method used in this work did not allow obtaining a Pd^{n+}/Pd^0 ratio within the range suitable to verify this relationship.

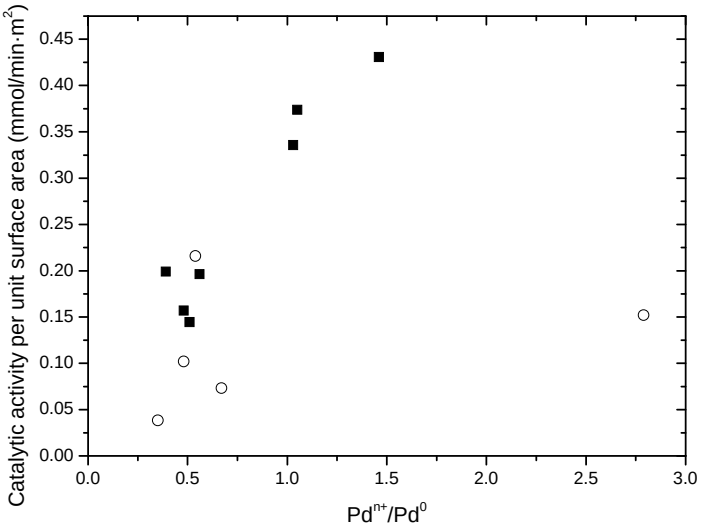

Figure 10. Catalytic activity per unit surface area vs. Pd^{n+}/Pd^0 ratio. (solid squares for methanol series, open circles for ethanol series)

Therefore, the increase of activity per unit surface with increasing nanoparticle diameter in the case of the methanol series may be related to changes in the coordination of Pd atoms and to a lower interaction potential with reactants and products, which reduces adsorption strength.

In the case of ethanol series, the influence of Pd^{n+}/Pd^{0} ratio was not so clearly observed, which can be attributed to the narrower Pd^{n+}/Pd^{0} ratio range provided by the Pd nanoparticles synthesis method based in the reduction with ethanol.

4. Conclusions

Pd nanoparticles have been synthesized and tested as catalysts in HDC of 4-CP at mild conditions (303-323 K, 1 atm.). The load of PVP, the alcohol used as reducing agent and its concentration affect to the particle size. Moreover, it seems that there is also a relationship between that particle size and Pd^{n+}/Pd^{0} ratio, the smaller particles showing Pd^{n+}/Pd^{0} ratios around 0.5. The Pd nanoparticles showed fairly active for 4-CP HDC but further phenol hydrogenation was not observed opposite to the reported for supported Pd catalysts. Decreasing particle size increases catalytic activity which can be mostly attributed to the higher surface area. However, the larger particles showed a more active surface looking at the activity per unit surface area in the case of the methanol series. The higher activity per unit surface area of larger particles may be related to their Pd^{n+}/Pd^{0} ratio and to coordination of Pd atoms and lower strength adsorption of reactants and products onto them. At equal others synthesis conditions, the nanoparticles synthesized using methanol as reducing agent were larger than those prepared with ethanol and at similar particle size, the former showed a higher activity. 4-CP disappearance upon HDC can be well described by a simple pseudo-first order rate equation. Apparent activation energy values within the range of 100-118 $kJ \cdot mol^{-1}$ were obtained for 4-CP disappearance, being significantly higher than the reported for supported Pd catalyst, indicating some important role of the supports on the reaction pathway.

Acknowledgements

We greatly appreciate financial support from the Spanish MCYT (CTQ2009-09983 and CSD2006-44) and CAM (REMTAVARES S-2009/AMB-1588 and CCG10-UAM/AMB-5521). J.A. Baeza thanks to the Spanish MICINN a research grant (BES-2010-030059).

References

[1] G. Yuan, M.A. Keane, Catal. Today 88 (2003) 27.

[2] C. Xia, Y. Liu, S. Zhou, C. Yang, S. Liu, J. Xu, J. Yu, J. Chen, X. Liang, J. Hazard. Mater. 169 (2009) 1029.

[3] G. Yuan, M.A. Keane, Chem. Eng. Sci. 58 (2003) 257.

[4] L. Calvo, M.A. Gilarranz, J.A. Casas, A.F. Mohedano, J.J. Rodríguez, Appl. Catal., B. 67 (2006) 68.

[5] K.V.R. Chary, P.V.R. Rao, V. Vishwanathan, Catal. Commun. 7 (2006) 974.

[6] S. Kovenklioglu, Z. Cao, D. Shah, R. J. Farrauto, E. N. Balko, AIChEm J. 38 (1992) 1003

[7] J.B. Hoke, G. A. Gramiccioni, E.N. Balko, Appl. Catal., B. 1 (1992) 285

[8] R. Muftikian, Q. Fernando, N. Korte, Water Res. 29 (1995) 2434.

[9] G. V. Lowry, M. Reinhard, Environ. Sci. Technol. 33 (1999) 1905.

[10] T.T. Bovkun, Y. Sasson, J. Blum, J. Mol. Catal. A: Chem. 242 (2005) 68.

[11] W. Wu, J. Xu, R. Ohnishi, Appl. Catal., B. 60 (2005) 129.

[12] K. Mackenzie, H. Frenzel, F. D. Kopinke, Appl. Catal. B-Environ. 63 (2006) 161.

[13] L. Calvo, M.A. Gilarranz, J.A. Casas, A.F. Mohedano, J.J. Rodríguez, Appl. Catal., B. 78 (2008) 259.

[14] M. Bonarowska, Z. Kaszkur, L. Kępiński, Z. Karpiński, Appl. Catal., B. 99 (2010) 248.

[15] A.Y. Stakheev, I.S. Mashkovskii, G.N. Baeva, N.S. Telegina, Russ. J. Gen. Chem. 80 (2010) 618.

[16] F. Murena, F. Gioia, Catal. Today 75 (2002) 57.

[17] G. Yuan, M.A. Keane, Catal. Commun. 4 (2003) 195.

[18] L. Calvo, A.F. Mohedano, J.A. Casas, M.A. Gilarranz, J.J. Rodríguez, Carbon 42 (2004) 1377.

[19] B.R. Cuenya, Thin Solid Films 518 (2010) 3127.

[20] J. Jolivet, S. Cassaignon, C. Chanéac, D. Chiche, O. Durupthy, D. Portehault, C. R. Chim. 13 (2010) 40.

[21] J. Park, J. Joo, S.G. Kwon, Y. Jang, T. Hyeon, Angew. Chem. , Int. Ed. 46 (2007) 4630.

[22] M.A. Keane, G. Pina, G. Tavoularis, Appl. Catal., B. 48 (2004) 275.

[23] S. Gómez-Quero, F. Cárdenas-Lizana, M.A. Keane, Chem. Eng. J. 166 (2011) 1044.

[24] E. Díaz, L. Faba, S. Ordóñez, Appl. Catal., B. 104 (2011) 415.

[25] X. Liu, J. Chen, J. Zhang, Ind. Eng. Chem. Res. 47 (2008) 5362.

[26] J.W. Bae, I.G. Kim, J.S. Lee, K.H. Lee, E.J. Jang, Appl. Catal., A 240 (2003) 129.

[27] M.A. Keane, C. Park, C. Menini, Catal. Lett. 88 (2003) 89-94.

[28] S. Ordóñez, E. Díaz, R.F. Bueres, E. Asedegbega-Nieto, H. Sastre, J. Catal. 272 (2010) 158.

[29] T. Janiak, J. Okal, Appl. Catal., B. 92 (2009) 384.

[30] M.A. Aramendía, V. Boráu, I.M. García, C. Jiménez, F. Lafont, A. Marinas, J.M. Marinas, F.J. Urbano, J. Catal. 187 (1999) 392.

[31] E. Diaz, A.F. Mohedano, J.A. Casas, L. Calvo, M.A. Gilarranz, J.J. Rodriguez, Appl. Catal., B. 106 (2011) 469.

[32] Y. Yang, L.D. Unsworth, N. Semagina, J. Catal. 281 (2011) 137.

[33] A. Binder, M. Seipenbusch, M. Muhler, G. Kasper, J. Catal. 268 (2009) 150.

[34] L. Kiwi-Minsker, N. Semagina, A. Renken, B. Corain, G. Schmid and N. Toshima (Eds.), Metal Nanoclusters in Catalysis and Materials Science, Elsevier, Amsterdam, 2008, p. 293.

[35] J.W. Kim, B. Lim, H. Jang, S.J. Hwang, S.J. Yoo, J.S. Ha, E.A. Cho, T. Lim, S.W. Nam, S. Kim, Int J Hydrogen Energy 36 (2011) 706.

[36] R. Narayanan, M.A. El-Sayed, Top. Catal. 47 (2008) 15.

[37] T. Teranishi, M. Miyake, Chem. Mater. 10 (1998) 594.

[38] J. Durand, E. Teuma, M. Gómez, Eur. J. Inorg. Chem 2008 (2008) 3577.

[39] S. Shen, X. Wang, Chem. Commun. 46 (2010) 6891.

[40] C. Luo, Y. Zhang, Y. Wang, J. Mol. Catal. A: Chem. 229 (2005) 7.

[41] A. Gniewek, A.M. Trzeciak, J.J. Ziółkowski, L. Kępiński, J. Wrzyszcz, W. Tylus, J. Catal. 229 (2005) 332.

[42] J. Cha, K. Kim, S. Choi, S. Yeon, H. Lee, C. Lee, J. Shim, Korean J. Chem. Eng. 24 (2007) 1089.

[43] K. Okitsu, H. Bandow, Y. Maeda, Y. Nagata, Chem. Mater. 8 (1996) 315.

[44] P. Yong, N.A. Rowson, J.P.G. Farr, I.R. Harris, L.E. Macaskie, Biotechnol. Bioeng. 80 (2002) 369.

[45] S. Domínguez-Domínguez, Á. Berenguer-Murcia, D. Cazorla-Amorós, Á. Linares-Solano, J. Catal. 243 (2006) 74.

[46] R. Narayanan, M.A. El-Sayed, J. Catal. 234 (2005) 348.

[47] A. Gniewek, J.J. Ziółkowski, A.M. Trzeciak, L. Kępiński, J. Catal. 239 (2006) 272.

[48] S.H. Joo, J.Y. Park, J.R. Renzas, D.R. Butcher, W. Huang, G.A. Somorjai, Nano Lett. 10 (2010) 2709.

[49] N. Krishnankutty, M.A. Vannice, J. Catal. 155 (1995) 312.

[50] M.A. Álvarez-Montero, L.M. Gómez-Sainero, M. Martín-Martínez, F. Heras, J.J. Rodriguez, Appl. Catal. B 96 (2010) 148.

[51] http://srdata.nist.gov/xps/

[52] M. Králik, A. Biffis, J. Mol. Catal. A: Chem.177 (2001) 113.

[53] T. Ashida, K. Miura, T. Nomoto, S. Yagi, H. Sumida, G. Kutluk, K. Soda, H. Namatame, M. Taniguchi, Surf. Sci. 601 (2007) 3898.

[54] L. Gomez-Sainero, X. Seoane, J. Fierro, A. Arcoya, J. Catal. 209 (2002) 279.

[55] F. Chen, Z. Zong, X. Xu, J. Luo, J. Mat. Sci. Lett. 40 (2005) 1517.

[56] H. Hirai, N. Yakura, Polym. Adv. Technol. 12 (2001) 724

[57] E. Diaz, A.F. Mohedano, J.A. Casas, L. Calvo, M.A. Gilarranz, J.J. Rodriguez, Appl. Catal., B 106 (2011) 469.

[58] M. Nutt, J. Hughes, M. Wong, Environ. Sci. Technol. 39 (2005) 1346.

[59] J. Xu, D. Bhattacharyya, Ind. Eng. Chem. Res. 46 (2007) 2348.

[60] Z. Jin, C. Yu, X. Wang, Y. Wan, D. Li, G. Lu, J. Hazard. Mater. 186 (2011) 1726.

[61] J. Le Bars, U. Specht, J.S. Bradley, D.G. Blackmond, Langmuir 15 (1999) 7621.

[62] Y. Li, E. Boone, M. El-Sayed, Langmuir 18 (2002) 4921.

[63] Z. Karpinski, K. Early, J.L. d'Itri, J. Catal. 164 (1996) 378.

[64] C. Thompson, R. Rioux, N. Chen, F. Ribeiro, J. Phys. Chem. B 104 (2000) 3067.

[65] A. Orlov, D.J. Watson, F.J. Williams, M. Tikhov, R.M. Lambert, Langmuir 23 (2007) 9551.

[66] J.L. Solomon, R.J. Madix, J. Stöhr, Surf. Sci. 255 (1991) 12.

[67] M.A. Keane, ChemCatChem 3 (2011) 800.

[68] E. Diaz, J.A. Casas, A.F. Mohedano, L. Calvo, M.A. Gilarranz, J.J. Rodriguez, Ind. Eng. Chem. Res. 47 (2008) 3840.

[69] H.M. Roy, C.M. Wai, T. Yuan, J. Kim, W.D. Marshall, Appl. Catal., A 271 (2004) 137.

[70] A.L. Dantas Ramos, P.d.S. Alves, D.A.G. Aranda, M. Schmal, Appl. Catal., A 277 (2004) 71.

[71] G. Yuan, M.A. Keane, Catal. Commun. 4 (2003) 195.

[72] E. Diaz, J.A. Casas, A.F. Mohedano, L. Calvo, M.A. Gilarranz, J.J. Rodriguez, Ind. Eng. Chem. Res. 48 (2009) 3351.

[73] Y. Shindler, Y. Matatov-Meytal, M. Sheintuch, Ind. Eng. Chem. Res. 40 (2001) 3301.

[74] G. M. Schwab, Adv. Catal. 27 (1978) 1

[75] M.A. Aramendía, V. Boráu, I.M. García, C. Jiménez, J.M. Marinas, F.J. Urbano, Appl. Catal. B 20 (1999) 101.

[76] C.E. Gigola, H.R. Aduriz, P. Bodnariuk, Appl. Catal. 27 (1986) 133.

[77] J. Estelle, J. Ruz, Y. Cesteros, R. Fernandez, P. Salagre, F. Medina, J. Sueiras, J. Chem. Soc. , Faraday Trans. 92 (1996) 2811.

[78] R.M. Rioux, C.D. Thompson, N. Chen, F.H. Ribeiro, Catal. Today 62 (2000) 269.

[79] F. Alonso, I.P. Beletskaya, M. Yus, ChemInform 34 (2003) no.

[80] J.W. Bae, E.J. Jang, D.H. Jo, J.S. Lee, K.H. Lee, J. Mol. Catal. A: Chem. 206 (2003) 225.

Nomenclature

a	Catalytic activity (mmol/g_{cat}·min)
C_{4-cp}	4-CP molar concentration (mmol/L)
d_s	Surface-area-weighted average mean diameter (m)
k	Rate constant (min^{-1})
m_{Pd}	Pd nanoparticles mass (g)
$-r_{4-cp}$	4-CP conversion rate (mmol/L·min)
S_a	Specific surface area (m^2/g)
t	Time (min)
ρ_{Pd}	Pd density (g/m^3)

CAPÍTULO II /CHAPTER II

Effect of size and oxidation state of size-controlled rhodium nanoparticles on the aqueous-phase hydrodechlorination of 4-chlorophenol

J.A. Baeza, L. Calvo, M.A. Gilarranz, J.J. Rodriguez. Chem Eng. J. 240 (2014) 271–280.

Abstract

Unsupported size-controlled Rh nanoparticles of different size and oxidation state were tested as catalysts models in aqueous phase hydrodechlorination (303-318 K, 1 atm) using 4-chlorophenol (4-CP) as target compound. A chemical reduction method was employed for the synthesis of the nanoparticles using methanol and poly(N-vinyl-2-pyrrolidone) (PVP) as reducing and capping agent, respectively. The size of Rh nanoparticles was in a narrow range (1.9 – 4.9 nm) whereas Rh^{n+}/Rh^{0} ratio values were found within a wide range (0.56 – 3.89).

High 4-CP conversion values (c.a. 100 %) were achieved at low Rh concentration ($2.45 \cdot 10^{-3}$ g·L^{-1}). Phenol, cyclohexanone, cyclohexanol and traces of cyclohexane were identified as reaction products. A wide range of activity values (1.7 – 29.4 mmol·g^{-1}·min^{-1}) were obtained, being equivalent to the measured in a previous work with unsupported Pd nanoparticles, in spite of the fact that Rh supported catalysts have generally been reported as less active than Pd ones in liquid phase hydrodechlorination. As the size of Rh nanoparticles decreased the activity increased reaching a maximum at 2.8 nm, lower size values leading to a significant decrease of activity. A remarkable dependence of activity on the Rh^{n+}/Rh^{0} ratio was found, thus a higher activity corresponded to a higher relative amount of zero-valent Rh in the nanoparticles samples. Regression models were developed in order to address the significance of nanoparticles size and oxidation state for the prediction of selectivity to cyclohexanone and cyclohexanol at varying reaction times. A crossed effect of particle size and Rh^{n+}/Rh^{0} ratio was identified as a significant factor influencing the selectivity.

Keywords: Rh nanoparticles, oxidation state, particle size, hydrodechlorination, 4-chlorophenol

1. Introduction

Liquid phase catalytic hydrodechlorination (HDC) is considered as a feasible alternative to treat wastewater bearing chlorophenolic compounds [1,2]. This type of xenobiotic compounds are toxic and carcinogenic [3,4] and have no natural ways of remediation, so chlorophenols persist in the environment and can produce both adverse ecological effects and severe impacts on public health [5]. The main advantages of HDC compared to other techniques of potential application have been reported in the literature [6-8] and can be summarized in the ability to treat a wide range of concentrations, the operation at mild conditions and the low reagents demand. Moreover, HDC shows a high selectivity towards less toxic by-products that could be recoverable, when waste valorization is possible, or safely delivered to a further biological treatment.

In spite of its high cost, Rh has been used in catalysis, it has been used for decades due to its exceptional features useful in a diversity of chemical reactions. Particularly, Rh has shown high catalytic action on carbonylation, hydroformylation, oxidation, reduction and HDC reactions [9-11]. Rh has also a higher melting point than other active metals used in catalysis and exhibits high resistance to acid and base attack, so Rh-based catalysts can be singularly stable, even under severe reaction conditions [9]. An adequate study of the factors affecting the catalytic performancesof the active phase, i.e. particle size, shape, oxidation state, interaction with the support

[12,13], is needed to acquire an in-depth knowledge on each individual contribution and the possible interrelations between factors in structure-sensitive reactions.

Singularly, the particle size of the metallic phase is a key variable regarding the performance of the catalysts in structure-sensitive reactions. A number of authors have reported that HDC is a structure-sensitive reaction [14-16], but there is no general agreement on this point [17]. In general, it is accepted that a higher surface-to-volume ratio, associated to a lower nanoparticle size of the active phase, increases the catalytic activity, although some limit has been reported for this effect [16,18]. Furthermore, variations in size could change the adsorption energies and provoke quite different effects, from the poisoning of the catalyst to the activation of the substrate, according to the nature of the molecule-particle surface adsorption [19]. The oxidation state of metal nanoparticles has also been claimed as an important factor influencing catalytic activity in structure-sensitive reactions and some authors have linked it to particle size [13], but there is no conclusive agreement on whether there is a direct or inverse relationship between size and the relative amount of electrodeficient species [13,20], and therefore, further research is needed.

In spite of the influence of metal particle size on the activity, the catalysts commonly used in structure-sensitive reactions are not prepared with an accurate control of that feature. In the last few years, the methods of synthesis that allow obtaining nanoparticles in a narrow range of size have attracted much attention enabling the investigation on chemical and physical size-dependent properties. Thus, the studies on the preparation and application in nano-sized catalysts have increased significantly [21]. Different methods of synthesis addressed to obtain size-controlled

nanoparticles have been reported [22-24]. Among them, chemical reduction has been frequently used due to its simple mechanism consisting on the reduction of a metal salt with a reducing agent (e. g. alcohols, potassium borohydride), using a capping agent (e. g. poly(N-vinyl-2-pyrrolidone), polivinyl alcohol, dodecylamine) in order to prevent undesired particle growth and aggregation. A number of authors have prepared colloidal Rh nanoparticles of controlled size using a chemical reduction method to test their behavior as catalysts in different reactions [9,25-27]. However, the dependence of activity on the particle size is so far not clear in HDC, where Rh-based catalysts have shown highly active [11,28].

Therefore, the objective of the current work is to address the effect of both initial size and oxidation state of unsupported Rh nanoparticles, used as catalysts models, on the activity and selectivity in 4-CP HDC in aqueous phase in order to gain an in-depth knowledge that could be useful for catalysts design. On the other hand, a direct comparison between the Rh nanoparticles synthesized in this work and those of Pd reported in our previous one [20] can provide a better understanding of the different behavior of both metals.

2. Experimental

2.1 Materials

Rh(III) chloride (98 %, Sigma Aldrich Co.) was used as precursor salt to synthesize Rh nanoparticles. Methanol (99.5 %, Panreac Quimica S.A.U.) was used as reducing agent and poly(N-vinyl-2-pyrrolidone) (PVP, average molecular weight: 40.000, Sigma-Aldrich Co.) was used as capping agent. Hydrogen (> 99 %, Praxair Spain, S.L.) was used to carry out catalytic HDC and for reducing Rh nanoparticles (sample 1

to sample 1R). $NaHCO_3$ (99.7 %, Merck, GmbH) and Na_2CO_3 (99.8 %, Panreac Quimica, S.A.U) were used to prepare a carbonate-bicarbonate buffer for the HDC runs at basic pH (10.4). All the reagents were used as received without previous purification.

2.2 Synthesis and characterization of Rh nanoparticles

A $2 \cdot 10^{-3}$ M Rh aqueous solution (pale pink colour) was obtained by mixing $RhCl_3$ (0.5 mmol), HCl (1 mmol) and distilled water up to a final volume of 250 mL. An aliquot of 30 mL of the acidic $2 \cdot 10^{-3}$ M Rh solution and 70 mL of methanol/water solution and PVP were mixed to obtain the colloidal synthesis of Rh nanoparticles. The mixture was refluxed in a flask connected to a Liebig condenser for 5 hours at 363 K under atmospheric pressure. In the case of the samples of nanoparticles prepared with the lowest concentration of methanol (10 %, v/v), it was necessary to increase the temperature from 363 to 368 K in order to achieve complete reduction of Rh. The colloidal suspension of nanoparticles (100 mL) was concentrated up to a final volume of approximately 10 mL in a rotary evaporator (Büchi). The synthesis of sample 1R was performed by reducing sample 1 under hydrogen flow (50 N mL·min^{-1}) at 363 K during 30 minutes. Different values of PVP/Rh ratio (5 - 35 mol/mol) and methanol concentration (10 - 40 %, v/v) were used in the synthesis with the aim of obtaining Rh nanoparticles samples of different sizes and Rh^{n+}/Rh^0 ratios. Table 1 summarizes the working conditions used for the synthesis of nanoparticles and the corresponding nomenclature.

Table 1. Mean particle size (d_s), size distribution (σ_s), Rh^{n+}/Rh^0 ratio and activity (a) of the Rh nanoparticles synthesized under different conditions.

Rh nanoparticles samples	Synthesis Temperature (K)	Vol Methanol (%)	PVP/Rh (mol/mol)	d_s (nm)	σ_s (nm)	Rh^{n+}/Rh^0 molar ratio	a (mmol/g_{cat}·min)
1	368	10	5	1.9	0.6	3.89	1.7
1R	363[1]	10	5	2.3	0.6	0.74	20.2
2	368	10	20	4.9	2.6	1.72	4.7
3	368	10	35	3.9	0.7	1.02	11.7
4	363	25	5	3.2	0.8	1.14	10.6
5	363	25	20	2.8	0.6	0.56	29.4
6	363	25	35	2.9	0.5	0.60	22.4
7	363	40	5	3.0	0.7	0.72	16.0
8	363	40	20	2.3	0.7	0.67	24.3
9	363	40	35	2.9	0.7	0.65	19.7

1R: obtained from reduction of sample 1 under hydrogen flow at 363 K

The size of Rh nanoparticles was measured by transmission electron microscopy (TEM) and X-ray photoelectron spectroscopy (XPS) was used to determine the Rh^{n+}/Rh^0 ratio. TEM micrographs were obtained in a JEM-3000F + XEDS microscope at 300 kV (JEOL). ImageJ 1.44i software was used for data treatment of digital TEM images (more than 200 particles were measured per sample). Surface-area-weighted mean diameters and size distribution, characterized by the standard deviation, were calculated as described in a previous work [20].

XPS profiles were obtained in an ESCA 5701 spectrometer equipped with a Mg-Kα X-ray excitation source (1253.6 eV) (Physical Electronics). A probing depth of at least several nanometres can be assumed. Thus, the Rh^{n+}/Rh^0 ratios obtained were ascribed to the whole particles and not only to their surface. Spectra deconvolutions were performed using Multipak v8.2b software in order to determine both electrodeficient and zero-valent species of the Rh nanoparticles synthesized. Shirley background subtraction, smoothing and mixed Gaussian-Lorentzian by a least-square method curve fitting were applied [20]. C 1s peak (284.8 eV) was used as internal standard for binding energies corrections due to sample charging. Doublet separation for Rh 3d was 4.74 eV as described elsewhere [29]. Binding energies for Rh $3d_{5/2}$ of deconvoluted peaks were in the range of 306.3 - 306.9 eV and 308.1 – 308.8 eV which can be ascribed to metallic or zero-valent (Rh^0) and electrodeficient (Rh^{n+}) Rh species, respectively. Those values are in good agreement with those reported in NIST X-ray Photoelectron Spectroscopy Database [29].

2.3 HDC experiments

HDC rus were performed in a three-necked jacketed glass reactor equipped with a H_2 supply. 150 mL of 4-CP aqueous solution (100 $mg \cdot L^{-1}$) were placed in the reactor and H_2 was continuously passed at 50 $NmL \cdot min^{-1}$. The reaction was maintained for 4 hours under vigorous stirring (800 rpm) and the temperature (303-318 K) was controlled by a thermostatic bath (Julabo). A cold trap at the vent was used to check any possible stripping, but no significant stripping was detected. The catalyst concentration in the reaction medium was $2.45 \cdot 10^{-3}$ $g \cdot L^{-1}$ of Rh.

Reaction samples (1 mL) were filtered (PTFE filter, pore size 0.45 μm) and analyzed by HPLC (Varian Prostar equipped with a UV-VIS detector) using a C_{18} column as stationary phase and a mixture of acetonitrile and water (1:1, v/v) as mobile phase. No reaction progress was observed once the samples were filtered and collected.

Cyclohexanone and cyclohexanol were analyzed by Gas Chromatography with FID detector (GC 3900 Varian) using a 30 m length and 0.25 mm internal diameter capillary column (CP-Wax 52 CB, Varian) and nitrogen as carrier gas. Cyclohexene was analyzed by Gas Chromatography with MS detector and an electron impact ionization source (Saturn 2100T). This chromatograph was equipped with a column Factor Four, Varian (30 m length, 0.25 mm internal diameter). In order to check the structural assignment of the identified compounds, the NIST 05 library and analytical standards were used. The quantification of chloride ion was performed by Ion Chromatography (Metrohm 790 Personal IC). The carbon and chlorine balances matched always above 90 and 95 %, respectively.

3. Results and discussion

3.1 Rh nanoparticles characterization

3.1.1 TEM characterization

Mean diameter and size distribution of Rh nanoparticles samples prepared using different PVP/Rh ratios and methanol concentrations are shown in Table 1. Though Pd and Rh are strongly electropositive metals ($E_0 \geq 0.7$ V) [30], the Rh^{3+}/Rh^0 redox couple ($E_0 = 0.76$ V) is lower than the Pd^{2+}/Pd^0 one ($E_0 = 0.95$ V), so it was necessary to use higher temperature and time of synthesis for Rh than for Pd [20]. As representative examples, TEM images and size distribution histograms of three selected samples are depicted in Figure 1. Rh nanoparticles showed mostly pseudo-spherical shapes. Moreover, the size of Rh nanoparticles samples synthesized was in a narrow range within 1.9 to 4.9 nm, although different size distributions were obtained. Sample 1 showed a narrower size distribution displaced towards lower values. Reduction of sample 1 with hydrogen (sample 1R) led to some widening of the size distribution, probably due to a moderate sintering. A much wider distribution can be observed for sample 5 showing the important influence of the synthesis conditions on nanoparticles size.

No significant changes in size were observed by varying the PVP/Rh ratio in the syntheses performed at 363 K with methanol concentrations of 25 % (d_s = 2.8 – 3.2 nm) and 40 % (d_s = 2.3 - 3.0 nm). On the contrary, the samples of nanoparticles synthesized at 368 K using a 10 % methanol concentration showed a wider range of size (1.9 – 4.9 nm). In principle, this effect cannot be ascribed solely to methanol concentration since the working temperature has been reported to affect to particle

size [31]. In a previous work [20] where Pd nanoparticles were synthesized in equivalent conditions, a wider range of particle size (3.1 – 12.9 nm) was obtained and different sizes were achieved by varying the methanol concentration and the PVP/Rh ratio.

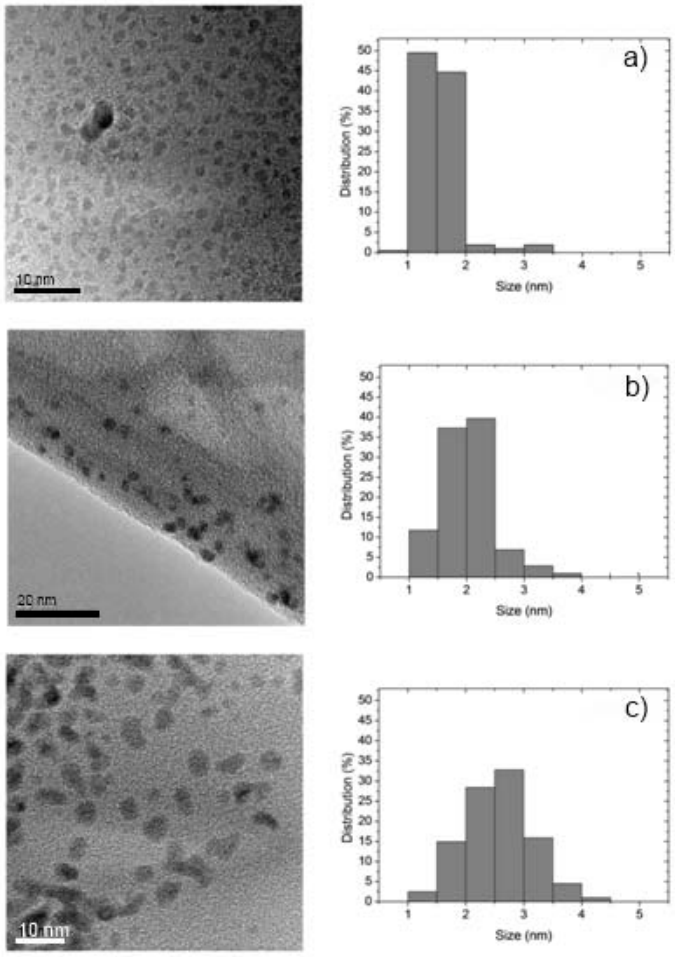

Figure 1. TEM images and size distribution histograms of three selected Rh nanoparticles samples: a) sample 1, b) sample 1R and c) sample 5.

3.2. XPS characterization

For the sake of determining the oxidation state of Rh nanoparticles samples, XPS spectra were obtained. Table 1 shows the values obtained for the Rh^{n+}/Rh^0 ratio from the deconvolution of the XPS Rh 3d region spectra. As can be observed, both Rh^{n+} and Rh^0 species are present in all the Rh nanoparticles samples synthesized. As representative examples, in Figure 2 can be seen the deconvoluted Rh 3d profiles for two selected Rh nanoparticles samples with extreme values of the Rh^{n+}/Rh^0 ratio (3.89 and 0.56 for samples 1 and 5, respectively). Sample 1 consists mainly of electrodeficient Rh whereas the zero-valent species is dominant in sample 5.

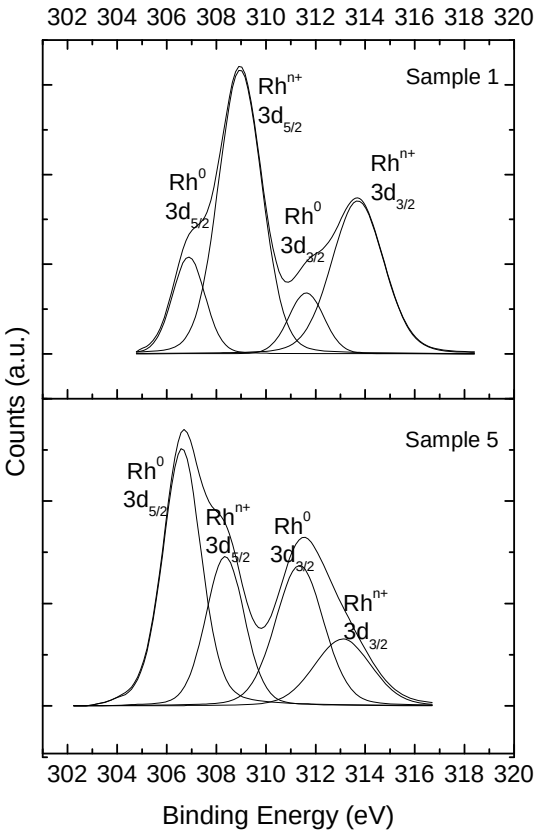

Figure 2. Deconvolved XPS spectra of Rh nanoparticles of samples 1 and 5.

In Figure 3, the Rh^{n+}/Rh^0 ratio is represented versus the mean nanoparticle size. It can be observed that there is a relationship between both variables and the Rh^{n+}/Rh^0 ratio acquired minimum values within the size range of around 2.3 to 3 nm. Although there is no general agreement on this issue, these results are consistent with the conclusions of some previous works in literature related to Pd where a higher relative amount of zero-valent metal was associated to a lower size of the Pd nanoparticles [20,32]. This fact may be due to the higher surface-to-volume ratio of smaller particles, which allows a higher surface availability of reducing agent per unit mass of nanoparticles. However, an exception can be observed in the case of the nanoparticles of lowest mean size (sample 1; d_s = 1.9 nm), where the Rh^{n+}/Rh^0 ratio showed the highest value. It has been reported that metal nanoparticles below 2.0-2.5 nm have no band structure characteristic of bulk metals and are electrodeficient [19].

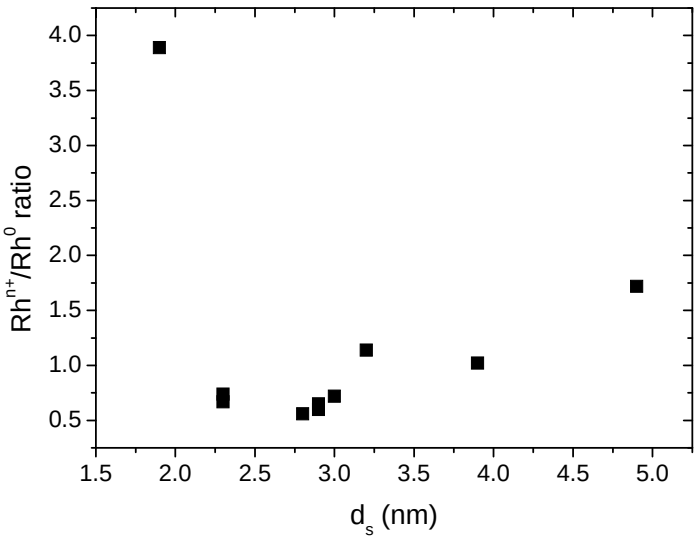

Figure 3. Rh^{n+}/Rh^0 ratio versus nanoparticles mean size.

3.3 HDC experiments

The synthesis conditions described above allowed obtaining Rh nanoparticles within a narrow range of sizes and a wide range of Rh^{n+}/Rh^0 ratios. Control experiments of 4-CP HDC were carried out at different PVP concentrations in the reaction medium in order to check the possible reaction between 4-CP, H_2 and PVP. Likewise, HDC experiments were carried out in the absence of nanoparticles (catalyst). No reaction was detected in any of the control runs and thus synergistic or inhibitory effects of PVP can be discarded. This fact is in good agreement with previous works in the literature where it has been reported that the presence of PVP in the reaction medium does not affect significantly to the catalytic activity of Pd nanoparticles [13,33]. On the other hand, different concentrations of catalyst and stirring rates were checked in the experiments of 4-CP HDC in order to address that the process takes place under chemical control. HDC rates per unit mass of catalyst showed no significant differences within the range of working conditions tested.

3.3.1 Activity of Rh nanoparticles

The evolution of 4-CP conversion upon reaction time with different Rh nanoparticles samples is represented in Figure 4. With the exception of samples 1 and 2 all the catalysts yielded high conversion values in relatively short reaction times. In most cases complete 4-CP conversion required no more than 1 hour. Samples 1 and 2 which provided by far the poorest results showed extreme values of size (1.9 and 4.9 nm, respectively) and the highest values of the Rh^{n+}/Rh^0 ratio (3.89 and 1.72, respectively). Some works on the influence of the oxidation state of Rh-based catalysts on activity can be found in the literature dealing mainly with oxidation reactions,

where electrodeficient Rh seems to play a determining role in enhancing the activity [26,27,34]. The role of Rh species has been analyzed also in NO_2 decomposition [35,36] and catalytic ignition of CH_4 [37]. This issue has been scarcely analyzed in hydrogenation reactions probably due to the the general assumption that zero-valent metal species is the only active in that case. Nevertheless, some authors have reported the active role of Rh^{n+} species in Rh-based catalysts used in the hydrogenation of olefinic and aromatic hydrocarbons [38-42].To the best of our knowledge, there are no studies on the influence of the oxidation state of Rh–based catalysts on their activity in liquid phase HDC. With cabon-supported Pd catalysts it has been reported in the literature [43] that both Pd^0 and Pd^{n+} are required for the catalytic HDC and a maximum activity was found at $Pd^{n+}/Pd^0 \approx 1$. In a previous work on HDC of 4-CP with Pd nanoparticles [20] we found that the activity lowered as the Pd^{n+}/Pd^0 decreased within the 1.5-0.3 range.

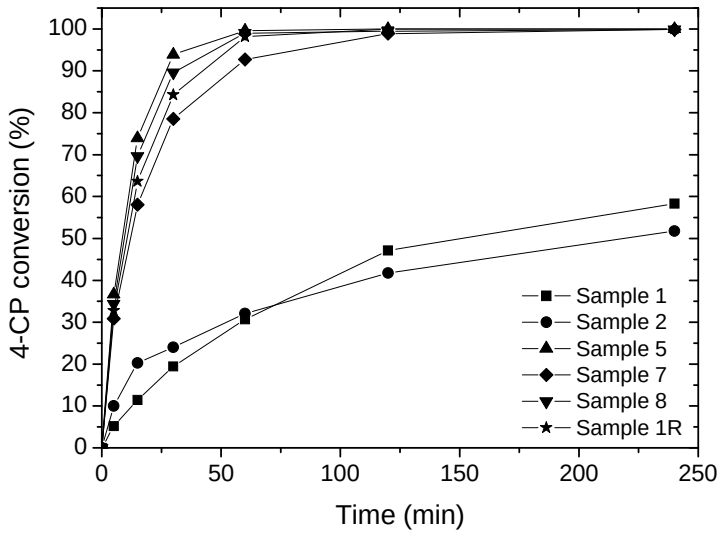

Figure 4. HDC of 4-CP with different Rh nanoparticles samples.

A kinetic analysis was performed in order to calculate the activity of Rh NPs. A simple pseudo-first order kinetic equation has been used to describe the rate of 4-CP disappearance. Since hydrogen is used in excess, its concentration was included into the pseudo-first-order rate constant (k_1):

$$(-r_{4-cp}) = \frac{-dC_{4-cp}}{dt} = k_1 \times C_{4-cp} \qquad [1]$$

$$t = 0; \quad C_{4-cp} = C_0$$

This simple equation served well in all cases to describe the experimental concentration versus time values. From the fitting the values of k1 were obtained and the activity (a) of the Rh nanoparticles was calculated by:

$$a = k_1 \times \frac{C_{0\,4-CP}}{C_{Rh}} \qquad [2]$$

The activity values for each Rh nanoparticles sample are collected in Table 1. As can be observed, those values fall within a wide a range (1.7 to 29.4 mmol·g^{-1}·min^{-1}). They compare closely compare with the obtained in our previous work on 4-CP HDC with Pd nanoparticles [20]. This is an important conclusion since in the case of supported catalysts Pd has been reported in general as more active than Rh in HDC [11,28,44,45] although in some cases equivalent activities have also been found [16].

Figure 5 depicts the values of activity versus mean size of the Rh nanoparticles. The highest values of activity corresponded to nanoparticles samples with sizes within the range of 2.3 to 3.0 nm, being the maximum around 2.8 nm. That range also corresponds with the lowest Rh^{n+}/Rh^0 ratios (0.56 – 0.72). Out of this range, the activity values decreased significantly. Thus, the activity increased as size decreased,

reaching a maximum at 2.8 nm. From this datum, the activity decreased. This can be explained for the higher presence of corner/edges in the nanoparticles of lower size, which can act as catalytic active sites. Moreover, as the particle size decreases, there is a lower number of particles surrounding each surface metal atom and that affects to the nature and strength of the interaction between the Rh particles surface and the 4-CP molecules [19]. Thus, changes in size are associated to changes in coordination affecting to adsorption energy. Below a certain size (less than 2.8 nm in the current work) the increase of adsorption energy can favor poisoning of the catalyst.

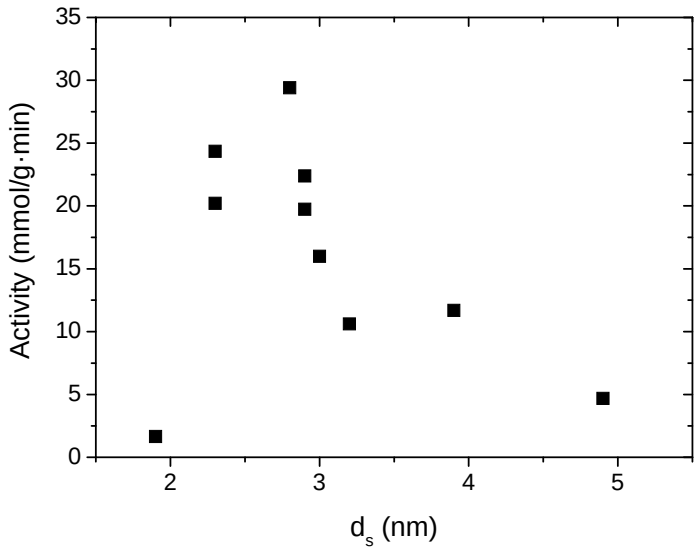

Figure 5. Activity versus mean size of the Rh nanoparticles.

Figure 6 shows an important dependence of activity on the Rh^{n+}/Rh^0 ratio. The activity becomes higher as the Rh^{n+}/Rh^0 ratio decreases, increasing dramatically for Rh^{n+}/Rh^0 ratios below c.a. 0.75; thus indicating the relevant role of Rh zero-valent species in the range studied (0.56 - 3.89). To the best our knowledge, no studies on the effect of Rh-based catalysts oxidation state on activity in aqueous phase HDC have been reported in the literature. This trend is quite different from that obtained in our

previous work [20] when Pd NPs were used as catalysts in 4-CP HDC where an optimum of Pd^{n+}/Pd^{0} ratio close to 1 was found in a range from 0.39 to 2.79. Thus, the presence of Rh electrodeficient species seems to be less relevant than in the case of Pd NPs in 4-CP HDC. Nevertheless, due to the limitations of the chemical reduction method to reach the Rh^{n+}/Rh^{0} ratios below 0.56, the possible synergistic effect between Rh electrodeficient and zerovalent species could not be addressed.

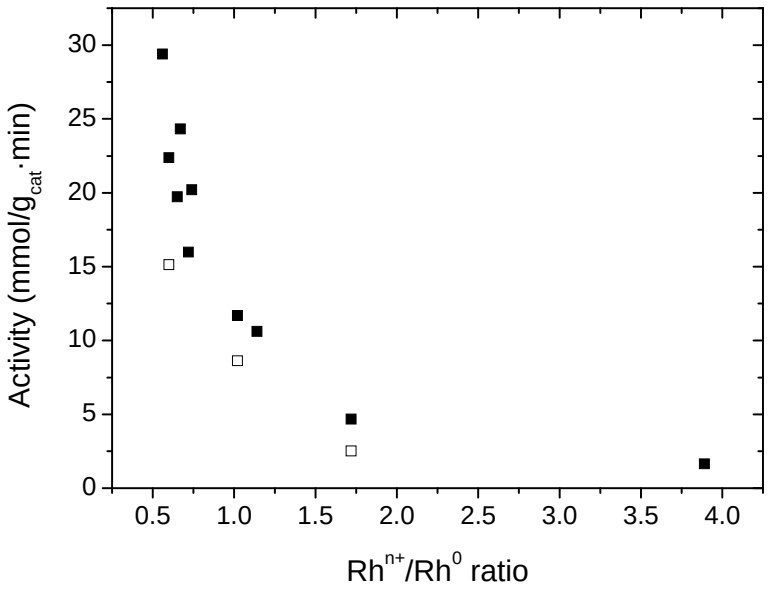

Figure 6. Activity versus Rh^{n+}/Rh^{0} ratio (solid squares: runs at uncontrolled pH; open squares: runs at pH = 10.4).

3.3.2 Selectivity of Rh nanoparticles

Differences in selectivity were found between the Rh nanoparticles samples. Figure 7 shows, as representative examples, the molar concentrations of 4-CP and the reaction products, phenol, cyclohexanone and cyclohexanol, versus time from the HDC experiments performed with two selected nanoparticles samples (samples 1 and 5). Cyclohexene was also identified but in very low concentrations (less than 2 $mg \cdot L^{-1}$) when detected and was not considered for the selectivity study. The occurrence of

cyclohexene can be ascribed to the dehydration of cyclohexanol by the HCl generated upon HDC [46]. In the experiments with sample 1 of nanoparticles, phenol appears as 4-CP is converted. Cyclohexanone was first detected at 15 minutes of reaction and cyclohexanol only at the end of the reaction, being phenol the main by-product along the 4 h of the experiment. In the case of sample 5, HDC of 4-CP and hydrogenation of phenol were significantly faster and both compounds were almost converted at 60 and 120 minutes, respectively. Cyclohexanone was detected at the same time than phenol (around 5 minutes) and cyclohexanol appeared beyond 15 minutes. Once all the phenol was practically converted, cyclohexanone concentration started decreasing whereas cyclohexanol continuously increased along the reaction.

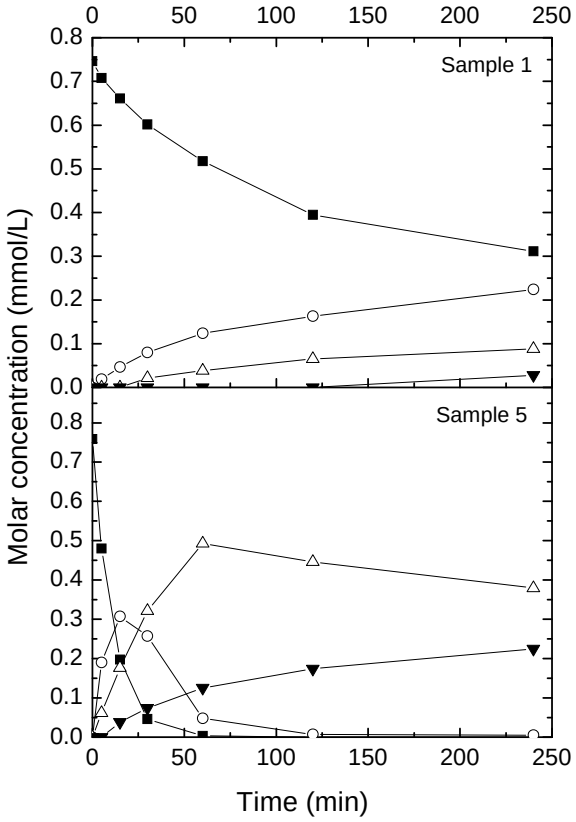

Figure 7. Molar concentrations of (■) 4-CP, (○) phenol, (Δ) cyclohexanone and (▼) cyclohexanol versus reaction time for HDC experiments with samples 1 and 5 of Rh nanoparticles.

On the basis of these results, the reaction scheme of Figure 8 is proposed, where 4-CP HDC is converted to phenol in a first step. This can be clearly observed with those Rh samples of low activity (i.e. sample 1) better than with the ones showing high activity (sample 5, for example), where phenol and cyclohexanone simultaneously appeared at 5 min of reaction time due to the faster hydrogenation of phenol. Cyclohexanone and cyclohexanol result from hydrogenation of phenol while cyclohexanol is also produced from cyclohexanone hydrogenation. This reaction scheme is in good agreement with that proposed by Fujita et al. [47] for the hydrogenation of phenol using supported Rh catalysts. Other useful reaction scheme has been proposed by Diaz et al. [11] for the HDC of 4-CP using alumina-supported Pd, Pt and Rh catalysts. This last work proposed the direct hydrogenation of 4-CP to phenol and cyclohexanone and the hydrogenation of phenol as the only path to cyclohexanol.

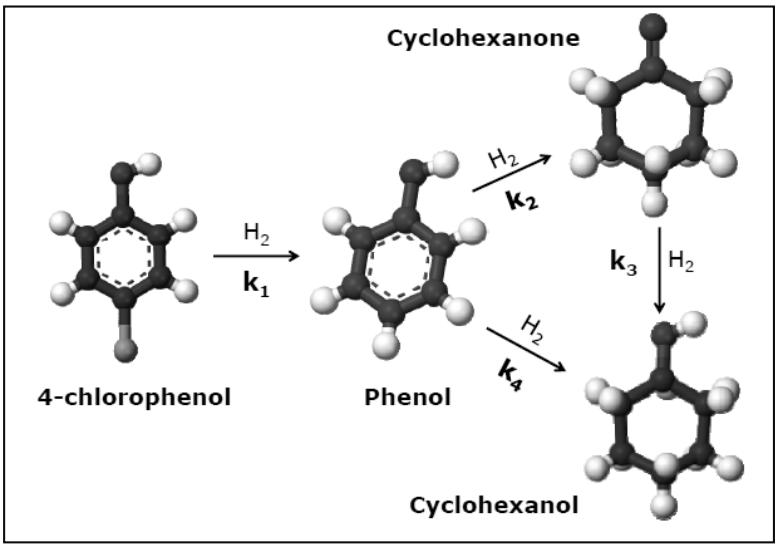

Figure 8. Reaction scheme proposed for liquid phase 4-CP HDC using Rh nanoparticles.

The influence of the nanoparticles characteristics on the selectivity towards reaction products was not as evident as the previously discussed for activity (Figures 3-6). With the objective of reaching a better understanding on the the differences in selectivity, second order regression models were developed in order to learn on the influence of nanoparticle size and Rh oxidation state, as well as the possible occurrence of some crossed effect between both variables. The response function was given by:

$$S_{i,t} = C + b \cdot D + d \cdot Ra + e \cdot D^2 + f \cdot Ra^2 + g \cdot D \cdot Ra \qquad [3]$$

where $S_{i,t}$ is the selectivity to product *i* at a *t* reaction time, *C* is a constant and *D* and *R*a are the coded variables for nanoparticle size and Rh^{n+}/Rh^0 ratio, respectively. IBM SPSS Statistics v19 software was used to perform regression, removing non significant terms for further model regression. A level of significance to entry equal or less than 0.05 and a level of significance to remove equal or more than 0.10 were the criteria used to include or exclude a given term into the model. Table 2 summarizes the ANOVA results and the coefficients for the final regression equations. In all cases, the significant effect influencing the selectivity was given by the product of the size and Rh^{n+}/Rh^0 ratio, indicating the strong interaction between these two variables. An inverse relationship between the values of that product and those of selectivity towards cyclohexanone and cyclohexanol was found. Thus, the selectivity was higher for the runs were the combination of nanoparticle size and Rh^{n+}/Rh^0 ratio was lower. Moreover, as the reaction time increased, the absolute values of the coefficients of the model increased as well, so the crossed-influence of size and Rh oxidation state on selectivity becomes more pronounced as reaction proceeds.

Table 2. ANOVA and parameters values of the regression equations developed for selectivity.

Model	Dependent variable	Independent variable	C	g value	R^2	F -value	p-value
1	$S_{c\text{-}one,15}$	D·Ra	43.49	-5.14	0.82	36.89	< 0.05
2	$S_{c\text{-}one,60}$	D·Ra	72.58	-5.95	0.65	14.81	< 0.05
3	$S_{c\text{-}one,240}$	D·Ra	85.17	-7.06	0.78	28.17	< 0.05
4	$S_{c\text{-}ol,15}$	D·Ra	9.74	-1.15	0.86	50.83	< 0.05
5	$S_{c\text{-}ol,60}$	D·Ra	21.55	-2.70	0.92	86.13	< 0.05
6	$S_{c\text{-}ol,240}$	D·Ra	38.19	-4.29	0.93	101.04	< 0.05

Figure 9 shows the experimental selectivities towards phenol, cyclohexanone and cyclohexanol versus 4-CP conversion. At low conversion values of 4-CP, both disappearance of 4-CP and the hydrogenation of phenol prevail with respect to cyclohexanone formation. Some competition for the active sites between 4-CP and phenol can be inferred from the sharp increase in cyclohexanone production once all 4-CP has been converted. In the same way, the less favored reaction step seems to be hydrogenation of cyclohexanone to cyclohexanol as a result of the competence for active sites, since the conversion of cyclohexanol increased substantially once both 4-CP and phenol were completely converted. These trends in selectivity seem to be independent on the nanoparticles size and structure, as can be seen from the alignment of data from the experiments performed with different nanoparticles samples. Two different behaviours were found for Rh^{n+}/Rh^{0} ratios values higher and lower than 1.7. The two samples with the highest Rh^{n+}/Rh^{0} ratios (samples 1 and 2) showed the highest selectivity towards phenol and the lowest selectivity towards cyclohexanol, even negligible in one of the cases. Though the samples with the Rh^{n+}/Rh^{0} ratio in the range between 0.56 - 1.14 showed a more homogeneous behaviour, some differences were found.

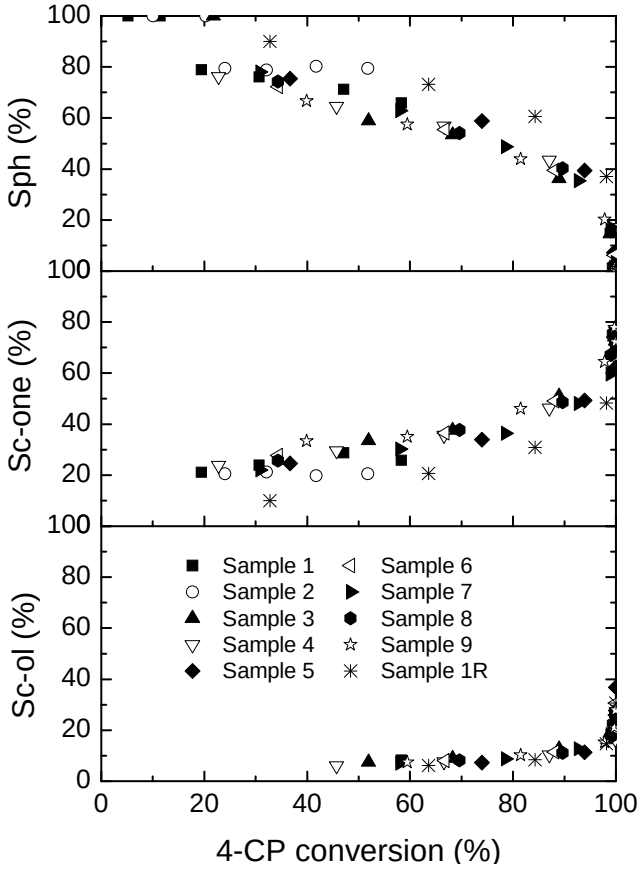

Figure 9. Selectivity towards phenol, cyclohexanone and cyclohexanol versus 4-CP conversion in HDC runs.

In the Figure 10 selectivity towards cyclohexanol and the Rh^{n+}/Rh^0 ratio were plotted. A clear relationship can be observed between the selectivity towards cyclohexanol and the Rh^{n+}/Rh^0 ratio within the 0.56 – 0.72 range, which corresponds to nanoparticles with size between 2.3-3.0 nm ratio. The point at a Rh^{n+}/Rh^0 ratio of 0.74 corresponds to Rh nanoparticles subjected to additional reduction (sample R1).

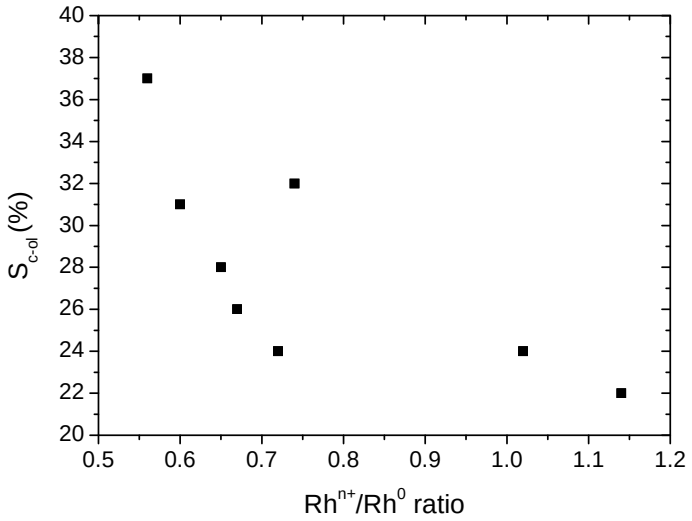

Figure 10. Selectivity towards cyclohexanol versus Rh^{n+}/Rh^0 ratio after 4 h reaction.

3.3.3 HDC runs at basic pH

Three HDC runs were performed at controlled basic pH (10.4) by using a carbonate-bicarbonate buffer in order to address possible changes in activity and/or selectivity. At this pH, 4-CP occurs mainly as 4-chlorophenolate, given the pKa value of 4-CP (9.3). Nanoparticles samples 1, 2 and 5 were selected as representative due to their differences in size and Rh^{n+}/Rh^0 ratio. As was seen in Figure 6, activity increased as Rh^{n+}/Rh^0 ratio decreased, in both uncontrolled and controlled (10.4) pH runs. The differences in activity between the runs performed at pH 10.4 and uncontrolled pH could be related with the different adsorption energy of 4-CP and 4-chlorophenolate on Rh nanoparticles.

Differences on selectivity between 10.4 and uncontrolled pH runs were also found. Figure 11 shows, as representative example, the selectivity to phenol, cyclohexanone and cyclohexanol versus time with the sample 5 of nanoparticles. As can be observed, the selectivity to phenol and cyclohexanone after the 4h reaction

time was higher at pH 10.4, whereas selectivity to cyclohexanol is lower than that found in the uncontrolled pH runs.

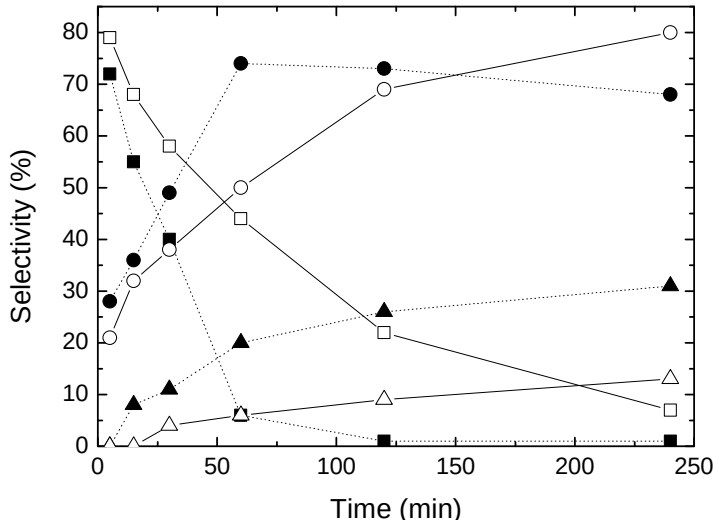

Figure 11. Selectivity to phenol (squares), cyclohexanone (circles) and cyclohexanol (triangles) versus time with sample 5 of nanoparticles in the HDC of 4-CP. Open symbols: pH 10.4. Solid symbols: uncontrolled pH.

3.4 Kinetic analysis

From the scheme of Figure 8, the following kinetic model is proposed for the HDC process to gain insight into the issue. This model is similar to that proposed by Fujita et al. [47] for the hydrogenation of phenol using Rh-based catalysts, but including the step of HDC of 4-CP to phenol.

$$\begin{aligned}
(-r_{4-cp}) &= \frac{-dC_{4-cp}}{dt} = k_1 \times C_{4-cp} \\
(r_{ph}) &= \frac{dC_{ph}}{dt} = k_1 \times C_{4-cp} - k_2 \times C_{ph} - k_4 \times C_{ph} \\
(r_{c-one}) &= \frac{dC_{c-one}}{dt} = k_2 \times C_{ph} - k_3 \times C_{c-one} \\
(r_{c-ol}) &= \frac{dC_{c-ol}}{dt} = k_3 \times C_{c-one} + k_4 \times C_{ph}
\end{aligned} \qquad [5]$$

$$t = 0; \quad C_{4-cp} = C_0; C_{ph} = 0; C_{c-one} = 0; \; C_{c-ol} = 0;$$

In Table 3, the values of the rate constants for the sample 5 of Rh nanoparticles are collected. As can be seen, k_1 and k_2 increase with temperature, whereas k_3 and k_4, associated to the production of cyclohexanol, do not show any significant change with temperature within the 15 ^{o}C range tested. Figure 12, as representative example, shows the validation of the rate curves of Rh sample 5.

Table 3. Values of the rate constants for 4-CP HDC with sample 5 of Rh nanoparticles.

Reaction temperature (K)	**Rate constants ($\cdot 10^3$) (min^{-1})**	**r^2**
303	$K_1 = 82 \pm 13$ $K_2 = 43 \pm 9$ $K_3 = 1 \pm 0.7$ $K_4 = 11 \pm 5$	0.984
308	$K_1 = 88 \pm 10$ $K_2 = 52 \pm 7$ $K_3 = 1 \pm 0.6$ $K_4 = 12 \pm 4$	0.992
318	$K_1 = 101 \pm 14$ $K_2 = 61 \pm 9$ $K_3 = 1 \pm 0.5$ $K_4 = 11 \pm 4$	0.992

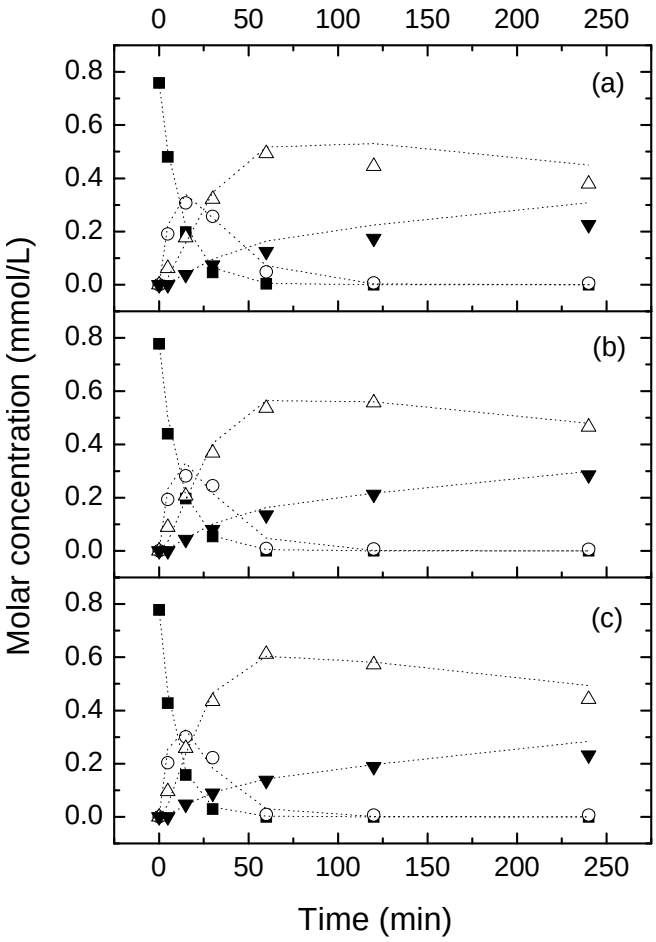

Figure 12. Molar concentration of (■) 4-CP, (○) phenol, (Δ) cyclohexanone and (▼) cyclohexanol versus reaction time for the 4-CP HDC runs with Rh sample 5 of nanoparticles. Reaction temperature: (a) 303 K, (b) 308 K, (c) 313 K. Predicted data in dashed lines.

3.5 Stability tests

Two different stability tests have been performed in the current work using Rh sample 6 as catalysts. The first one was a 60 hours-long reaction, with the objective of improving the knowledge on the hydrogenation ability of the Rh NPs, once all the 4-CP and phenol were converted. The other one consisted in the successive addition of two pulse of highly concentrated 4-CP solution (3 mL, 5000 $mg \cdot L^{-1}$) to achieve the initial 4-CP concentration, once all the 4-CP is converted, thus completing three reaction cycles.

Figure 13 shows the concentration of 4-CP and by-products versus reaction time. After the complete 4-CP and phenol conversion in 2 hours, the hydrogenation of cyclohexanone led to obtain cyclohexanol. Cyclohexanone reduction is not completed in 60 hours, although progressive conversion of cyclohexanone to cyclohexanol is observed. These results support the reaction mechanism proposed in this work where the hydrogenation of cyclohexanone can lead to obtain cyclohexanol, in contrast to other reaction mechanisms proposed for Rh-supported catalysts [11]

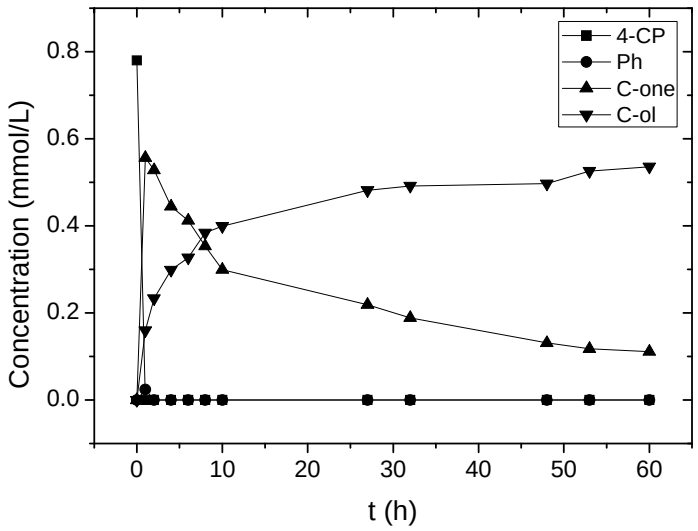

Figure 13. 4-CP and by-products concentration versus time using Rh sample 6.

Figure 14 shows the 4-CP conversion versus time for the three pulses. As can be observed, the complete HDC is obtained before 240 min reaction in all the cases, but as the number of cycle increased, the complete conversion is delayed up to 120 and 210 min for the cycle #2 and cycle #3, respectively, when it is compared to the cycle #1 (60 min). Moreover, the activity significantly decreased to 10.4 $mmol \cdot g^{-1} \cdot min^{-1}$ and 6.4 $mmol \cdot g^{-1} \cdot min^{-1}$, for the cycle #2 and cycle #3, respectively, in comparison with the cycle

#1 (22.4 mmol·g^{-1}·min^{-1}). The fall in activity as the number of cycles increased, could also be explained by the competition between the substrates for the active sites as the concentrations of by-products increased with time. Thus, phenol and cyclohexanone can compete with 4-CP for the active sites, diminishing the activity. Likewise, other causes such as loss of catalyst with samples (13 % at the end of three cycles), the high concentration of chlorine in the medium or changes in the structure of the nanoparticles as reaction time increased, could be related to the loss of activity.

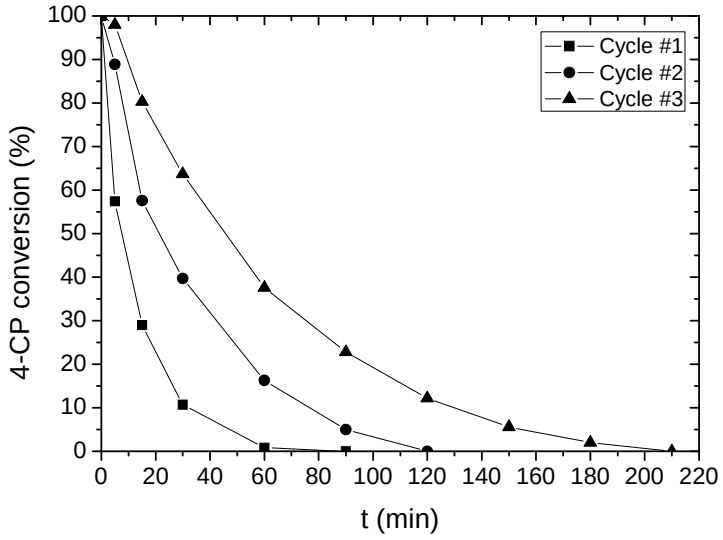

Figure 14. 4-CP conversion versus time for the 3 cycles using Rh sample 6.

4. Conclusions

Rh nanoparticles were synthesized and used as catalysts in aqueous phase 4-CP HDC at mild conditions (303 - 318 K, 1 atm.). The load of PVP and the concentration of methanol affected to particle size and Rh oxidation state. The Rh nanoparticles showed high activity for 4-CP HDC equivalent to that previously obtained for Pd nanoparticles, in spite of the fact that in the case of supported catalysts Rh has generally been

reported less active than Pd. The size and the oxidation state of the Rh nanoparticles showed a significant influence on the activity, which increased as size decreased up to a maximum at 2.8 nm. A high dependence between the activity and the Rh^{n+}/Rh^{0} ratio was found. Increasing the relative amount of zero-valent Rh, increased the activity. Such specific influence of zero-valent Rh in aqueous phase HDC of 4-CP had not been reported before. Regression equations were developed in order to acquire a better understanding on the differences of selectivity to cyclohexanone and cyclohexanol found with the different Rh nanoparticles samples. The crossed influence of particle size and Rh^{n+}/Rh^{0} ratio was the only significant effect in those equations predicting selectivity at different times. On the basis of the experimental curves of products distribution upon reaction time a reaction scheme has been proposed and a kinetic model was derived from it.

Acknowledgements

We greatly appreciate financial support from the Spanish MCYT (CTQ2009-09983 and CTQ2012-32821) and CAM (REMTAVARES S-2009/AMB-1588). J.A. Baeza thanks to the Spanish MICINN a research grant (BES-2010-030059).

References

[1] C. Xia, Y. Liu, S. Zhou, C. Yang, S. Liu, J. Xu, J. Yu, J. Chen, X. Liang, The Pd-catalyzed hydrodechlorination of chlorophenols in aqueous solutions under mild conditions: A promising approach to practical use in wastewater, J. Hazard. Mater. 169 (2009) 1029-1033.

[2] M. Zheng, J. Bao, P. Liao, K. Wang, S. Yuan, M. Tong, H. Long, Electrogeneration of H_2 for Pd-catalytic hydrodechlorination of 2,4-dichlorophenol in groundwater, Chemosphere 87 (2012) 1097-1104.

[3] M. Czaplicka, Sources and transformations of chlorophenols in the natural environment, Sci. Total Environ. 322 (2004) 21-39.

[4] P. Lampi, K. Tolonen, T. Vartiainen, J. Tuomisto, Chlorophenols in lake bottom sediments: a retrospective study of drinking water contamination, Chemosphere 24 (1992) 1805-1824.

[5] M.A. Keane, Supported transition metal catalysts for hydrodechlorination reactions, ChemCatChem 3 (2011) 800-821.

[6] G. Yuan, M.A. Keane, Catalyst deactivation during the liquid phase hydrodechlorination of 2,4-dichlorophenol over supported Pd: influence of the support, Catal. Today 88 (2003) 27-36.

[7] G. Yuan, M.A. Keane, Liquid phase catalytic hydrodechlorination of 2,4-dichlorophenol over carbon supported palladium: an evaluation of transport limitations, Chem. Eng. Sci. 58 (2003) 257-267.

[8] L. Calvo, M.A. Gilarranz, J.A. Casas, A.F. Mohedano, J.J. Rodríguez, Hydrodechlorination of 4-chlorophenol in aqueous phase using Pd/AC catalysts prepared with modified active carbon supports, Appl. Catal. B: Environ. 67 (2006) 68-76.

[9] A.J. Biacchi, R.E. Schaak, The solvent matters: kinetic versus thermodynamic shape control in the polyol synthesis of rhodium nanoparticles, ACS Nano 5 (2011) 8089-8099.

[10] Y. Yuan, N. Yan, P.J. Dyson, Advances in the rational design of rhodium nanoparticle catalysts: control via manipulation of the nanoparticle core and stabilizer, ACS Catal. 2 (2012) 1057-1069.

[11] E. Díaz, J.A. Casas, A.F. Mohedano, L. Calvo, M.A. Gilarranz, J.J. Rodríguez, Kinetics of the hydrodechlorination of 4-chlorophenol in water using Pd, Pt, and Rh/Al_2O_3 catalysts, Ind. Eng. Chem. Res. 47 (2008) 3840-3846.

[12] B.R. Cuenya, Synthesis and catalytic properties of metal nanoparticles: size, shape, support, composition, and oxidation state effects, Thin Solid Films 518 (2010) 3127-3150.

[13] G. Somorjai, J. Park, Molecular factors of catalytic selectivity, Angew. Chem. Int. Ed. 47 (2008) 9212-9228.

[14] M.A. Keane, G. Pina, G. Tavoularis, The catalytic hydrodechlorination of mono-, di- and trichlorobenzenes over supported nickel, Appl. Catal. B: Environ. 48 (2004) 275-286.

[15] S. Ordóñez, E. Díaz, R.F. Bueres, E. Asedegbega-Nieto, H. Sastre, Carbon nanofibre-supported palladium catalysts as model hydrodechlorination catalysts, J. Catal. 272 (2010) 158-168.

[16] E. Diaz, A.F. Mohedano, J.A. Casas, L. Calvo, M.A. Gilarranz, J.J. Rodriguez, Comparison of activated carbon-supported Pd and Rh catalysts for aqueous-phase hydrodechlorination, Appl. Catal. B: Env. 106 (2011) 469-475.

[17] T. Janiak, J. Okal, Effectiveness and stability of commercial Pd/C catalysts in the hydrodechlorination of meta-substituted chlorobenzenes, Appl. Catal. B: Environ. 92 (2009) 384-392.

[18] M.A. Aramendía, V. Boráu, I.M. García, C. Jiménez, F. Lafont, A. Marinas, J.M. Marinas, F.J. Urbano, Influence of the reaction conditions and catalytic properties on the liquid-phase hydrodechlorination of chlorobenzene over palladium-supported catalysts: activity and deactivation, J. Catal.187 (1999) 392-399.

[19] A.Y. Stakheev, I.S. Mashkovskii, G.N. Baeva, N.S. Telegina, Specific features of the catalytic behavior of supported palladium nanoparticles in heterogeneous catalytic reactions, Russ. J. Gen. Chem. 80 (2010) 618-629.

[20] J.A. Baeza, L. Calvo, M.A. Gilarranz, A.F. Mohedano, J.A. Casas, J.J. Rodriguez, Catalytic behavior of size-controlled palladium nanoparticles in the hydrodechlorination of 4-chlorophenol in aqueous phase, J. Catal. 293 (2012) 85-93.

[21] N. Yan, C. Xiao, Y. Kou, Transition metal nanoparticle catalysis in green solvents, Coord. Chem. Rev. 254 (2010) 1179-1218.

[22] A. Gniewek, A.M. Trzeciak, J.J. Ziółkowski, L. Kępiński, J. Wrzyszcz, W. Tylus, Pd-PVP colloid as catalyst for Heck and carbonylation reactions: TEM and XPS studies, J. Catal. 229 (2005) 332-343.

[23] K. Okitsu, H. Bandow, Y. Maeda, Y. Nagata, Sonochemical preparation of ultrafine palladium particles, Chem. Mater. 8 (1996) 315-317.

[24] P. Yong, N.A. Rowson, J.P.G. Farr, I.R. Harris, L.E. Macaskie, Bioreduction and biocrystallization of palladium by *Desulfovibrio desulfuricans* NCIMB 8307, Biotechnol. Bioeng. 80 (2002) 369-379.

[25] H. Hirai, Y. Nakao, N. Toshima, Colloidal rhodium in polyvinyl-alcohol as hydrogenation catalyst of olefins, Chem. Lett. (1976) 905-910.

[26] M.E. Grass, Y. Zhang, D.R. Butcher, J.Y. Park, Y. Li, H. Bluhm, K.M. Bratlie, T. Zhang, G.A. Somorjai, A reactive oxide overlayer on rhodium nanoparticles during CO oxidation and its size dependence studied by in situ ambient-pressure X-ray photoelectron spectroscopy, Angew. Chem. Int. Ed. 47 (2008) 8893-8896.

[27] S. Kim, K. Qadir, S. Jin, A.S. Reddy, B. Seo, B.S. Mun, S.H. Joo, J.Y. Park, Trend of catalytic activity of CO oxidation on Rh and Ru nanoparticles: role of surface oxide, Catal. Today 185 (2012) 131-137.

[28] E. Diaz, J.A. Casas, A.F. Mohedano, L. Calvo, M.A. Gilarranz, J.J. Rodriguez, Kinetics of 4-chlorophenol hydrodechlorination with alumina and activated carbon-supported Pd and Rh catalysts., Ind. Eng. Chem. Res. 48 (2009) 3351-3358.

[29] http://srdata.nist.gov/xps/

[30] D. Goia V., E. Matijevic, Preparation of monodispersed metal particles, New J. Chem. 22 (1998) 1203-1215.

[31] J. Turkevich, P.C. Stevenson, J. Hillier, A study of the nucleation and growth processes in the synthesis of colloidal gold, Discuss. Faraday Soc. 11 (1951) 55-75 .

[32] F. Chen, Z. Zhong, X. Xu, J. Luo, Preparation of colloidal Pd nanoparticles by an ethanolamine modified polyol process, J. Mater. Sci. 40 (2005) 1517-1519.

[33] H. Hirai, N. Yakura, Y. Seta, S. Hodoshima, characterization of palladium nanoparticles protected with polymer as hydrogenation catalyst, React. Funct. Polym. 37 (1998) 121-131.

[34] C. Fontaine-Gautrelet, J. Krafft, G. Djéga-Mariadassou, C. Thomas, Evidence for Rh electron-deficient atoms ($Rh^{\delta+}$) as the catalytic species for CO oxidation when supported on $Ce_{0.68}Zr_{0.32}O_2$: a combined N_2-FTIR, benzene hydrogenation, and kinetic study, J. Catal. 247 (2007) 34-42.

[35] H. Beyer, J. Emmerich, K. Chatziapostolou, K. Köhler, Decomposition of nitrous oxide by rhodium catalysts: effect of rhodium particle size and metal oxide support, Appl. Catal. A: Gen. 391 (2011) 411-416.

[36] P.S.S. Reddy, N. Seshu Babu, N. Pasha, N. Lingaiah, P.S. Sai Prasad, Influence of microwave irradiation on catalytic decomposition of nitrous oxide over Rh/Al_2O_3 catalyst, Catal. Commun. 9 (2008) 2303-2307.

[37] C. Cao, A. Bourane, J.R. Schlup, K.L. Hohn, In situ IR investigation of activation and catalytic ignition of methane over Rh/Al_2O_3 catalysts, Appl. Catal. A: Gen. 344 (2008) 78-87.

[38] N.L. Holy, Versatile polymer-bound hydrogenation catalysts. Rhodium(I)-catalyzed hydrogenation, J. Org. Chem. 44 (1979) 239-243.

[39] T. Eumatsu, T. Kawakami, F. Saitho, M. Miura, H. Hashimoto, Hydrogenation and isomerization of olefins on heterogenized rhodium complexes, J. Mol. Catal. 12 (1981) 11-26.

[40] P. Ferreira-Aparicio, B. Bachiller-Baeza, I. Rodriguez-Ramos, A. Guerrero-Ruiz, M. Fernandez-Garcia, Correlation between metal oxidation state and catalytic activity: hydrogenation of crotonaldehyde over Rh catalysts, Catal. Lett. 49 (1997) 163-167.

[41] P.C. Selvaraj, V. Mahadevan, Polymer-supported palladium and rhodium species as hydrogenation catalysts, J. Pol. Sci. A: Pol. Chem. 35 (1997) 105-122.

[42] P. Reyes, C. Rodriguez, G. Pecchi, J.L.G. Fierro, Promoting effect of Mo on the selective hydrogenation of cinnamaldehyde on Rh/SiO_2 catalysts, Catal. Lett. 69 (2000) 27-32.

[43] L.M. Gómez-Sainero, X.L. Seoane, J.L Fierro, A. Arcoya, Liquid-phase hydrodechlorination of CCl4 to CHCl3 on Pd/C catalysts: Nature and role of Pd active species, J. Catal. 209 (2002) 279-288.

[44] G. Yuan, M.A. Keane, Liquid phase catalytic hydrodechlorination of chlorophenols at 273 K, Catal. Commun. 4 (2003) 195-201.

[45] G.S. Pozan, I. Boz, Catalytic hydrodechlorination of 2,4-dichlorophenol on Pd/Rh/C catalysts, J. Hazard. Mater. 136 (2006) 917-921.

[46] T.T. Bovkun, Y. Sasson, J. Blum, Conversion of chlorophenols into cyclohexane by a recyclable Pd-Rh catalyst, J. Mol. Catal. A: Chem. 242 (2005) 68-73.

[47] S. Fujita, T. Yamada, Y. Akiyama, H. Cheng, F. Zhao, M. Arai, Hydrogenation of phenol with supported Rh catalysts in the presence of compressed CO_2: Its effects on reaction rate, product selectivity and catalyst life, J. Supercrit. Fluids 54 (2010) 190-201.

Nomenclature

a	Catalytic activity (mmol/g_{cat}·min)
$C_{4\text{-}cp}$	4-CP molar concentration (mmol/L)
C_{ph}	Phenol molar concentration (mmol/L)
$C_{c\text{-}one}$	Cyclohexanone molar concentration (mmol/L)
$C_{c\text{-}ol}$	Cyclohexanol molar concentration (mmol/L)
C_{Rh}	Rh nanoparticles concentration (g/L)
d_s	Surface-area-weighted average mean diameter (nm)
k_x	Rate constant (min^{-1})
$-r_{4\text{-}cp}$	4-CP conversion rate (mmol/L·min)
r_{ph}	Phenol conversion rate (mmol/L·min)
$r_{c\text{-}one}$	Cyclohexanone conversion rate (mmol/L·min)
$r_{c\text{-}ol}$	Cyclohexanol conversion rate (mmol/L·min)
$S_{c\text{-}one}$	Selectivity towards cyclohexanone
$S_{c\text{-}ol}$	Selectivity towards cyclohexanol
S_i	Selectivity towards compound i (%), defined as moles of compound i per mole of 4-CP converted
S_{ph}	Selectivity towards phenol
t	Reaction time (min)

CAPÍTULO III /CHAPTER III

Kinetic analysis of 4-chlorophenol hydrodechlorination by Rh nanoparticles based on the two-step reaction and Langmuir-Hinshelwood mechanisms.

Submitted to Catalysis Letters (Accepted)

Abstract

In this work kinetic analysis based on the two-step reaction and Langmuir-Hinshelwood mechanisms are applied to the aqueous phase catalytic hydrodechlorination of 4-chlorophenol by unsupported Rh nanoparticles. The theoretical predictions of models based on the two-step and Langmuir-Hinshelwood methods showed good agreement with experimental activity data (turn over frequency) of reaction runs carried out at 303 K with nanoparticles of different size (1.9-4.9 nm). Theoretical peaks in activity (29-30 h^{-1}) for nanoparticle sizes of 2.5-2.7 nm were very close to experimental values (ca. 28 h^{-1}, 2.8 nm). The applicability of the two-step model and Langmuir-Hinshelwood mechanism to unsupported metal nanoparticles is proved and mechanistic information is obtained. An important difference in the Gibbs replacement adsorption energy (100-130 kJ/mol) of hydrogen by chlorophenol has been found between edges and terraces.

1. Introduction

Catalytic hydrodechlorination(HDC) in aqueous phase is considered an effective technique to treat wastewater polluted with chlorophenolic compounds [1] that leads to less toxic and more biodegradable reaction products [2-3], and that can even be a route to waste valorization [4].

Noble metals have been used extensively in HDC as catalysts due to their excellent properties in terms of stability, activity and selectivity. Among the noble metals used, Rh-based catalysts have not only shown high activity, but also a remarkable ability to hydrogenate HDC reaction products, thus leading to additional reduction of toxicity [5].

In order to reach high-performance catalysts, a rational design is needed, taking into consideration factors that have influence on activity and selectivity, such as the size of the metallic phase clusters. Thus, previous works have reported on the use of non-supported noble metal nanoparticles to stablish relationships between the characteristics of the metal nanoparticles and their catalytic performance [6-7]. This type of experimental results provides a deeper understanding and can drive new approaches in catalysts design. In addition to this, in the last few years kinetic analysis has emerged as a theoretical approach to study the effect of cluster size on activity for supported catalysts [8]. The results obtained in former studies revealed a reasonably good fitting between predicted values and experimental data for a variety of reactions [9], which opens a field for the theoretical design of catalysts. However, to the best of our knowledge, this approach has not been applied yet to unsupported metallic catalysts. This is a very interesting approach since the potential effect of the interaction between the active phase and support in the activity can be avoided.

In a previous work [10], the effect of nanoparticle size was experimentally explored by using unsupported Rh nanoparticles, as model catalysts, in the 4-chlorophenol (4-CP) HDC in aqueous phase at 303 K. The activity *vs.* size plot revealed a volcano-shaped curve, evidencing a maximum for activity at c.a. 2.8 nm. In the present work, a kinetic analysis based on the two-step reaction and Langmuir-Hinshelwood mechanism is performed to assess the theoretical effect of Rh nanoparticle size on activity in the 4-CP HDC in aqueous phase and check the applicability of the models.

2. Two-step reaction mechanism.

The two-step reaction mechanism has been commonly used in the literature [11-12] to explain catalytic kinetics for reactions where only two main steps are assumed. In particular, the two-step method has been used to account for catalytic kinetics of hydrodechlorination reactions [13]. Thus, the mechanism is described in Equation (1), where A_1 and A_2 are reactants, B_1 and B_2 are products, ZH is the surface active site with adsorbed hydrogen and *I* is the adsorbed Cl. This mechanism is an extension of a classical two step sequence with only one most abundant surface intermediate.

1. $ZH + A_1 \leftrightarrow Z\text{-}I + B_1$
2. $Z\text{-}I + A_2 \leftrightarrow ZH + B_2$ (1)

$A_1 + A_2 \leftrightarrow B_1 + B_2$

Where A_1 = C_6H_4OHCl; Z-I = Z-Cl; A_2 =H_2; B_1 =C_6H_5OH; B_2 = HCl. The catalytic cycle given in (1) does not include an initial step of cycle initiation by hydrogen adsorption.

According to [12], the reaction rate for this mechanism is:

$$r(d) = \frac{k_1 C_{A_1} k_2 C_{A_2} - k_{-1} C_{B_1} k_{-2} C_{B_2}}{k_1 C_{A_1} + k_2 C_{A_2} + k_{-1} C_{B_1} + k_{-2} C_{B_2}} \qquad (2)$$

Where C_{xn} are concentrations and k_n kinetic constants of elementary steps in eq. (1).

For the sake of easier applicability of the model, some assumptions previous to the kinetic analysis have been reported [14], which can be summarized as a) the alterations of the chemical potential of nanoparticles in comparison with bulk metal are the same, independent of the surface coverage; b) only terraces and edges are sites with different reactivity; c) cubo-octahedral shape of the Rh nanoparticles.

Thus, the rate constants are

$$k_1(d) = k_1 e^{-\alpha_1 \chi/d} \; ; \qquad k_{-1}(d) = k_{-1} e^{(1-\alpha_1)\chi/d} \qquad (3)$$

$$k_2(d) = k_2 e^{(1-\alpha_2)\chi/d} \; ; \qquad k_{-2}(d) = k_{-2} e^{-\alpha_2 \chi/d}$$

where α_n is the Polanyi parameter for step n, d is the nanoparticle size and χ is defined as

$$\chi = \frac{(\Delta G_{ads,edges} - \Delta G_{ads,terraces})}{RT} \qquad (4)$$

With ΔG_x being the Gibbs energy of replacement adsorption of hydrogen with Cl (reaction 1) on edges or terraces, R the gas constant, and T the reaction temperature.

Note that the original treatment of the two step in [14] was limited to adsorption to and from bare surfaces. In fact eq. (1) is presented in a form which allows to use the mathematical treatment developed in [14] also for the case of replacement adsorption with the only difference that instead of adsorption of chlorophenol on bare surfaces, the modified analysis considers the replacement of adsorbed hydrogen by chlorophenol incoming from the fluid phase.

The reaction rate is expressed as

$$r(d) = \frac{\left(k_1 C_{A_1} k_2 C_{A_2} - k_{-1} C_{B_1} k_{-2} C_{B_2}\right) e^{(1-\alpha_1-\alpha_2)\chi/d}}{(k_1 C_{A_1} + k_{-1} C_{B_1} e^{\chi/d}) e^{-\alpha_1 \chi/d} + (k_{-2} C_{B_2} + k_2 C_{A_2} e^{\chi/d}) e^{-\alpha_2 \chi/d}} \qquad (5)$$

In order to simplify, considering that the 4-CP HDC reaction is irreversible, three cases can be taken into account:

a) Irreversibility of both steps 1 and 2 ($k_{-1} \approx k_{-2} \approx 0$); the reaction rate is described by

$$r(d) = \frac{\omega_2 e^{(1-\alpha_2)\chi/d}}{1 + \frac{\omega_2}{\omega_1} e^{(1+\alpha_1-\alpha_2)\chi/d}} \qquad (6)$$

where $\omega_n = k_n C_{Xn}$ (i.e. $\omega_1 = k_1 C_{A1}$) according to Temkin notation [12]. Then, the reaction rate can be arranged as

$$r(d) = \frac{p_1 e^{(1-\alpha_2)\chi/d}}{1 + p_2 e^{(1+\alpha_1-\alpha_2)\chi/d}} (7)$$

where $p_1 = \omega_2$, $p_2 = (\omega_2/\omega_1)$

b) Irreversibility of step 1 ($k_{-1} \approx 0$). The reaction rate is described by

$$r(d) = \frac{\omega_2 e^{(1-\alpha_2)\chi/d}}{1 + \frac{\omega_2}{\omega_1} e^{(1+\alpha_1-\alpha_2)\chi/d} + \frac{\omega_{-2}}{\omega_1} e^{(\alpha_1-\alpha_2)\chi/d}} \qquad (8)$$

Then, the reaction rate can be arranged as

$$r(d) = \frac{p_1 e^{(1-\alpha_2)\chi/d}}{1 + p_2 e^{(1+\alpha_1-\alpha_2)\chi/d} + p_3 e^{(\alpha_1-\alpha_2)\chi/d}} \qquad (9)$$

where $p_1 = \omega_2$, $p_2 = (\omega_2/\omega_1)$, $p_3 = (\omega_{-2}/\omega_1)$.

c) irreversibility of step 2 ($k_{-2} \approx 0$). The reaction rate is described by

$$r(d) = \frac{\omega_2 e^{(1-\alpha_2)\chi/d}}{1 + \frac{\omega_2}{\omega_1} e^{(1+\alpha_1-\alpha_2)\chi/d} + \frac{\omega_{-1}}{\omega_1} e^{\chi/d}} \qquad (10)$$

$$r(d) = \frac{p_1 e^{(1-\alpha_2)\chi/d}}{1 + p_2 e^{(1+\alpha_1-\alpha_2)\chi/d} + p_4 e^{\chi/d}} \qquad (11)$$

where $p_1 = \omega_2$, $p_2 = (\omega_2/\omega_1)$ and $p_4 = (\omega_{-1}/\omega_1)$

In a simplified case, when it is assumed that $\alpha_1 = \alpha_2 = \alpha$, the equation (11) can be rearranged as

$$r(d) = \frac{p_1 e^{(1-\alpha)\chi/d}}{1 + p_5 e^{\chi/d}} \qquad (12)$$

Where $p_1 = \omega_2$ and $p_5 = (\omega_2+\omega_{-1})/\omega_1$

3. Langmuir-Hinshelwood mechanism

The Langmuir-Hinshelwood mechanism has also been used to explain kinetics in hydrodechlorination [15-17]. This mechanism assumes the adsorption of the reactants on different active sites. If the coverage of the product is neglected and adsorption is considered as non-competitive, it can be described by equation. (13).

1. Z + A ↔ Z-A (quasi-equilibrium)
2. Z* + B ↔ Z*-B (quasi-equilibrium) (13)
3. Z-A + Z*-B → C+D

A + B→ C+D

where A, B, C and D are respectively 4-CP, H_2, phenol and HCl and Z and Z* are different sites.

The reaction rate is given by equation (14)

$$r(d) = \frac{k_3 K_1 C_A K_2 C_B}{(1 + K_1 C_A)(1 + K_2 C_B)} \qquad (14)$$

Where C_{xn} are concentrations, k_3 is the kinetic constant and K_n equilibrium constants of elementary steps in equation (14).

As in the two-step approach, for the sake of easier applicability of the model, some assumptions previous to the kinetic analysis have been reported [14], which can be summarized as a) the alterations of the chemical potential of nanoparticles in comparison with bulk metal are the same, independent of the surface coverage; b) only terraces and edges are sites with different reactivity; c) cubo-octahedral shape of the Rh nanoparticles. Thus, the reaction rate is expressed as

$$r(d) = \frac{k_3 e^{\alpha(\chi_A + \chi_B)/d} K_1 C_A K_2 C_B}{(1 + K_1 C_A e^{\chi_A/d}) \left(1 + K_2 C_B e^{\chi_B/d}\right) d} \qquad (15)$$

Where α is the Polanyi parameter for the step 3, *d* is the nanoparticle size and χ_x is the parameter for 4-CP and H_2, respectively, defined in equation (4) as the difference between adsorption of edges and terraces of 4-CP or hydrogen.

Then, the reaction rate can be arranged as

$$r(d) = \frac{p_6 e^{\alpha(\chi_A + \chi_B)/d}}{(1 + p_7 e^{\chi_A/d}) \left(1 + p_8 e^{\chi_B/d}\right) d} \qquad (16)$$

where $p_6 = k_3 K_1 K_2 C_A C_B$, $p_7 = K_1 C_A$ and $p_8 = K_2 C_B$

4. Results and discussion

In the previous work [10], experimental data were obtained for the catalytic HDC of 4-CP by Rh nanoparticles with different sizes (1.9‑4.9 nm). The Rh nanoparticles were prepared by a chemical reduction method using $RhCl_3$ as a precursor salt, methanol as a reducing agent and polyvinylpyrrolydone (PVP) as a capping agent.

These unsupported nanoparticles were tested as model catalysts in the aqueous phase 4-CP HDC in excess of H_2. The highest values of activity were obtained by Rh nanoparticles within a range of 2.3–3.0 nm, reaching a maximum ca. 2.8 nm. These results indicated that the aqueous phase HDC of 4-CP by Rh nanoparticles is a structure sensitive reaction. The activity increased as size decreased up to ca. 2.8 nm. Below this size, the activity decreased. The number of atoms surrounding each surface metal atom decreases as the particle size decreases, affecting the nature and strength of the interactions between the surface of Rh particles surface and 4-CP molecules [18]. Therefore, changes in the coordination related to the nanoparticle size have a strong effect on the adsorption energy and may be the reason for lower activity.

Model Discrimination. Ten kinetics model (M1 – M10) were proposed based on the two-step (M1-M8) and Langmuir-Hinshelwood mechanism (M9 and M10). Table 1 summarizes the main parameter values for all the models. Models M1, M2 and M3 were proposed considering that both steps are irreversible. M4 and M5 were proposed considering only step 1 as irreversible and, in the case of M7, M8 and M9, considered only step 2 as irreversible. A relevant difference between models lies on the different assumptions made for α. Only in models M1 and M8 α_1 is assumed to be different from α_2. Table 1 also shows the models where the value of either α or α_1 was fixed at 0.5.

Table 1. Parameter values obtained from all the models proposed.

Parameter	M1	M2	M3	M4	M5	M6	M7	M8	M9	M10
P1	0.16 ±0.03	0.32 ±0.04	0.03 ±0.01	0.26 ±0.01	0.39 ±37.6	0.32 ±0.03	0.03 ±0.01	1.14 ±0.19	-	-
P2	1.8E-8 ±4.3E-8	5.6E-10 ±4.6E-10	1.9E-7 ±1.6E-7	1.8E-9 ±1.7E-9	3.1E-4 ±2.9E-4	-	-	-0.39 ±0.05	-	-
P3	-	-	-	0.3 ±0.1	13.95 ±1429.92	-	-	-	-	-
P4	-	-	-	-	-	-	-	0.12 ±0.02	-	-
P5	-	-	-	-	-	5.6E-10 ±4.6E-10	1.9E-7 ±1.7E-7		-	-
P6	-	-	-	-	-	-	-		0.04 ±0.01	0.01 ±0.0001
P7	-	-	-	-	-	-	-		5.8E-10 ±4.2E-10	9.8E-8 ±6E-8
P8	-	-	-	-	-	-	-		3.3E-16 ± 0*	6.8E-17 ±0*
α1	1.00 ±0.46	-	-	-	-	-	-	0.5	-	-
α2	0.51 ±0.30	-	-	-	-	-	-	0.78 ±0.01	-	-
α	-	0.76 ±0.10	0.5	0.74 ±0.01	0.5	0.76 ±0.01	0.5		0.30 ±0.1	0.5
χ	30.02 ±18.43	51.91 ±1.86	41.06 ±2.20	49.43 ±1.73	40.94 ±6.01	51.91 ±1.86	41.05 ±2.16	7.78 ±0.37	-	-
χA	-	-	-	-	-	-	-	-	52.09 ±1.64	41.98 ±1.67
χB	-	-	-	-	-	-	-	-	3.7E-16 ±0*	6.8E-14 ±0*
Chi^2/DoF	0.093	0.076	0.103	0.074	0.089	0.073	0.082	0.043	0.051	0.061
R2	0.912	0.932	0.916	0.948	0.923	0.934	0.928	0.969	0.956	0.918

*very small values with no reliable standard error

In Figures 1-4 activity (TOF) versus nanoparticle size are plotted and it can be observed that all the models proposed fitted reasonably well with experimental data. Nevertheless, some of the models can be discarded due to that they do not fulfill physical criteria which is the case of M1, M5 and M8, i.e., with parameters lacking of physical sense.

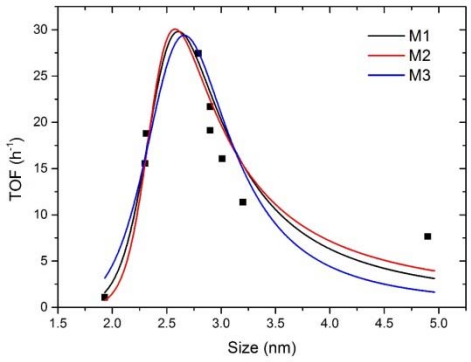

Figure 1. TOF versus Rh nanoparticles size. Solid squares: experimental data. Lines: values predicted from M1, M2 and M3.

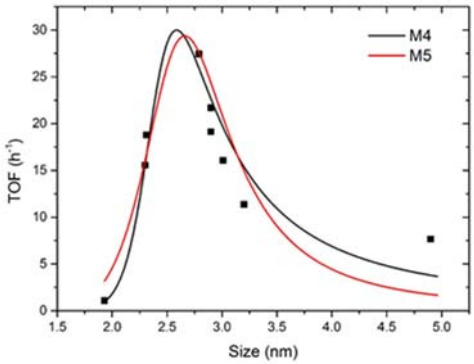

Figure 2. TOF versus Rh nanoparticles size. Solid squares: experimental data. Lines: values predicted from M4 and M5.

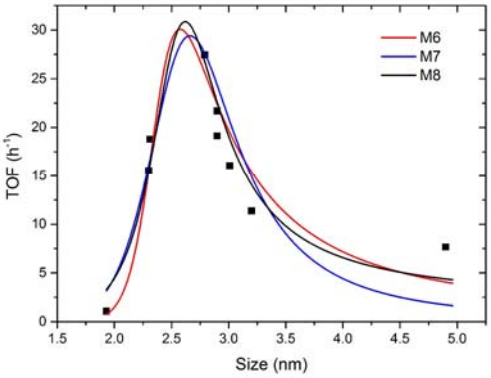

Figure 3. TOF versus Rh nanoparticles size. Solid squares: experimental data. Lines: values predicted from M6, M7 and M8.

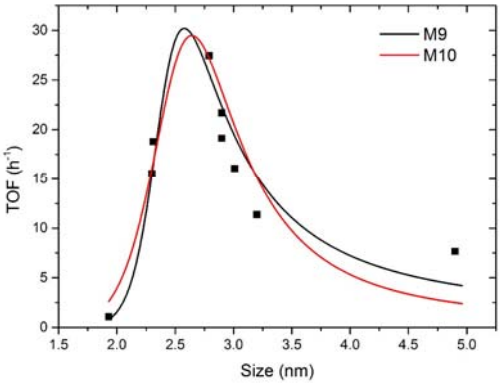

Figure 4. TOF versus Rh nanoparticles size. Solid squares: experimental data. Lines: values predicted from M9 and

For all the models, the theoretical maximum activity obtained (2.5 – 2.7 nm, 29-30 h^{-1}) is quite close to the experimental maximum (ca. 2.8 nm, 28 h^{-1}), although significant differences are observed in the predictions at high nanoparticle size values, with a higher drop in activity and lack of fit for M3, M5, M7 and M10 models. In these models the alpha values were fixed to 0.5.

Based on the parameter values obtained for all the models, additional insight in the reaction mechanism can be obtained. Thus, the difference in adsorption energy of 4-

CP between adsorption on edges and terraces, calculated from equation (4) for all the models, is higher (100-130 kJ/mol) than that reported for Pd/TiO_2 in the hydrogenation of ethene (55 kJ/mol) [14]. Such a high values suggests that 4-CP is strongly adsorbed on terraces and barely adsorbed on edges. Thus, maybe due to steric restrictions or low efficiency of the interaction, 4-CP is barely adsorbed on edges and smaller cluster would be less active. This is consistent with the experimental results showed in Figures 1-4 where a very low activity is observed for the HDC experiments carried out with sizes below 2 nm. On the other hand, when the alpha values were not fixed in the models based on the two-step mechanism, the value of the Polanyi parameter ($\alpha \approx 0.75$) is higher than those usually reported in heterogeneous catalysis ($\alpha \approx 0.5$) [12], but close to the range of values ($\alpha = 0.3 - 0.7$) that Temkin [12] reported for the ammonia synthesis using different catalysts. This value ($\alpha \approx 0.75$) is also close to that reported in the crotonaldehyde hydrogenation using a gold supported on TiO_2 catalysts ($\alpha = 0.67$) [19]. When the model is based on Langmuir-Hinshelwood mechanism, the value of the Polanyi parameter is lower ($\alpha = 0.3$).

The most noticeable aspect of the prediction of the two-step model and Langmuir-Hinshelwood approach is the maximum in catalytic activity. For instance, the particle size for which this maximum occurs when the two-step mechanism, assuming step 2 as irreversible, and $\alpha_1 = \alpha_2 = \alpha$ is considered is given by

$$d_{maxTOF} = \frac{\chi}{\ln(\frac{1-\alpha}{\alpha p_5})} \qquad (17)$$

Therefore, it depends on the p_5, which is related to partial concentrations of the reactants [14]. Thus, some shift of the maximum in activity is expected as reaction

conditions (i.e. concentrations) are changed. In general, the maximum in activity could be explained as an interplay of adsorption and desorption on edges and terraces as cluster size changes.

5. Conclusions

The two-step method and Langmuir-Hinshelwood mechanism have been applied to model the aqueous phase HDC of 4-clorophenol by unsupported Rh nanoparticles. A good agreement has been found between the theoretical predictions and the experimental data, probing the applicability of the kinetic analysis to unsupported Rh nanoparticles and providing mechanistic interpretation to results. A significant difference between adsorption on edges and terraces can be estimated based on the kinetic analysis.

Acknowledgements

We acknowledge the financial support from MINECO (CTQ2012-32821) and CAM (REMTAVARES S-2009/AMB-1588). J.A. Baeza is grateful to the Spanish MICINN for a research grant (BES-2010-030059).

References.

[1] Keane MA (2011) ChemCatChem 3:800.

[2] Calvo L, Gilarranz MA, Mohedano AF, Casas JA, Rodríguez JJ (2006) Appl Catal B 67:68

[3] Al Bahri M, Calvo L, Polo AM, Gilarranz MA, Mohedano AF, Rodriguez JJ (2013) Chemosphere 91:1317

[4] Gómez-Quero S, Cárdenas-Lizana F, Keane MA (2011) Chem Eng J 166:1044

[5] Díaz E, Casas JA, Mohedano AF, Calvo L, Gilarranz MA, Rodríguez JJ (2008) Ind Eng Chem Res 47:3840

[6] Binder A, Seipenbusch M, Muhler M, Kasper G (2009) J Catal 268:150

[7] Joo SH, Park JY, Renzas JR, Butcher DR, Huang W, Somorjai G (2010) Nano Lett 10:2709

[8] Murzin DYu (2011) Catal Sci Technol 1:380

[9] Murzin DYu, Parmon VN (2011) Catalysis-Special Periodical Reports, RSC, Cambridge

[10] Baeza JA, Calvo L, Gilarranz MA, Rodriguez JJ (2014) Chem Eng J 241:271

[11] Boudart M (1968) Kinetics of Chemical Processes, Prentice-Hall, New Jersey

[12] Temkin MI (1979) Adv Catal 28:173

[13] Keane MA, Murzin DYu (2001) Chem Eng Sci 56:3185

[14] Murzin DYu (2010) J Catal 276:85

[15] Ordoñez S, Diez FV, Sastre H (2002) Ind Eng Chem Res 41:505

[16] Lopez E, Ordoñez S, Sastre H, Diez FV (2003) J Hazard Mater B97:281

[17] Chen N, Rioux RM, Barbosa LAMM, Ribeiro FH (2010) Langmuir 26:16615

[18] Stakheev AY, Mashkovskii IS, Baeva GN, Telegina NS (2010) Russ J Gen Chem 80:618

[19] Murzin DYu (2009) Chem Eng Sci 64:1046

CAPÍTULO IV /CHAPTER IV

Activity enhancement and selectivity tuneability in aqueous phase hydrodechlorination by use of controlled growth Pd-Rh nanoparticles.

Submitted to ACS Nano

Abstract

Colloidal bimetallic PdRh nanoparticles (NPs) of controlled size and structure were synthesized and tested as catalysts models in aqueous phase hydrodechlorination (303 K, 1 atm) using 4-chlorophenol (4-CP) as target compound. The colloidal bimetallic PdRh NPs were synthesized by chemical reduction, using methanol as reducing agent and poly(N-vinyl-2-pyrrolidone) (PVP) as capping agent. Two methods of synthesis (co-reduction, successive reduction) and three different Pd/Rh molar ratios (0.2, 1, 5) were used. The NPs were characterized by means of TEM, HAADF-STEM/EDS and XPS.

High 4-CP conversion values (85–100%) were achieved at very low metal concentration ($1.23 \cdot 10^{-3}$ $g \cdot L^{-1}$). Phenol, cyclohexanone, cyclohexanol and cyclohexene were the reaction by-products detected. Core-shell and cluster-in-cluster NP structures were obtained by varying the method of synthesis and the Pd/Rh molar ratio. No relationship between method of synthesis and type of structure obtained (core-shell/cluster-in-cluster) were found. The activity increases with the Pd/Rh ratio. Activity values up to 67.0 $mmol \cdot g \cdot min^{-1}$, which are significantly higher than those obtained in previous works with monometallic Pd (39.1 $mmol \cdot g \cdot min^{-1}$) and Rh (29.4 $mmol \cdot g \cdot min^{-1}$) under equivalent conditions, were achieved. Significant differences in activity and selectivity were found between the nanoparticles with Pd/Rh ratios of 0.2-1 synthesized by co-reduction and successive reduction. The results indicate that the study of the performance of Pd/Rh bimetallic catalysts in HDC requires some consideration about the structure of the nanoparticles, since the metal arrangement can determine both synergistic and antagonist effects in the activity and selectivity of the catalysts.

1. Introduction

Chlorophenols constitute a group of hazardous compounds which can be found as pollutants in different industrial wastewaters since they are involved in the preparation of several chemical products such as pesticides, germicides or wood preservatives, among others [1]. In particular, monochlorophenols have been used as antiseptics since 19th century [2] and have been widely used in the extraction of nitrogen and sulphur compounds from coal, dye and pesticide industry. The most used among monochlorophenols has been 4-chlorophenol (4-CP) [3].

Among the potential techniques that could be used to treat wastewater containing chlorophenols, liquid phase catalytic hydrodechlorination (HDC) has been found as a suitable alternative to remove this sort of hazardous compounds. The operation at mild conditions, the ability to treat a wide range of concentrations and the high selectivity towards less toxic by-products, which could allow the waste valorization, have been remarked in the literature as the main advantages [4-8]. Besides, HDC could be appropriate as a detoxifying step previous to a biological treatment. Likewise, 4-CP is among the most used model compound in studies dealing with aqueous phase HDC.

Noble metal-based catalysts have been widely used in aqueous phase HDC due to their highactivity [9-11]. Among those catalysts, the bimetallic ones have attracted much attention in the last few years due to the unique properties and catalytic behavior derived from the presence of the second metal [12]. In this sense, it has been reported that the selectivity and activity can be improved significantly by using bimetallic instead of monometallic catalysts due to the synergy between both metals

[13]. Likewise, the structural stability can also be enhanced by using bimetallic catalysts [14]. Thus, in addition to the size, shape, oxidation state or the type of support, the composition of the metal NPs is considered a crucial factor for the catalyst performance [15].

Like monometallic NPs, bimetallic ones can be synthesized by physical (e.g. laser ablation, evaporation) and chemical methods (e.g. 'conventional chemical', sonochemical, photochemical or electrochemical). Chemical methods have been widely used due to their simplicity for controlling the primary structures of the NPs such as size, shape or composition. In general, chemical methods used to synthesize bimetallic NPs can be divided into two categories: co-reduction and successive reduction, which can lead to different types of structures such as core/shell, nanoalloy or cluster-in-cluster with potential different effects on activity and selectivity [16].

In our previous works [17, 18], non-supported monometallic Pd and Rh NPs were used as catalysts models in the aqueous phase HDC of 4-chlorophenol (4-CP), in order to gain insight into the effect of size and oxidation state of the metal NPs on activity/selectivity in the absence of support. Differences between both metals have been addressed, such as the specific hydrogenation ability (negligible in the case of PVP-based Pd NPs) or the effect of the electrodeficient to zerovalent species ratio on the activity within the ranges tested.

One step further, in the present work, PdRh bimetallic NPs of different Pd/Rh molar ratios (0.2, 1 and 5) have been synthesized using co-reduction and successive reduction methods. Then, they have been used unsupported as catalyst models in the aqueous phase HDC of 4-CP to acquire an in-depth knowledge on the effect of the

synthesis method on the activity and selectivity. The results can contribute to a better understanding of the relationship between properties and structure for HDC reaction, useful for rational catalyst design.

2. Experimental

2.1 Materials

Sigma Aldrich Co. Pd(II) and Rh(III) chloride (99 % and 98 %, respectively) were used as precursor salts to synthesize bimetallic PdRh NPs. 4-CP (>99 %, Sigma-Aldrich Co) was used as model compound. HCl (37 %, Panreac Quimica, S.A.U.) was used to dissolve metal precursors. Methanol (99.5 %, Panreac Quimica S.A.U.) was used as reducing agent and poly(N-vinyl-2-pyrrolidone) (PVP, average molecular weight: 40.000, Sigma-Aldrich Co.) was used as capping agent. Hydrogen (> 99 %, Praxair Spain, S.L.) was used to carry out HDC. All the reagents were used as received without additional purification.

2.2 Synthesis and characterization of bimetallic PdRh NPs

A $2 \cdot 10^{-3}$ M Rh(III) aqueous solution (pale pink colour) was obtained by mixing $RhCl_3$ (0.5 mmol), HCl 0.2N (1 mmol) and deionized water up to a final volume of 250 mL.Pd (II) chloride (0.5 mmol), HCl 0.2N (1 mmol) and deionized water (250 mL) were mixed to obtain a $2 \cdot 10^{-3}$ M Pd(II) aqueous solution (pale yellow colour). Co-reduction synthesis was performed by mixing 30 mL of a mixture of known volumes from the Pd and Rh aqueous solutions with 70 mL of 25 % methanol/water solution and PVP ($PVP_{monomer}$/metal ratio = 20 mol/mol) to obtain the colloidal synthesis of bimetallic PdRh NPs. The mixture was refluxed in a flask connected to a Liebig condenser for 5 hours at 363 K under atmospheric pressure. Successive reduction synthesis was carried

out using monometallic NPs of the selected metal as seeds, prepared as described above, and then a known volume of the other metal solution and additional reducing agent (methanol/metal ratio of 7200 mol/mol) was added under agitation. Three Pd/Rh molar ratios were used: 0.2, 1 and 5. The colloidal suspension of bimetallic NPs was concentrated up to a final volume of approximately 10 mL in a rotary evaporator (Büchi). Table 1 summarizes the working conditions used for the synthesis of bimetallic NPs and the corresponding nomenclature for them.

Table 1. Method of synthesis, Pd/Rh ratio, mean diameter (d_s), size distribution (σ_s), Pd^{n+}/Pd^0 ratio, Rh^{n+}/Rh^0 ratio, activity per unit mass (a_m). All ratios are molar.

Samples	Method of synthesis	Pd/Rh	d_s (nm)	σ_s (nm)	Pd^{n+}/Pd^0 ratio	Rh^{n+}/Rh^0 ratio	a (mmol/g_{cat}·min)
CR0.2	Co-reduction	0.2	2.7	0.8	2.06	0.99	11.2
CR1	Co-reduction	1	3.5	1.0	3.05	0.95	12.1
CR5	Co-reduction	5	4.4	2.2	0.59	0.62	46.2
SRPd0.2	Successive reduction[a]	0.2	3.1	0.5	1.83	0.68	13.4
SRPd1	Successive reduction[a]	1	3.8	1.2	1.10	1.05	63.4
SRPd5	Successive reduction[a]	5	4.2	1.6	0.51	1.44	67.0
SRRh0.2	Successive reduction[b]	0.2	4.0	0.7	1.18	0.54	17.2
SRRh1	Successive reduction[b]	1	2.4	0.8	2.28	1.26	21.6
SRRh5	Successive reduction[b]	5	5.0	2.0	0.99	1.18	35.8
B1	Blank[c]	1	8.5(Pd) 2.8(Rh)	4.6(Pd) 0.6(Rh)	1.03(Pd)	0.56(Rh)	67.2
B0.2	Blank[c]	0.2					50.7
B5	Blank[c]	5					24.2

[a] 1st Pd, 2nd Rh

[b] 1st Rh, 2nd Pd

[c] Mixture of monometallic nanoparticles,

The size of PdRh NPs was measured by transmission electron microscopy (TEM), high-angle annular dark field scanning transmission electron microscopy (HAADF-STEM) coupled with energy-dispersive X-ray spectroscopy (EDS) was used to determine the structure/composition of the bimetallic NPs and X-ray photoelectron spectroscopy (XPS) was used to determine the Pd^{n+}/Pd^{0} and Rh^{n+}/Rh^{0} ratio. TEM micrographs were obtained in a JEM-3000F + XEDS microscope at 300 kV (JEOL). ImageJ 1.44i software was used for data treatment of digital TEM images (more than 200 particles were measured per sample). Surface-area-weighted mean diameters and size distribution, characterized by the standard deviation, were calculated as described in a previous work [17]. HAADF-STEM images were obtained in a Titan 200 KV ChemiSTEM microscope (FEI Company), equipped with probe Cs corrector. Previously to characterization in Titan 200 KV ChemiSTEM, samples were exposed to 5 seconds cycles of oxygen/argon plasma in a Fischione Instrument 1020 plasma cleaner, in order to remove the PVP.

XPS profiles were obtained in an ESCA 5701 spectrometer equipped with a Mg-Kα X-ray excitation source (1253.6 eV) (Physical Electronics). A probing depth of at least several nanometres can be assumed. Thus, the Rh^{n+}/Rh^{0} ratios obtained were ascribed to the whole particles and not only to their surface. Spectra deconvolution was performed using Multipak v8.2b software in order to determine both electrodeficient and zero-valent species of the PdRh bimetallic NPs synthesized. Shirley background subtraction, smoothing and mixed Gaussian-Lorentzian by a least-square method curve fitting were applied. C 1s peak (284.8 eV) was used as internal standard for binding energies corrections due to sample charging. Doublet separation for Pd 3d was 5.26 and for Rh 3d was 4.74 eV as described elsewhere [19]. Binding energies for

$Pd3d_{5/2}$ of deconvoluted peaks were in the range of 334.65 eV and 335.76 eV which can be ascribed to metallic or zero-valent (Pd^0) and electrodeficient (Pd^{n+}) Pd species, respectively. Binding energies for Rh $3d_{5/2}$ of deconvoluted peaks were in the range of 306.00 eV and 307.32 eV which can be ascribed to metallic or zero-valent (Rh^0) and electrodeficient (Rh^{n+}) Rh species, respectively. These values are in good agreement with those reported in NIST X-ray Photoelectron Spectroscopy Database [19].

2.3 HDC experiments

A three-necked jacketed glass reactor equipped with a H_2 supply was used to carry out the HDC runs. A 4-CP aqueous solution (150 mL, 100 $mg \cdot L^{-1}$) was introduced into the reactor and H_2 was continuously passed at 50 $NmL \cdot min^{-1}$. The reaction took place during 4 hours under vigorous stirring (800 rpm) and the temperature (303 K) was controlled by a thermostatic bath (Julabo). A cold trap at the vent was used to check any possible stripping, but no significant stripping was detected. The catalyst concentration in the reaction medium was $1.23 \cdot 10^{-3}$ $g \cdot L^{-1}$ of metal.

Reaction samples (1 mL) were filtered (PTFE filter, pore size 0.45 µm) and 4-CP and phenol were analyzed by HPLC (Varian Prostar equipped with a UV-VIS detector) using a C_{18} column as stationary phase and a mixture of acetonitrile and water (1:1, v/v) as mobile phase. No reaction progress was observed once the samples were filtered and collected.

Cyclohexanone and cyclohexanol were analyzed by Gas Chromatography with FID detector (GC 3900 Varian) using a 30 m length and 0.25 mm internal diameter capillary column (CP-Wax 52 CB, Varian) and nitrogen as carrier gas. Cyclohexene was analyzed by Gas Chromatography with MS detector and an electron impact ionization

source (Saturn 2100T). This chromatograph was equipped with a column Factor Four, Varian (30 m length, 0.25 mm internal diameter). In order to check the structural assignment of the identified compounds, the NIST 05 library and analytical standards were used. No chlorinated compounds were detected in addition to 4-CP. The quantification of chloride ion was performed by Ion Chromatography (Metrohm 790 Personal IC). The carbon and chlorine mass balances matched always above 90 (90.8 – 98.3 %) and 95 % (95.9 – 99.4 %), respectively.

3. Results and discussion

3.1 Bimetallic PdRh NPs characterization

3.1.1 TEM/STEM characterization

Table 1 shows the mean diameter of the bimetallic PdRh NPs samples synthesized at fixed 25 % (v/v) methanol/water concentration and a PVP/metal molar ratio of 20, using different synthesis procedures (co-reduction and successive reduction) and Pd/Rh molar ratios. TEM images of selected samples are shown in Figure 1 as representative examples. It can be observed that the bimetallic PdRh NPs samples showed different shapes, mostly irregular globular or polyhedral-shaped. The mean diameter was estimated using the diameter of the smallest circle in which the nanoparticle fits. The sizes of the bimetallic PdRh samples were in a narrow range from 2.4 to 5.0 nm. As general trend, larger sizes were observed for the NPs with higher content of Pd, regardless the method used in the synthesis. This fact is in agreement with previous results where different range of sizes were found for Pd and Rh monometallic NPs, 2.7-22.1 nm and 1.9-4.9 nm, respectively [17, 18].

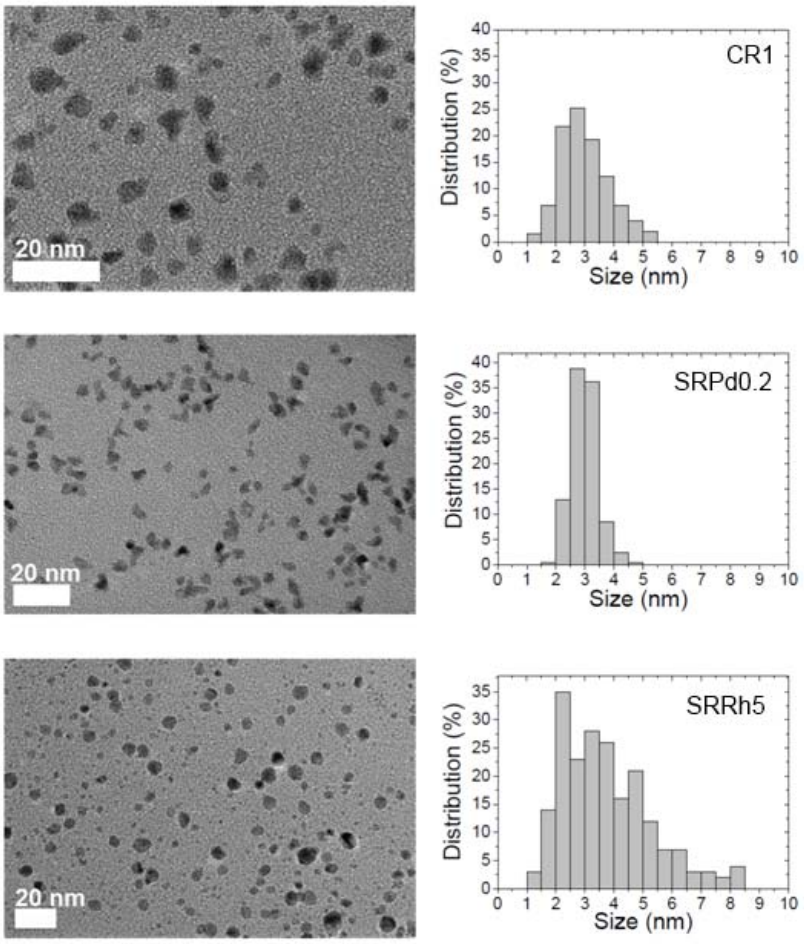

Figure 1. TEM images and size distributions of three samples (CR1, SRPd0.2 and SRRh5) of PdRh bimetallic NPs.

Moreover, the preparation of bimetallic NPs always led to obtain lower sizes when compared to the monometallic Pd NPs synthesized under the same conditions (methanol/water 25 %, v/v; PVP/metal molar ratio of 20). The presence of both metals in each sample was confirmed by EDS. Samples CR1, SRPd1 and SRPd5 were also analyzed by HAADF-STEM/EDS in order to address their nanoparticle structure. Figures 2, 3 and 4 show the elemental composition of representative nanoparticles of these three samples. The nanoparticle structures obtained in sample CR1 are mainly core-

shell-like (Pd core, Rh shell), although it is possible to find some nanoparticles with a non-completely developed shell as shown in Figure 2.

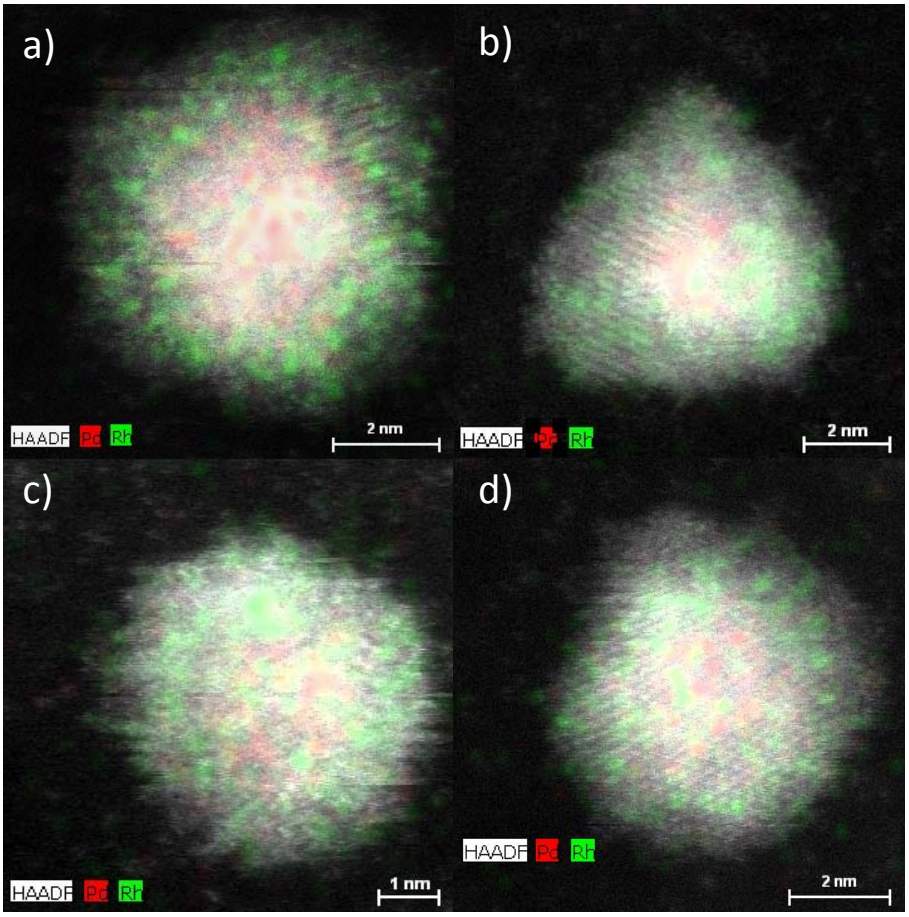

Figure 2. HAADF-STEM/EDS elemental maps of 4 representative nanoparticles (a, b, c and d) of sample CR1.

In the case of sample SRPd1 (Figure 3), core-shell is also the predominant nanoparticle structure (Pd core, Rh shell) but the contribution of Pd in the shell is clearly higher than in sample CR1.

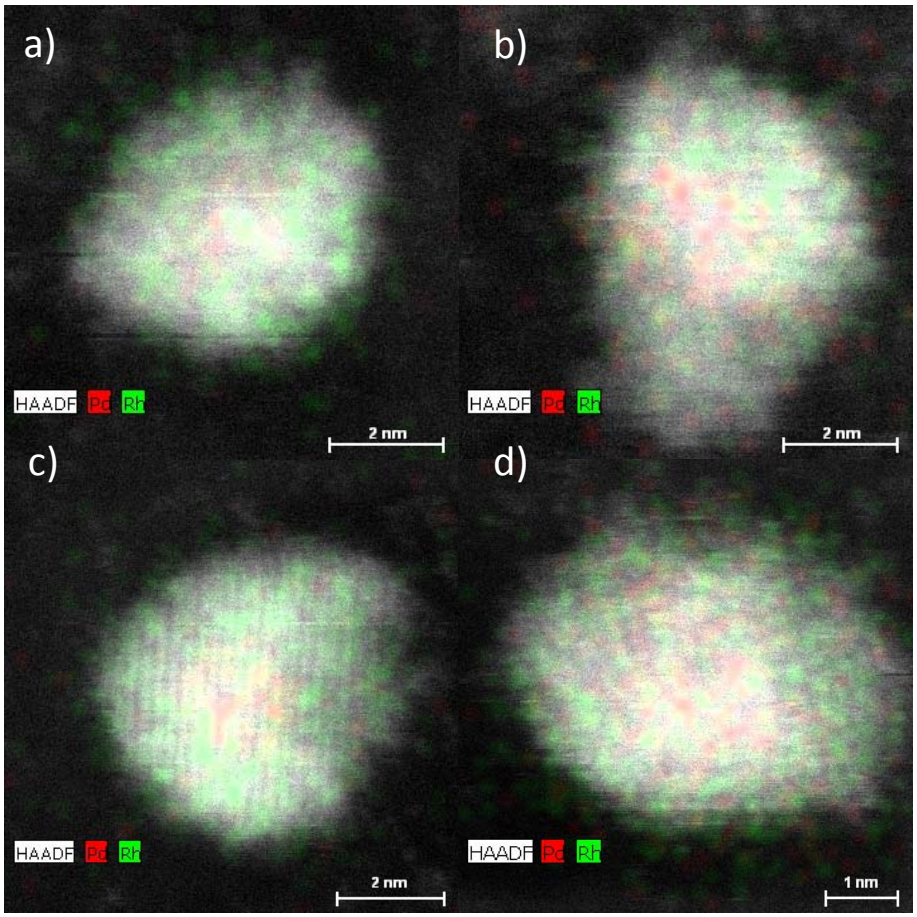

Figure 3. HAADF-STEM/EDS elemental maps of 4 representative nanoparticles (a, b, c and d) of sample SRPd1.

In Figure 4 it can be observed that sample SRPd5 exhibits nanoparticles where cluster-in-cluster structures were the most abundant. No relationship between nanoparticle structure and method of synthesis were found, since samples CR1 and SRPd1 were synthesized by co-reduction and successive reduction, respectively, and both led to a core-shell-like structure. This could be related to the difference in redox potential between Pd^{2+}/Pd^{0} and the Rh^{3+}/Rh^{0}, with values close to 0.95 eV and 0.76 eV, respectively, which favors the reduction of Pd before Rh. Moreover, different nanoparticle structures can be obtained using the same method of synthesis, by changing the molar ratio between metals Pd/Rh as can be observed in samples SRPd1

and SRPd5. Migration of Pd or Rh has been previously reported for Pd/Rh core-shell nanoparticles [20], which could explain the occurrence of cluster-in-cluster structures when successive reduction was used in synthesis at a Pd/Rh molar ratio of 5.

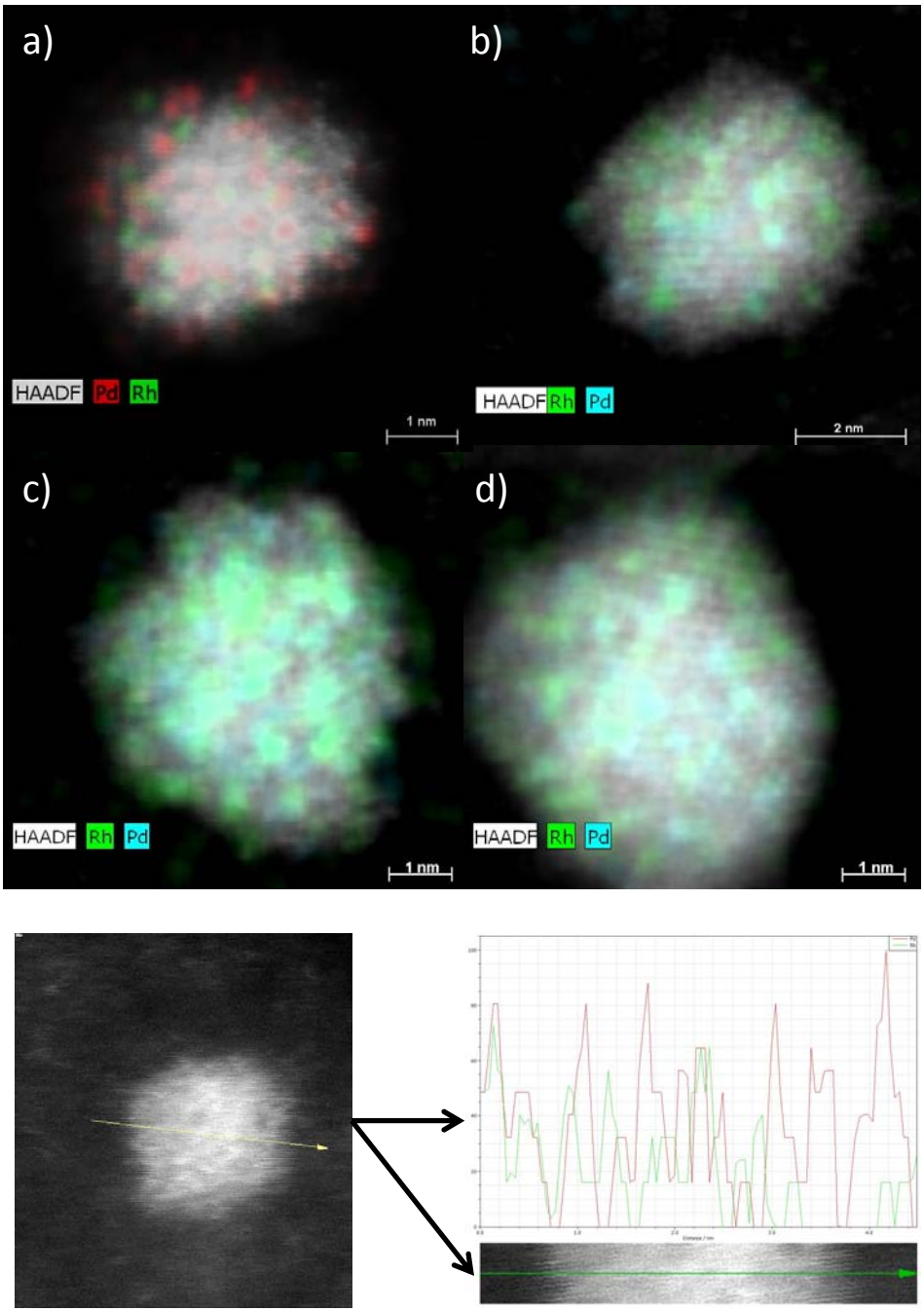

Figure 4. HAADF-STEM/EDS elemental maps of 4 representative nanoparticles (a, b, c and d) and a scanline of nanoparticle a) (Pd red, Rh green) of sample SRPd5.

3.2. XPS characterization

XPS spectra were obtained in order to determine the oxidation state of PdRh bimetallic NPs. Table 1 summarizes the values of Pd^{n+}/Pd^0 and Rh^{n+}/Rh^0 ratios obtained from the deconvolution of the 3d region spectra of Pd and Rh XPS. Both electrodeficient and zerovalent species of Pd and Rh were identified in all samples. The Rh^{n+}/Rh^0 ratio values were in the range from 0.54 to 1.44, whereas those of Pd^{n+}/Pd^0 covered a wider range of 0.51 – 3.05. As representative examples, Figure 5 shows the Pd and Rh 3d deconvolved spectra for a selected sample of NPs (SRPd1). In general, from the results of Table 1 it can be seen that co-reduction led to NPs with lower Rh^{n+}/Rh^0 ratios, except for the samples with the highest Rh contents (SRPd0.2 and SRRh0.2). Though the reduction method does not show a clear effect on the Pd^{n+}/Pd^0 ratio, it can be pointed out that the NPs prepared with the highest Pd/Rh molar ratio (5) showed lower proportion of electrodeficient Pd.

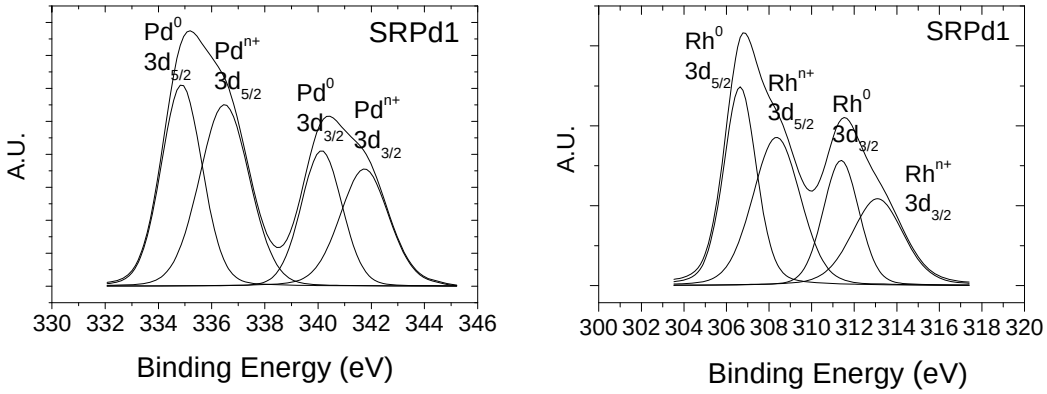

Figure 5. Pd 3d and Rh 3d deconvolved XPS spectra of SRPd1 sample.

Figure 6 depicts the Pd^{n+}/Pd^0 and Rh^{n+}/Rh^0 ratios versus the mean size of NPs. Lower Pd^{n+}/Pd^0 ratios (0.51 – 0.99), were obtained for the larger size NPs (>4 nm). This behavior differs from data previously reported for monometallic Pd NPs [17], where the lower Pd^{n+}/Pd^0 ratios ranging (0.35 - 0.67) corresponded to the smaller particles (2.7 to 4.2 nm).

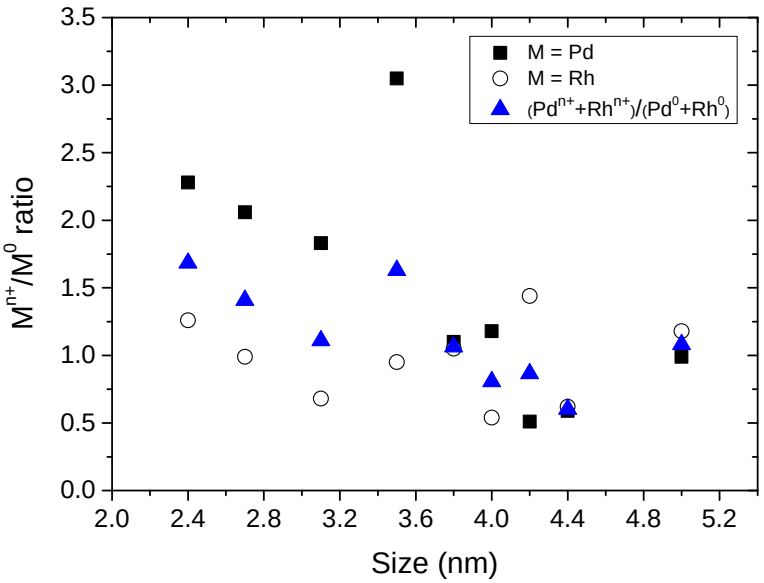

Figure 6. Pd^{n+}/Pd^0, Rh^{n+}/Rh^0 and$(Pd^{n+}+Rh^{n+})/(Pd^0+Rh^0)$ ratio versus NP mean size.

The reduction of Pd seems to be favored by the presence of Rh, which can be explained by the difference in standard electrode potential of Pd^{2+}/Pd^0 and Rh^{3+}/Rh^0, with values close to 0.95 eV and 0.76 eV, respectively. No defined trend was observed for the Rh^{n+}/Rh^0 ratios, being all the values within a narrower range. Comparing the Pd^{n+}/Pd^0 and Rh^{n+}/Rh^0 ratios with those of the corresponding monometallic NPs synthesized at the same conditions, different behavior was observed for the two metals. Thus, the proportion of Rh^{n+} species in the bimetallic NPs remained unaltered or increased in comparison with monometallic NPs, whereas the proportion of

Pd^{n+}species increased for Pd/Rh ratios of 0.2-1 and decreased for a ratio of 5. Therefore, redox interactions between both metals are significant, as it has been reported for other bimetallic systems [21]. Moreover, largest bimetallic NPs (>4 nm) were related to higher Pd/Rh ratios.

3.3. HDC experiments

Control runs of 4-CP HDC using different PVP concentrations were performed in order to check its possible interaction with H_2 between 4-CP, H_2 and PVP. Additionally, control experiments were also carried out in the absence of catalysts. No effect of PVP was observed and no reaction products were detected in the absence of metal NPs. Different loads of catalyst and stirring velocities were also checked in previous experiments in order to confirm that the process takes place under chemical control.

3.3.1 Activity of PdRh NPs

4-CP conversion versus reaction time with all the NPs series is showed in Figure 7. All the catalysts tested achieved 4-CP conversion values within the range from 85 % to 100 % after 4h reaction time. That Figure also includes the runs carried out mixing the Rh and Pd monometallic NPs, which were synthesized at the same conditions than the bimetallic ones and were considered as blanks. Important differences in activity can be observed depending on the method followed for the preparation of the NPs. Comparison with the blanks indicates that not only synergistic, but also antagonist effects occur.

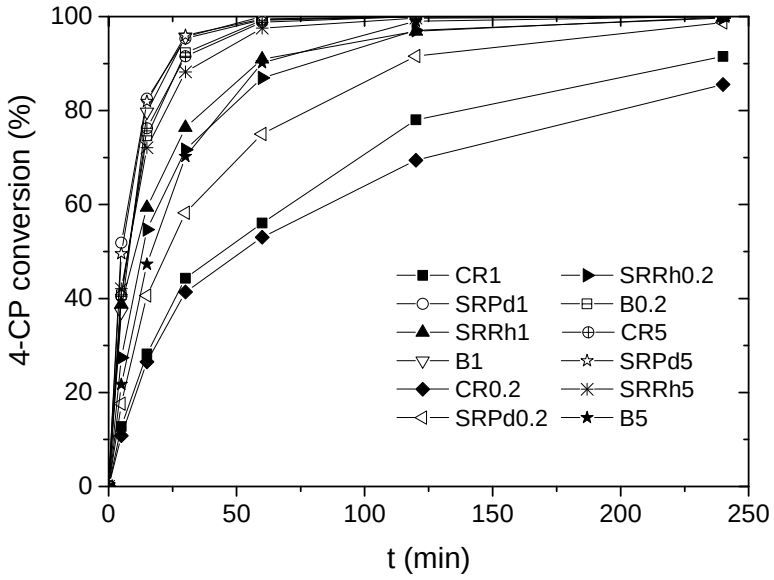

Figure 7. 4-CP conversion versus reaction time for all the catalysts tested.

The rate of 4-CP disappearance was calculated from a simple pseudo-first order equation:

$$(-r_{4-cp}) = \frac{-dC_{4-cp}}{dt} = k_1 \times C_{4-cp} \qquad [1]$$

$$t = 0; \quad C_{4-cp} = C_0$$

Since hydrogen is in great excess, its concentration can be included in the pseudo-first-order rate constant (k_1), whose values are given in Table 2, together with those of the correlation coefficient. Good fitting results were obtained, as can be observed from the regression coefficients in Table 2, which also makes possible to assume that there is no catalysts deactivation after 4 h of reaction.

Table 2. Values of the pseudo-first order rate constant (min^{-1}) of 4-CP HDC

Samples	k_1 ($\cdot 10^{-3}$)	r^2
CR0.2	11.05	0.98
CR1	14.55	0.99
CR5	76.40	0.95
SRPd0.2	25.64	0.99
SRPd1	108.48	0.99
SRPd5	125.13	0.98
SRRh0.2	23.35	0.99
SRRh1	56.12	0.98
SRRh5	72.04	0.95

The initial activity (a) of PdRh bimetallic NPs was calculated from the k_1 values, the 4-CP initial concentration and the Pd-Rh dose used in the experiments, according to equation [2]. The values are included in Figure 1.

$$a = k_1 \times \frac{C_{0\,4-CP}}{C_{Pd-Rh}} \quad [2]$$

A wide range of activity values from 11.2 to 67.0 $mmol \cdot g^{-1} \cdot min^{-1}$ can be observed. The highest activity values (63.4 – 67.0 $mmol \cdot g^{-1} \cdot min^{-1}$) were significantly above those obtained in previous works using monometallic Pd (39.1 $mmol \cdot g^{-1} \cdot min^{-1}$) or Rh (29.4 $mmol \cdot g^{-1} \cdot min^{-1}$) NPs as catalysts [17, 18], thus showing the synergy between these metals when bimetallic NPs are synthesized under adequate conditions.

The lowest activity values (11.2 and 12.1 $mmol \cdot g^{-1} \cdot min^{-1}$) were obtained with the NPs synthesized by co-reduction, with the exception of the sample CR5 (46.2 $mmol \cdot g^{-1} \cdot min^{-1}$) prepared with the highest Pd/Rh molar ratio (5). The NPs synthesized by successive reduction using Pd NPs as seeds showed the highest activity values (67.0 and 63.4 $mmol \cdot g^{-1} \cdot min^{-1}$), except for sample SRPd0.2 (13.4 $mmol \cdot g^{-1} \cdot min^{-1}$) which contains the lowest Pd/Rh molar ratio (0.2). On the other hand, successive reduction synthesis using Rh NPs as seed showed intermediate to high activity values (17.2 – 35.8 $mmol \cdot g^{-1} \cdot min^{-1}$). Significant differences in activity between the NPs synthesized with the highest load of Pd (35.8 – 67.0 $mmol \cdot g^{-1} \cdot min^{-1}$) and those synthesized with the lowest one (11.2 – 17.2 $mmol \cdot g^{-1} \cdot min^{-1}$) were found. The NPs with equimolar ratio of Pd and Rh yielded a wide range of activity values, from 12.1 to 63.4 $mmol \cdot g^{-1} \cdot min^{-1}$, showing a higher influence of the synthesis procedure.

In the case of the binary mixtures of monometallic NPs (blanks), fairly high activities were obtained at Pd/Rh ratios of 0.2-1, suggesting that to take advantage of the synergy between Pd and Rh their arrangement in bimetallic particles is not essential at low Pd/Rh ratios. However, among NPs of equimolar Pd/Rh (1) a substantial effect of the of the NPs synthesis method is observed. The NPs from CR1 sample exhibited a clear core-shell structure with a higher proportion of Rh at the shell (Figure 2). This structure seems to be detrimental, since it leads to lower activities than the blank (Figure 7). This can be related with a higher competence for active centers between 4-CP and the subsequent hydrogenation by-products in the case of Rh-based NPs [17, 18]. On the contrary, the sample SRPd1 also showed a core-shell arrangements (Figure 3), but with higher contribution of NPs where the core-shell structure is not so clear and with higher exposure of Pd, thus yielding a remarkable

activity. In the case of the samples with the highest Pd/Rh ratio (5) a substantial difference is observed between the activity of the blank (24.2 $mmol \cdot g^{-1} \cdot min^{-1}$) and that of the bimetallic NPs prepared by different procedures (35.8-67.0 $mmol \cdot g^{-1} \cdot min^{-1}$), showing the highest activity the SRPd5 sample, which is characterized for a cluster-in-cluster structure with presence of both Pd and Rh domains on the surface of the NPs (Figure 4). The activity is represented versus the mean size of the bimetallic PdRh NPs in Figure 8. As shown, bimetallic NPs smaller than 3.5 nm showed lower activity values (11.2 - 21.6 $mmol \cdot g^{-1} \cdot min^{-1}$) than those with higher size (35.8 – 67.2 $mmol \cdot g^{-1} \cdot min^{-1}$), with the exception of sample SRRh0.2 (4.0 nm; 17.2 $mmol \cdot g^{-1} \cdot min^{-1}$). The main difference between this sample and those with sizes beyond 3.5 nm is its lower Pd content, this effect prevailing over that of particle size. Thus, it can be concluded that a high activity is also associated with a high relative content of Pd.

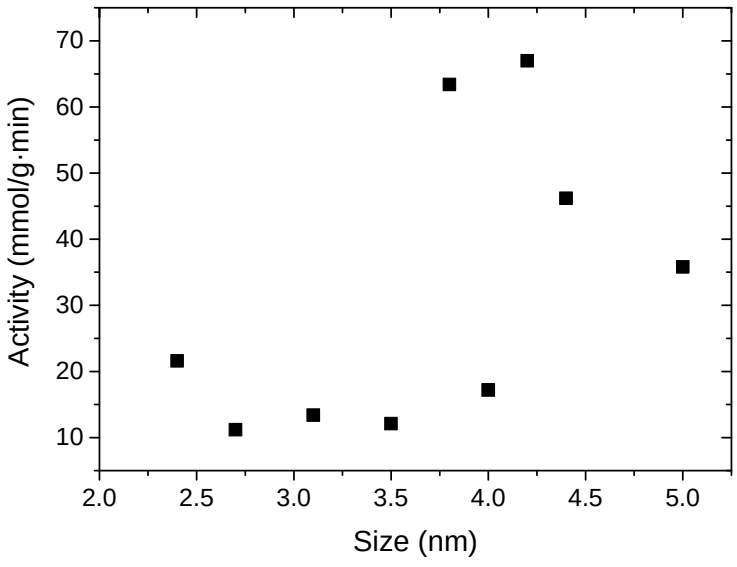

Figure 8. Activity versus mean size of the bimetallic RhPd nanoparticles.

Figure 9 depicts the activity against the starting Pd^{n+}/Pd^0 and Rh^{n+}/Rh^0 ratios. As can be seen, the highest activity values were achieved with the NPs with starting Pd^{n+}/Pd^0ratio around or below 1. No relationship between the activity and the Rh^{n+}/Rh^0 ratio was found, although this may be due to the narrower range covered of that ratio compared to the Pd^{n+}/Pd^0 one. As indicated before, the sample SRRh0.2, characterized by a remarkably low Rh^{n+}/Rh^0 ratio, yielded a low activity. This is an interesting result, since in a previous work the important role of the Rh^0 species in the activity of Rh NPs was shown [18].

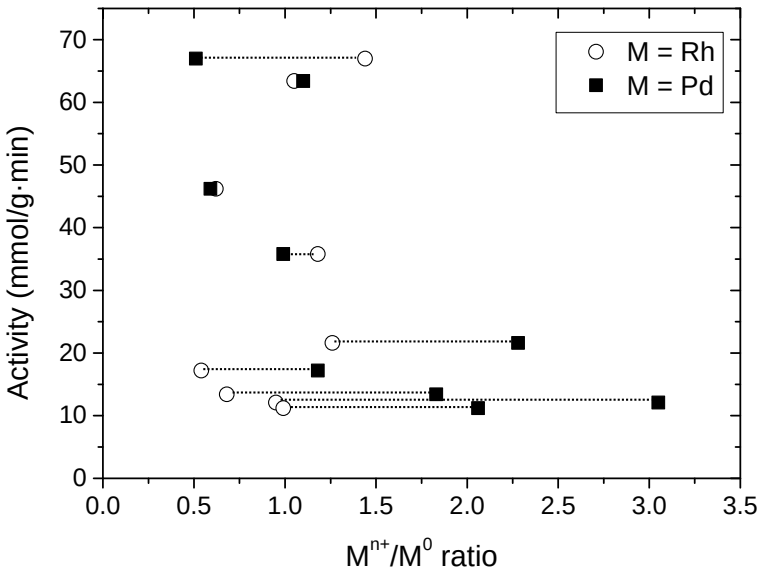

Figure 9. Pd^{n+}/Pd^0 and Rh^{n+}/Rh^0 ratio versus activity.

3.3.2 Selectivity of PdRh bimetallic NPs

Phenol, cyclohexanone and cyclohexanol were identified as by-products of 4-CP HDC in all the cases, but differences in selectivity were found between the bimetallic samples tested. Cyclohexene was in very low concentrations (less than 2 $mg \cdot L^{-1}$) when

detected and was not considered for the selectivity study. The occurrence of cyclohexene has been attributed to the dehydration of cyclohexanol and the products distribution is consistent with the mechanism described in previous works [22]. Thus, phenol has been proposed as the only HDC product from 4-CP, undergoing subsequent hydrogenation to cyclohexanone and this last to cyclohexanol.

Figure 10 shows the evolution of the selectivity to phenol, cyclohexanone and cyclohexanol with 4-CP conversion for the NPs prepared with a Pd to Rh equimolar ratio (samples CR1, SRPd1, SRRh1 and B1). Important differences in selectivity can be observed depending on the different methods of synthesis. For CR1 sample, the relationship between the selectivity towards phenol and 4-CP conversion was rather linear, indicating that phenol is easily hydrogenated to cyclohexanol even when the concentration of 4-CP in the reaction medium is still high. On the contrary, with the NPs prepared by successive reduction SRPd1 and SRRh1, HDC of 4-CP leads essentially to phenol (selectivity around 90%) until conversion values well above 80%. This behavior is even more pronounced in the case of the blank (B1). Cyclohexanol was the minor reaction product in all cases and the selectivity to it was only relevant at high 4-CP and phenol conversion values, although much earlier occurrence was observed with the CR1 sample.

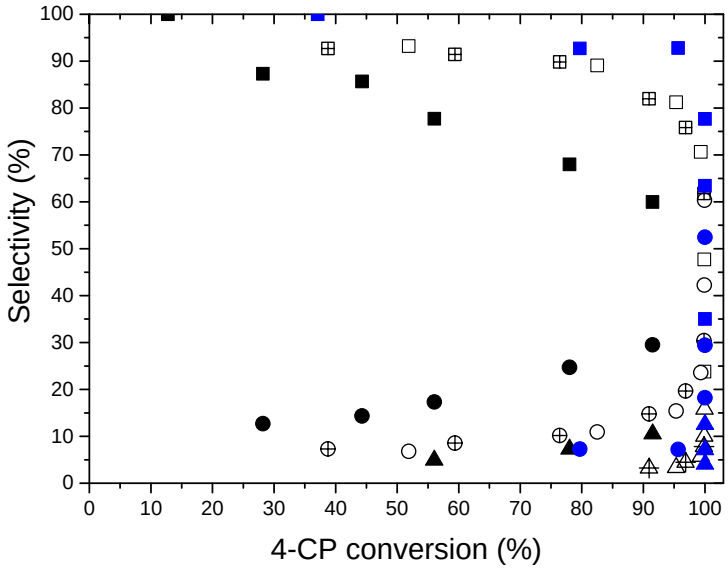

Figure 10. Selectivity towards phenol (squares), cyclohexanone (circles) and cyclohexanol (triangles) versus 4-CP conversion for samples CR1 (solid), SRPd1 (open), SRRh1 (crossed-open) and B1 (solid blue).

As shown in Figure 2 and 3, core-shell nanoparticle structures are characteristic of CR1 and SRPd1 samples, where the proportion of Rh is higher in the shell. CR1 and SRPd1 samples showed similar size (3.5 and 3.8 nm, respectively) and Rh^{n+}/Rh^{0} ratio (0.95 and 1.05, respectively), but fairly different Pd^{n+}/Pd^{0} ratio (3.05 and 1.10, respectively). The HAADF-STEM/EDS characterization of CR1 sample showed a higher concentration of Rh at the outer surface of the NPs, which may be behind the higher selectivity to phenol hydrogenation products. Besides, the presence of Pd in the structure of the NPs seems to have a role in the hydrogenation activity, as can be observed from the low conversion of phenol achieved with the blank.

The results in Figure 10 indicate that for the equimolar mixture of monometallic NPs (B1) the competition for active sites on the metal surface is more evident,

prevailing the interaction between 4-CP and the surface, and the occurrence of phenol, cyclohexanone and cyclohexanol only become important when the conversion of 4-CP is high. This effect is attenuated, but still evident when the NPs are synthesized by co-reduction, with some differences in behavior depending on the metal used as seeds, as can be seen in Figure 11, where 4-CP, phenol, cyclohexanone and cyclohexanol concentration versus reaction time have been plotted for samples B1, SRPd1 and SRRh1. At 100 % 4-CP conversion (4 h reaction time) the selectivity towards cyclohexanol is significantly higher in the case of SRPd1 (16 %) than with SRRh1 (8 %), which also can be related with the higher proportion of Rh at the outer part of the NPs. This seems to lead to higher competence for active sites, since with SRPd1 (open symbols in Figure 8) the occurrence of cyclohexanol takes place at higher 4-CP conversion values. This strong competition has also been observed for monometallic Rh NPs [18].

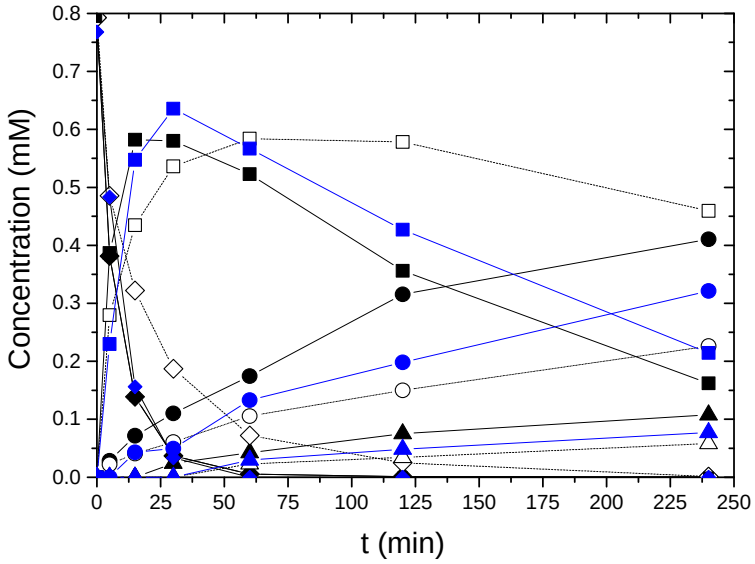

Figure 11. 4-CP (rhombuses), phenol (squares), cyclohexanone (circles) and cyclohexanol (triangles) concentration versus time with NPS of the SRPd1 (solid), SRRh1 (open) and B1 (blue) series.

Interestingly, the catalysts with higher hydrogenation ability (CR1) showed a remarkably low activity in dechlorination, well below that of the blank. Compared to the blank, CR1, SRPd1 and SRRh1 samples showed a higher selectivity towards cyclohexanone and cyclohexanol at shorter reaction times and lower 4-CP conversions, suggesting that in the blank experiments only Rh NPs are involved in hydrogenation and there is a synergy between both metals in the bimetallic NPs. SRPd1 and B1 showed a quite similar activity (63.4 versus 67.2 $mmol \cdot g^{-1} \cdot min^{-1}$, respectively, but at 95 % 4-CP conversion SRPd1 showed selectivities of 15% and 3% towards cyclohexanone and cyclohexanol ,respectively, whereas those values reached only 7 % and 0% with B1

For the NPs with the lowest Pd/Rh molar ratio (CR0.2, SRPd0.2 and SRRh0.2 samples), the activity order in the hydrogenation of phenol and cyclohexanone was: CR0.2 > SRPd0.2 > SRRh0.2 > B0.2, the most active leading to higher selectivity to cyclohexanone and cyclohexanol and hydrogenation from low 4-CP conversion values. Thus, when compared to the blank (B0.2), co-reduction and successive reduction with Pd NPs as seeds led to bimetallic NPs with higher hydrogenation ability, suggesting again the role of the Rh allocated at the outer part of the NPs and the synergy between both metals.

Figure 12 depicts the evolution of the selectivities to the different reaction products upon 4-CP conversion with the NPs prepared with a Pd/Rh molar ratio of 5 (samples CR5, SRPd5, SRRh5 and B5), the highest tested. The three former yielded significantly higher selectivities to cyclohexanone (> 27 %) compared to the blank (B5, < 4 %). Moreover, they showed ability to hydrogenate cyclohexanone to cyclohexanol, which is not the case of the blank. When comparing the selectivities of the samples synthesized by successive reduction (Figure 13) lower hydrogenation ability can be observed with the NPs prepared using Rh seeds (SRRh5), which can be associated to a lower presence of Pd at the outer surface.

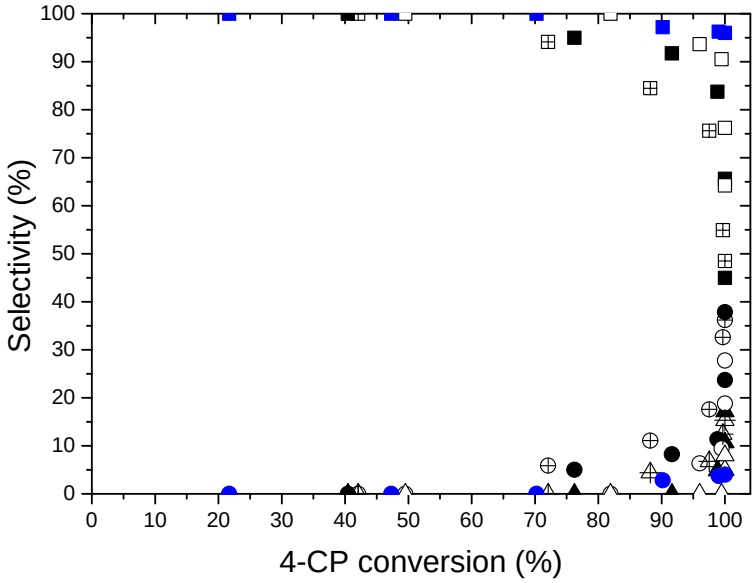

Figure 12. Selectivity towards phenol (squares), cyclohexanone (circles), cyclohexanol (triangles) versus 4-CP conversion with NPs of the CR5 (solid), SRPd5 (open) and SRRh5 (crossed-open) and B5 (blue) series.

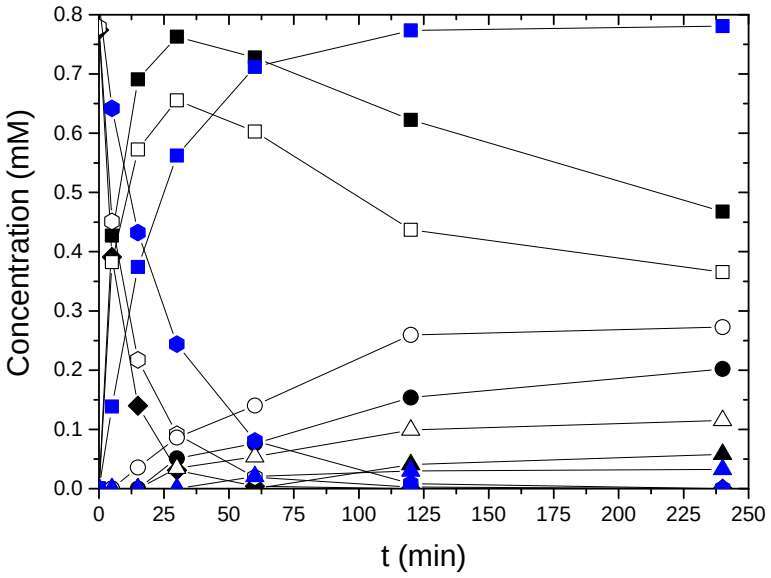

Figure 13. 4-CP (rhombuses), phenol (squares), cyclohexanone (circles) and cyclohexanol (triangles) concentration versus time with the NPs of SRPd5 (solid), SRRh5 (open) and B5 (blue) series.

4. Conclusions

Bimetallic PdRh NPs were synthesized and tested in 4-CP HDC under mild conditions (303 K, 1 atm). The method of synthesis (co-reduction and successive reduction) and the Pd/Rh molar ratio had a clear influence in the NPs structure, although no relationship between method of synthesis and type of NPs structure obtained (core-shell/cluster-in-cluster) was found. All the catalysts tested achieved high 4-CP conversion values after 4 h of reaction time in the range from 85 % to 100 % at very low metal concentration.

The results indicated that the study of the performance of Pd/Rh bimetallic catalysts in HDC cannot be evaluated without some consideration about the structure of the NPs,

since the metal arrangement can lead to both synergistic and antagonist effects in the activity and selectivity of the catalysts.

The activity in 4-CP HDC was enhanced by a high content of Pd in the metal NPs, although a clear improvement in comparison to the activity of mixtures of monometallic NPs was only observed for Pd/Rh ratios of 5. A lower activity in the HDC of 4-CP was observed for metal arrangements in the nanoparticles where Rh was in higher proportion at the outer surface of the NPs. However, this arrangement was found to lead to much higher hydrogenation ability. Therefore, these opposite effects must be balanced basis on the purpose of the catalysts.

In spite of the prominent role of Rh in the hydrogenation ability, the presence of Pd in the structure of the NPs was essential to achieve high selectivity towards phenol hydrogenation products, as shown by the comparison to the mixtures of metallic nanoparticles.

Acknoledgements

We acknowledge the financial support from MINECO (CTQ2012-32821) and CAM (REMTAVARES S-2009/AMB-1588). J.A. Baeza is grateful to the Spanish MICINN for a research grant (BES-2010-030059).

References

[1] M. Munoz, Z.M. de Pedro, N. Menendez, J.A. Casas, J.J. Rodriguez, AppliedCatalysis B: Environmental 136–137 (2013) 218.

[2] Paul M. McKee, Richard P. Scroggins, David M. Casson., Chlorinated phenols in the aquatic environment. Scientific criteria document for standard development no. 2-84. , Queen's printer for Ontario. Ontario Ministry of Environment., Ontario, 1984.

[3] P.D. Warrington, Ambient Water Quality Guidelines for Chlorophenols, BC Ministry of Environment, Water Management Branch, British Columbia, Canada, 1997.

[4] G. Yuan, M.A. Keane, Catalysis Today 88 (2003) 27.

[5] C. Xia, Y. Liu, S. Zhou, C. Yang, S. Liu, J. Xu, J. Yu, J. Chen, X. Liang, Journal of Hazardous Materials 169 (2009) 1029.

[6] G. Yuan, M.A. Keane, Chemical Engineering Science 58 (2003) 257.

[7] L. Calvo, M.A. Gilarranz, J.A. Casas, A.F. Mohedano, J.J. Rodríguez, AppliedCatalysis B: Environmental 67 (2006) 68.

[8] K.V.R. Chary, P.V.R. Rao, V. Vishwanathan, Catalysis Communications 7 (2006) 974.

[9] M. Bonarowska, Z. Kaszkur, L. Kępiński, Z. Karpiński, Applied Catalysis B: Environmental 99 (2010) 248.

[10] E. Diaz, A.F. Mohedano, J.A. Casas, L. Calvo, M.A. Gilarranz, J.J. Rodriguez, AppliedCatalysis B: Environmental 106 (2011) 469.

[11] S. Gómez-Quero, F. Cárdenas-Lizana, M.A. Keane, Journal of Catalysis 303 (2013) 41.

[12] D. Wang, Y. Li, Adv Mater 23 (2011) 1044.

[13] N. Toshima, H. Yan, Y. Shiraishi, in: B. Corain, G. Schmid and N. Toshima (Eds.), Metal Nanoclusters in Catalysis and Materials Science, Elsevier, Amsterdam, 2008, p. 49.

[14] K. Shin, D.H. Kim, S.C. Yeo, H.M. Lee, Catalysis Today 185 (2012) 94.

[15] B.R. Cuenya, Thin Solid Films 518 (2010) 3127.

[16] N. Toshima, T. Yonezawa, New J. Chem. 22 (1998) 1179.

[17] J.A. Baeza, L. Calvo, M.A. Gilarranz, A.F. Mohedano, J.A. Casas, J.J. Rodriguez, Journal of Catalysis 293 (2012) 85.

[18] J.A. Baeza, L. Calvo, M.A. Gilarranz, J.J. Rodriguez, Chem. Eng. J. 240 (2014) 271.

[19] http://srdata.nist.gov/xps/.

[20] F. Tao, M. Grass, Y. Zhang, D. Butcher, J. R. Renzas, Z. Liu, J. Y. Chung, B.S. Mun, M. Salmeron, G. Somorjai, Science, 2008, 322, 5903, 932

[21] M.Harada, K. Asakura, N. Toshima, J. Phys. Chem., 1993, 97, 5103

[22] T.T. Bovkun, Y. Sasson, J. Blum, Journal of Molecular Catalysis A: Chemical 242 (2005) 68.

CAPÍTULO V /CHAPTER V

Unsupported PVA and PVP stabilized Pd nanoparticles as catalyst for nitrite hydrogenation in aqueous phase

Y. Zhao, J.A. Baeza, N. Koteswara Rao, L. Calvo, M.A. Gilarranz, Y.D. Lib, L. Lefferts, J. Catal. 318 (2014) 162-169

Abstract

Pd colloids stabilized with polyvinyl alcohol (PVA) and polyvinylpyrrolidone (PVP) have been prepared, characterized with TEM, zeta-potential measurements, CO chemisorption in aqueous phase and ATR-IR spectroscopy using CO as a probe molecule, and finally tested for performance in nitrite hydrogenation as unsupported nanoparticles. Polymer coverage on Pd surface was significant for both Pd-PVA and Pd-PVP colloid, blocking active sites. The turn-over-frequency (TOF) of the remaining sites as well as selectivity to ammonium was not influenced by PVA; however, the ammonium selectivity increased with increasing Pd particle size. In contrast, increasing PVP coverage on Pd surface increased the TOF, while the ammonium formation was suppressed. This has been attributed to an effect of PVP on the surface reaction intermediates, based on the observation that chemisorbed CO was also influenced by PVP.

Keywords: Pd, colloid, PVA, PVP, nitrite hydrogenation

Introduction

Colloidal methods are widely used to prepare model catalyst with accurately controlled particle sizes and shapes. [1-3] Such colloids, containing metallic nanoparticles, can be used either to prepare supported catalysts via immobilization on support material, or to apply directly as a catalyst after dispersion in liquid reaction medium. [4]

To prepare colloid, stabilizers are usually necessary during colloid preparation to limit crystal growth and particle agglomeration in order to control the size of the nanoparticles. [3, 5-8] Polymers, such as polyvinyl alcohol (PVA) and polyvinylpyrrolidone (PVP), are commercially available, relatively inexpensive, well water-soluble, nontoxic, and very effective stabilizers for colloid preparation. [9] These two polymers both contain a long-carbon-chain back-bone with different functional groups, where PVA contains hydroxyl groups whereas PVP contains pyrrolidone groups, as shown in Scheme 1.

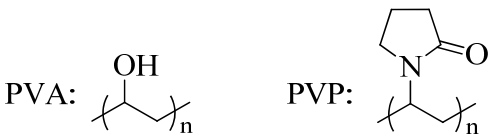

Scheme 1. Molecular structure of PVA and PVP

Obviously, stabilizers interact with the surface of the nanoparticles competing with reactant molecules, acting as a (partial) surface poison by blocking active sites [10-12] . Therefore, obtaining “clean” particles without significant change of size and shape of the nanoparticles has become a major challenge in the case of supported catalysts prepared via colloidal methods. Methods based on exposure to ozone with UV-light, [13] as well as thermal treatments in oxidative, reducing and inert atmosphere have been explored with limited success, often

resulting in deteriorating particle size and shape or incomplete removal and formation of carbonaceous deposits blocking the surface. [14-19] On the other hand, partial removal of polymer stabilizer already increases activity significantly of e.g. Pt/TiO_2 catalyst for CO oxidation in gas phase and alcohol oxidation in liquid phase. [20].

Also, favourable effects of polymer stabilizers, such as PVP, on catalyst performance have been reported. Quintanilla et al. reported that PVP increases the activity of Au/Al_2O_3 for liquid phase oxidation of benzyl alcohol. [11] When using colloid metal particles directly, without a support material, stabilizers are clearly necessary to prevent agglomeration during the catalytic experiment. Evangelisti et al. reported PVP was responsible for high stereo-selectivity to *cis*-alkenes for hydrogenation of aliphatic alkynes with Pd-PVP colloid. [21] PVP was also reported to enhance activity of Au-PVP colloid for aerobic oxidation of alcohols especially for very small nanoparticles (<1.5 nm). [22, 23]

In this contribution, unsupported Pd-PVA and Pd-PVP colloids were used as catalysts to ensure absence of any support effect in nitrite hydrogenation. Colloids with different Pd particle sizes were prepared by altering the concentration of these two commonly used polymer stabilizers. It will be shown that the functional groups influence the catalytic performance of the Pd colloid.

2. Experimental

5.2.1 Chemicals. Sodium tetrachloropalladate (II) (Na_2PdCl_4 ≥ 99.995% (metal basis)), polyvinyl alcohol (PVA, average MW = 13000 – 23000, 87% – 89% hydrolyzed), polyvinylpyrrolidone (PVP, average MW = 40000), and sodium borohydride ($NaBH_4$, ≥ 96% (gas-volumetric) were purchased from Sigma-Aldrich. Sodium nitrite (> 99%) was purchased from Merck. All the aqueous solutions were prepared using ultra purified water obtained on water purification system (Millipore, Synergy).

5.2.2 Pd-PVA Colloid Preparation. PVA was dissolved in water at 70°C with stirring for 2 hours. The solution (2 wt %) was then cooled down to room temperature. Aqueous solution of Na_2PdCl_4 (20 mL, containing 0.086 mmol Pd) and 1.76 mL of freshly prepared PVA solution (2 wt %) were added to 240 mL water, obtaining a yellow-brown solution. After 3 min, $NaBH_4$ solution (1.72 mL, 0.172 mmol) was added with a syringe pump under vigorous stirring. Brown Pd colloid solution was immediately formed. The final pH was around 9. The procedure as described leads to a molar ratio of polymer-monomer/Pd ($polymer_{mono}$/Pd) equal to 9.3 (mol/mol); this ratio was varied between 1.2 and 9.3 by varying the volume of the polymer solution.

5.2.3 Pd-PVP Colloid Preparation. Similar to Pd-PVA colloid preparation, PVP aqueous solution (5.04 wt %) was prepared at room temperature. Aqueous solution of Na_2PdCl_4 (20 mL, containing 0.086 mmol Pd) and 1.76 mL of freshly prepared PVP solution (5.04 wt %) were added to 240 mL water ($polymer_{mono}$/Pd = 9.3, mol/mol). After 3 min, $NaBH_4$ solution (1.72 mL, 0.172 mmol) was added with a syringe pump under vigorous stirring. Brown Pd colloid solution

was immediately formed. The final pH was around 9. Also in this case the $polymer_{mono}$/Pd ratio was varied by varying the volume of the polymer solution.

5.2.4 Electron Microscopy. Pd particle size distribution was determined using TEM (Philips CM300ST-FEG) with a resolution of 1 nm. Typically 2 µL colloidal suspension was dropped and dried on a copper grid covered with hollow carbon for TEM image taking. Pd particle sizes were determined with ImageJ at minimal 7 locations on the grid, and at least 500 Pd particles were measured. A Cu grid covered with graphene modified lacey carbon grid was used instead when HRTEM images was taken on the same apparatus.

5.2.5. Zeta Potential. The zeta potential of the Pd colloid dispersed in the reaction suspension after reaction at pH = ~8.5 was characterized by a Zetasizer Nano ZS ZEN3600 instrument (Malvern Instruments) at 25^{o}C using laser with wavelength of 633 nm.

5.2.6 ATR-IR of Adsorbed CO. The as-prepared colloidal suspension was sprayed on a ZnSe crystal (Internal Reflection Element) to form a catalyst layer of a few micron thick. Then the crystal was mounted in a home-build *in-situ* ATR-IR(Attenuated Total Reflection Infrared Spectroscopy) cell which has been described in detail elsewhere.[24] The cell was mounted in the sample compartment of an infrared spectrometer (Bruker Tensor 27) equipped with a MCT detector. All the measurements were done at room temperature (293 K) with a resolution of 4 cm^{-1}. Typically the sample was reduced in a H_2 flow for 2 h, followed by flushing in Ar for 30 min. The last spectrum in Ar was used as background. IR spectra were recorded every minute with 128 scans during exposing the sample to pure CO for 30 min, followed by flushing with Ar for 30 min.

5.2.7. CO Chemisorption in Aqueous Phase. The accessibility of surface Pd atoms of the colloid in aqueous phase was characterized by CO chemisorption, in a home-built apparatus equipped with a glass vial and a Teflon coated magnetic stir-bar with a stirring rate of at least 500 rpm. 4 mL of 3.3×10^{-4} mol_{Pd} L^{-1} of Pd colloid was first reduced in H_2 flow for 1 h followed by flushing in He for 30 min. Then CO pulses were introduced via a six-port valve with a 50 µL loop and the response in the exiting gas stream was measured on-line with a quadrupole mass spectrometer (MS, Pfeiffer AG Balzers, OmniStar, (m/z=28)). The amount CO in every pulse was estimated based on the integrated area of the response signal recorded as a function of time. Pulsing was repeated until saturation occurred, implied by that the peak area of subsequent CO peaks became constant and equal to the peak area of the original pulse. The total amount of chemisorbed CO was calculated by summing the amounts of CO adsorbed during each individual pulse. A typical result is shown in Figure S-2 in the Supporting Information.

5.2.8. Nitrite Hydrogenation. The reactions involved in nitrite hydrogenation are given in Equations (1) and (2).

$$2NO_2^- + 3H_2 + 2H^+ \xrightarrow{Pd} N_2 + 3H_2O \qquad (1)$$

$$NO_2^- + 3H_2 + 2H^+ \xrightarrow{Pd} NH_4^+ + 2H_2O \qquad (2)$$

All the as-prepared colloids were stored in a refrigerator and were used in catalytic experiments without any further separation or washing. The reaction was performed in a home-build apparatus including a glass tank reactor (φ 98 mm with four 5 mm baffles), equipped with a mechanical 6-blade-stirrer (φ 44 mm, 1000 rpm) with the propeller positioned at the centre of liquid. Typically, 70 mL as-prepared colloidal suspension was mixed with 230 mL

phosphate (KH_2PO_4 + NaOH) buffer solution under vigorous stirring in 40 vol% H_2 in He (total flow rate 100 mL min^{-1}) at 1 bar for 1 h. The initial pH of the reaction was 8.5, resulting in significant selectivity to ammonium, in order to obtain accurate data. Then 3 mL 4.4 mmol L^{-1} $NaNO_2$ solution was introduced, starting the reaction. Samples were taken using a 1 mL syringe (BD Plastipak), in which the sample was filtered through 40 mg of α-Al_2O_3 and a syringe filter (PTFE, 0.2 μm, Whatman) in order to remove the colloid. The sample was diluted with a factor of 5 before injection into IC to determine the concentrations of nitrite and ammonium. Selectivity to ammonium of the colloids was defined as:

$$\text{ammonium selectivity (\%)} = \frac{\text{mole of ammonium formed}}{\text{mole of nitrite consumed}} \times 100 \qquad (3)$$

Any G-L mass transfer limitation was experimentally ruled out by varying catalyst amount as shown in Figure S-6 in the *Supporting Information*.

3. Results

3.1. TEM

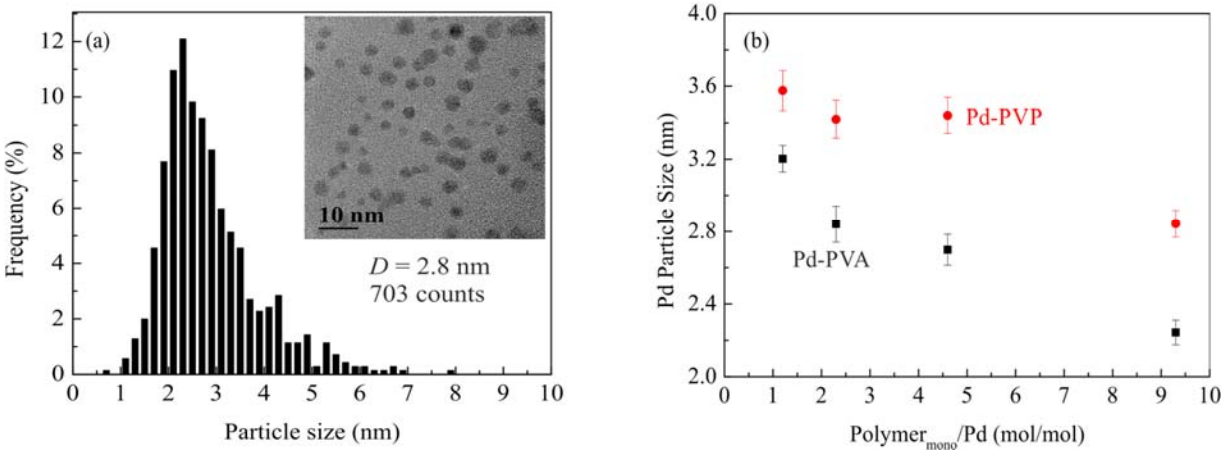

Figure 1. Pd particle size observed by TEM: (a) TEM image and particle size distribution for Pd-PVP colloid with polymer$_{mono}$/Pd = 9.3 (mol/mol); (b) Mean diameters of the Pd colloids prepared using different capping agents and polymer$_{mono}$/Pd mole ratio. The error bars represent error margin of 95% confidential intervals.

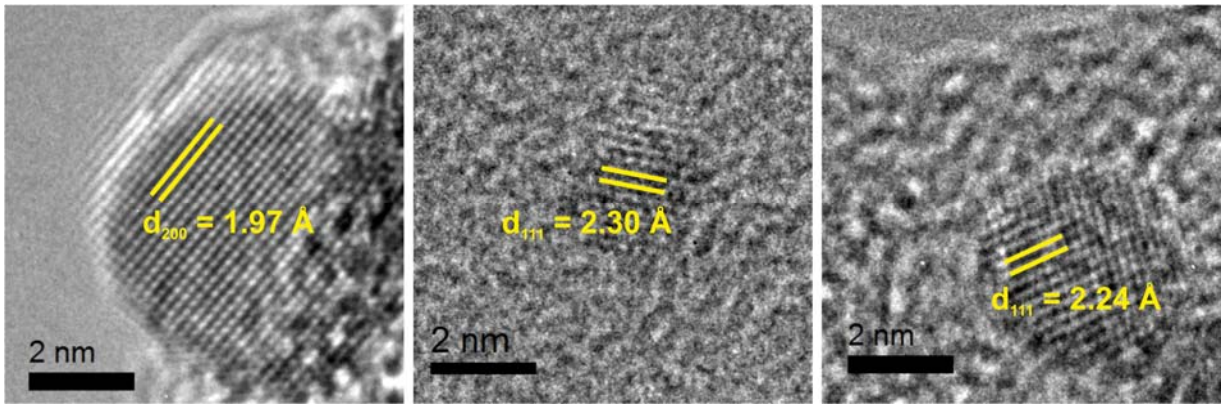

Figure 2. HRTEM images of Pd-PVA colloid (polymer$_{mono}$/Pd = 9.3, mol/mol).

Figure 1 shows a typical TEM image and size distribution for Pd-PVP colloid with $polymer_{mono}$/Pd mole ratio of 9.3; similar results were obtained for all catalysts and the results are presented in Figure S-1 in the *Supporting Information*. These results are summarized in Figure 1(b), showing that the Pd particle size increase with decreasing the amount of polymer, which is in good agreement with previous studies. [7, 25] The polymers act as a protecting agent during colloid synthesis, avoiding uncontrolled nanoparticles growth and preventing aggregation. [26, 27] The particle sizes obtained with PVP are systematically larger as compared to PVA at constant $polymer_{mono}$/Pd mole ratio in this study. In general, relatively small particle size (2 – 4 nm) of Pd NPs were achieved in this study using $NaBH_4$ as reducing agent, as compared to literature reporting typically Pd particle sizes in the range of 5 to13 nm by using a weaker reducing agent like ethanol or methanol, [25] indicating the importance of reduction rate on Pd particle size. [7] The HRTEM image in Figure 2 illustrates that the Pd-polymer colloids as synthesized appear sphere-like shaped and no specific other shapes were observed.

3.2. Zeta potential

The influence of the $polymer_{mono}$/Pd mole ratio on the zeta potential of Pd-polymer colloid is depicted in Figure 3. Both Pd-PVA and Pd-PVP colloids were negatively charged at pH = 8.5, and PVA resulted in lower zeta potential values as compared to PVP. Both Pd-PVA and Pd-PVP revealed decreasing negative charge with increasing amount of polymer and this trend was also observed when additional polymer was added after Pd nanoparticle synthesis. Apparently, polymer is able to partly neutralize the negative charge on Pd nanoparticles after its formation.

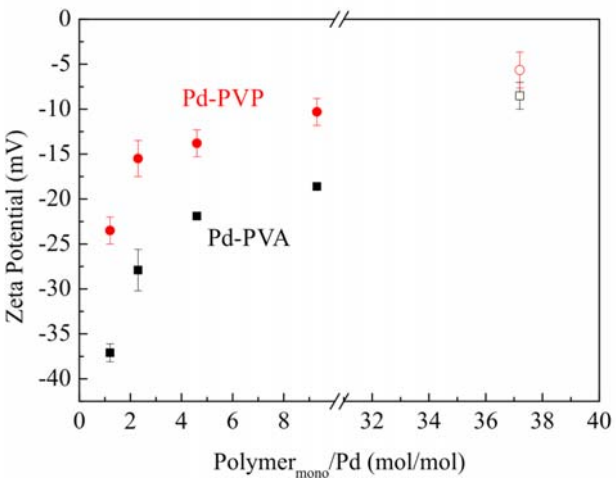

Figure 3. Zeta potential of Pd colloid with different polymer$_{mono}$/Pd mole ratio in reaction slurry at pH = 8.5. The solid symbols (■ and ●) represent as-prepared Pd-polymer colloid, while the open symbols (□ and ○) represent colloids added with additional polymer to as-prepared colloid with polymer$_{mono}$/Pd mole ratio of 1.2.

3.3. ATR-IR of CO chemisorption

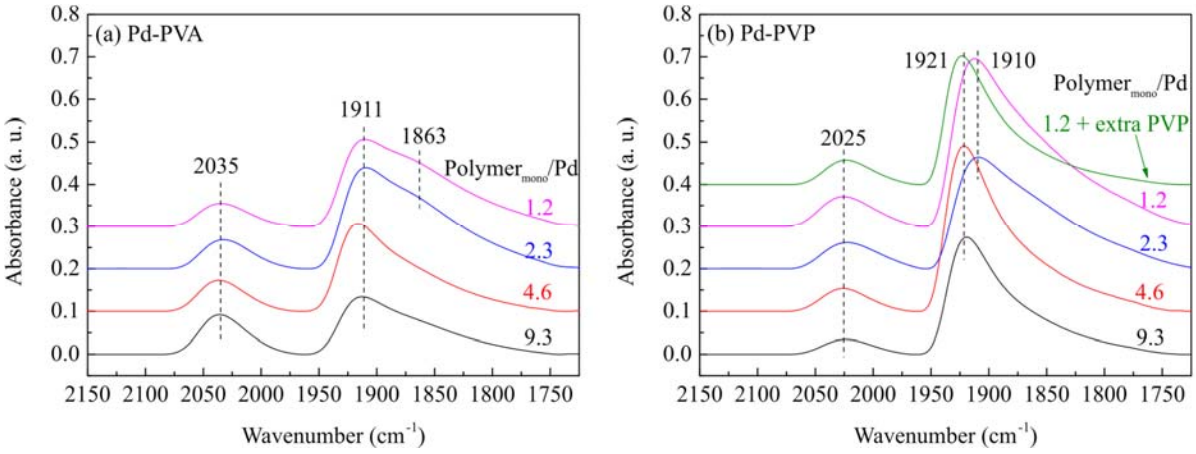

Figure 4 ATR-IR spectra of irreversibly chemisorbed CO on Pd in Ar: (a) Pd-PVA, (b) Pd-PVP. Note the intensity of the peaks is only qualitatively comparable between samples because the Pd amount was not identical.

Figure 4 shows ATR-IR spectra of irreversibly chemisorbed CO on thin layers of Pd-PVA and Pd-PVP colloid on a ZnSe wafer, collected in Ar flow after CO adsorption. Two distinct peaks are assigned to linearly chemisorbed CO on Pd surface atoms (CO_L) at higher wavenumber (1960 – 2100 cm^{-1}), and CO chemisorbed on bridged or hollow Pd sites (CO_{B+H}) at lower wavenumber (1950 – 1750 cm^{-1}), respectively. These peak assignments are in agreement with previously reported results for Pd-PVA and Pd-PVP colloids. [28-30] However, the wavenumbers of these peaks presented here were lower than what is generally reported for supported Pd catalysts on e.g. Al_2O_3 or SiO_2 at room temperature [31-33]. This observation hints to a significant effect of the polymer on chemisorbed CO molecules.

The position of the CO_L peak was not influenced by the polymer amount. In contrast, the position of the CO_{B+H} peak was red shifted with decreasing $polymer_{mono}$/Pd ratio for Pd-PVP colloid as shown in Figure 4(b). Remarkably, extra PVP added to the Pd-PVP colloid with $polymer_{mono}$/Pd of 1.2, after colloid synthesis, caused a blue shift of the CO_{B+H} peak to the same position observed for the colloid prepared with higher $polymer_{mono}$/Pd ratios. Note that position of the CO_{B+H} peak did not vary at all with the PVA $polymer_{mono}$/Pd ratio in Figure 4(a)

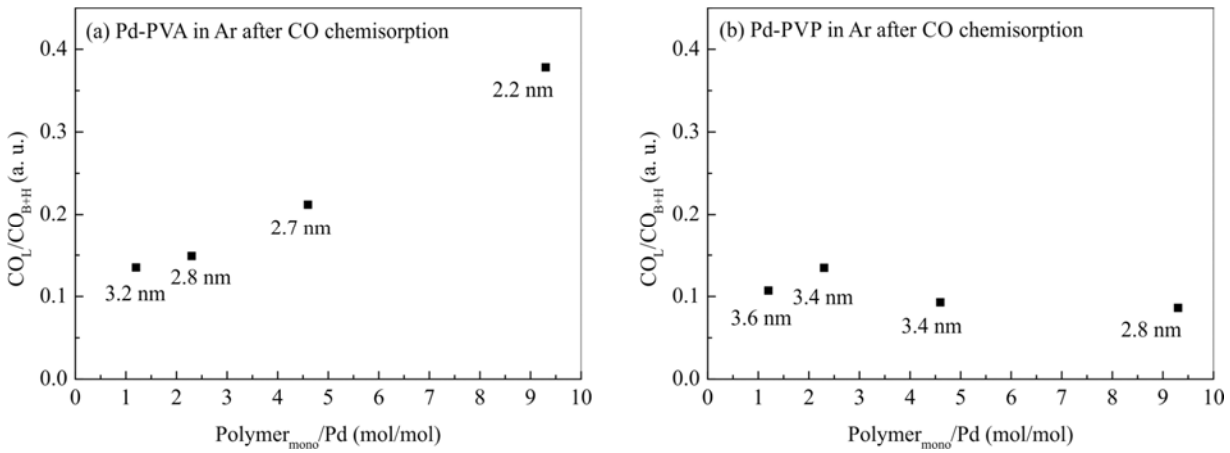

Figure 5. The ratio of integrated area of peaks of CO_L and CO_{B+H} as function of the mole ratio of polymer monomer and Pd.

The ratios of integrated peak area of irreversibly adsorbed CO_L and CO_{B+H} are compared in Figure 5. The CO_L/CO_{B+H} ratio increased with decreasing Pd particle size with Pd-PVA colloid (Figure 5a), agreeing well with extensively reported similar trends for supported Pd nanoparticles in the range of 2 – 4 nm in diameter, [34-37] which is rationalised based on a higher fraction of low coordinated Pd atoms in the surface of smaller particles, favourable for linearly adsorbed CO. In contrast, no significant change in the CO_L/CO_{B+H} ratio was observed

with Pd-PVP (Figure 5b), indicating a significant effect of PVP on chemisorbed CO with the bonding configuration.

3.4. CO chemisorption in aqueous phase

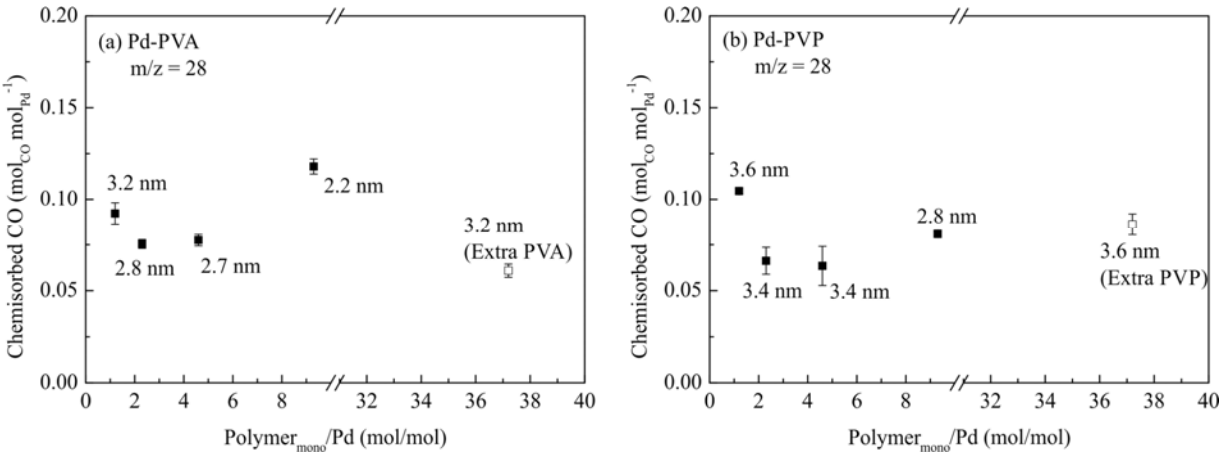

Figure 6. Amount of chemisorbed CO on Pd colloid in aqueous phase determined by MS with m/z ratio = 28: (a) Pd-PVA colloid, (b) Pd-PVP colloid. The hollow squares are results for colloid with additional polymer. Error bars represent error margin of 95% confidential interval.

As shown in Figure 6, the amount of CO chemisorbed on the Pd NPs tends to first decrease and then increased with increasing of polymer$_{mono}$/Pd ratio for both Pd-PVA and Pd-PVP colloid. The decrease is unexpected, whereas the increase is probably due to the concurrent decrease of Pd particles size and increase of dispersion. Importantly, addition of extra PVA or PVP to colloid with the largest particles (3.2 and 3.6 nm respectively) caused the amount of chemisorbed CO to decrease, indicating enhanced blocking by both polymers.

3.5. Nitrite hydrogenation

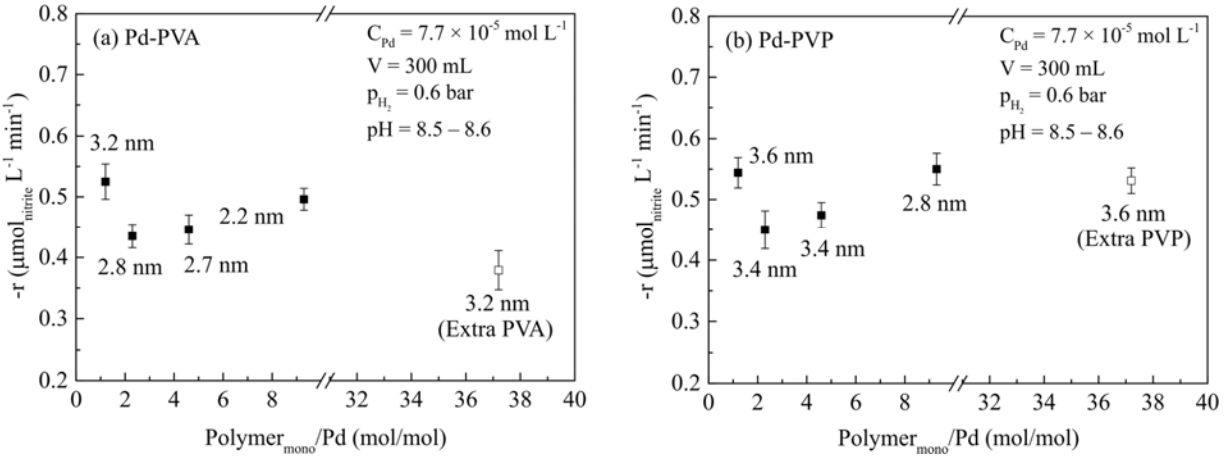

Figure 7. Initial reaction rates of nitrite hydrogenation using (a) Pd-PVA and (b) Pd-PVP colloids with different polymer$_{mono}$/Pd mole ratios.

Figure 7(a) and (b) show how the initial reaction rates were influenced by the polymer$_{mono}$/Pd mole ratio, changing as well the Pd particle sizes. The shape of both curves is rather similar to the shape in Figure 6, observing a minimum at intermediate polymer$_{mono}$/Pd ratios. The activity of the largest PVA stabilized Pd NPs (3.2 nm) was found to decrease on adding additional PVA after colloid synthesis. Remarkably, the same experiment with the largest PVP stabilized Pd NPs (3.6 nm) did not cause a significant change in initial activity.

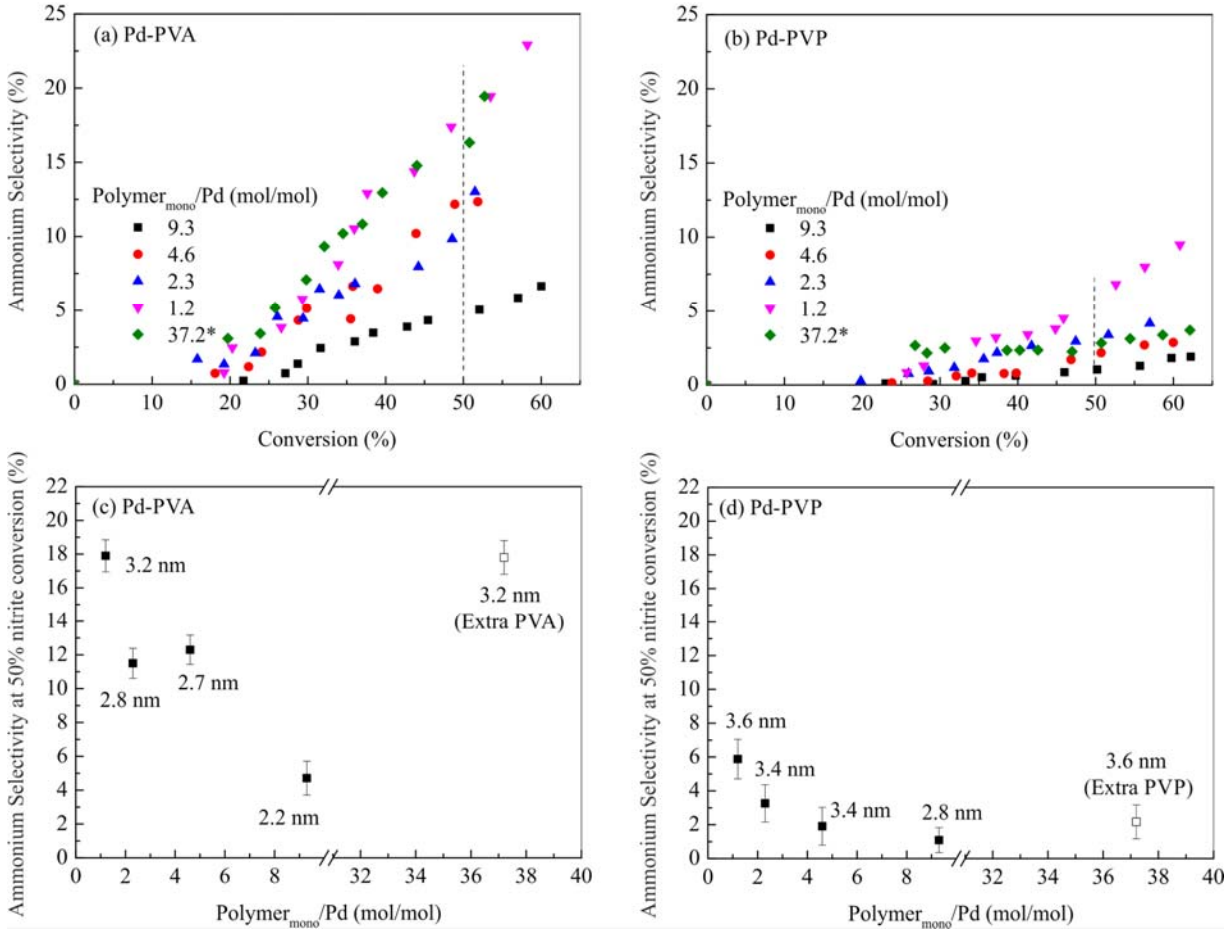

Figure 8. Selectivity to ammonium as function of nitrite conversion for (a) Pd-PVA and (b) Pd-PVP colloids; ammonium selectivity at 50% conversion as function of the polymer$_{mono}$/Pd ratio for (c) Pd-PVA and (d) Pd-PVP colloids. (Extra polymer added, open squares, after formation of Pd colloid originally prepared with polymer$_{mono}$/Pd = 1.2.)

The selectivity to ammonium using different Pd colloids is compared in Figure 8; other products ending up in the gas-phase, comprising mainly N_2 and possibly some N_2O [38, 39], are not analysed. As shown in Figure 8(a) and 8(b), ammonium selectivity increased with nitrite conversion level, thus selectivity to ammonium should be compared at the same nitrite conversion level. Therefore, Figure 8(c) and (d) present the selectivity to ammonium for all samples at 50% nitrite conversion. The selectivity to ammonium tends to decrease with

increasing amount of polymer and decreasing Pd particle size. This effect is clearly significant for Pd-PVA and much less so for Pd-PVP. Generally, Pd-PVP results in lower selectivity to ammonium as compared to Pd-PVA. Remarkably, ammonium selectivity unchanged when adding extra PVA to the Pd-PVA colloid with the largest particle size (3.2 nm, Figure 8(a)), whereas ammonium selectivity was found to decrease when adding extra PVP (Figure 8(b)).

4. Discussion

4.1. Activity of Pd-PVA and Pd-PVP colloids for Nitrite Hydrogenation

Figure 1 shows that the Pd particle size increased when decreasing the amount of polymer used in colloid preparation. As Pd particle sizes were increased from 2.2 nm to 2.8 nm and from 2.8 nm to 3.4 nm for Pd-PVA and Pd-PVP, respectively, the number of active sites accessible for CO (Figure 6) as well as the observed catalytic activity decreased (Figure 7). These observations are very similar to what is generally observed for structure insensitive reaction: metal surface area and activity increase with decreasing particle size. Surprisingly, the number of active sites as well as observed activity increased when the Pd particle size was further increased, by decreasing the amount of stabilizer, to 3.2 nm for Pd-PVA and 3.6 nm for Pd-PVP colloid, as shown in Figure 6 and 7. When extra polymer was added, after colloid preparation, the number of active sites decreased for Pd-PVA and to lesser extent also for Pd-PVP.

These observations indicate that the polymer blocks part of active sites, in agreement with many previous studies. [10, 11, 40] The coverage of the Pd surface by polymer can now be estimated based on the CO-chemisorption data, in aqueous phase, and the TEM observations

(Figure 1), resulting in Figure 9. It is assumed that the Pd particles are spheres with an average size as determined with TEM. The CO-Pd stoichiometry is assumed to be one, which obviously may induce a systematic error. In any case, it seems that the coverage of the Pd surface with polymer was significantly high for all colloids, while relatively low coverage existed with the colloid prepared with the lowest amount of polymer resulting in relatively large particle sizes (3.2 nm for Pd-PVA and 3.6 nm for Pd-PVP colloid).

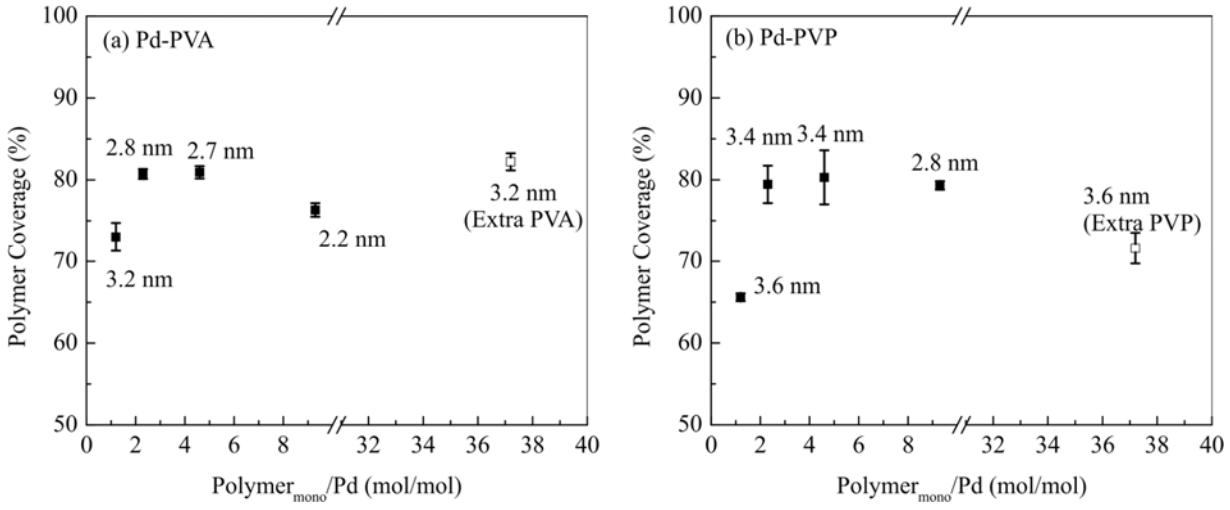

Figure 9. Polymer coverage as function of polymer amount: (a) Pd-PVA; (b) Pd-PVP. Hollow squares represent sample with extra polymer after Pd nanoparticle formation. The polymer coverage was estimated by subtracting number of surface Pd atoms estimated based on TEM and number of Pd available for chemisorbed CO in aqueous phase. The error bars represent 95% confidential intervals.

The CO chemisorption data in aqueous phase also allow estimation of the turn-over-frequency (TOF) based on the initial reaction rates reported in Figure 7. Figure 10(a) shows a constant TOF for Pd-PVA colloid, independent of particle size and polymer concentration, except for the catalyst with the smallest particle size (2.2 nm). The constant TOF agrees well with the claim in literature that nitrite hydrogenation is structure independent, based on studies with supported Pd catalyst with Pd particle size ranging from 1.5 to 20 nm.[38, 41] It is not clear at this point why very small particles stabilized with PVA seem to deviate.

Figure 10(b) shows that no correlation is found between particle size and TOF in the case of Pd-PVP. Instead, Figure 10(c) shows that the TOF increases with the PVP coverage. In other words, the activity of the accessible sites increases when fewer sites are accessible.

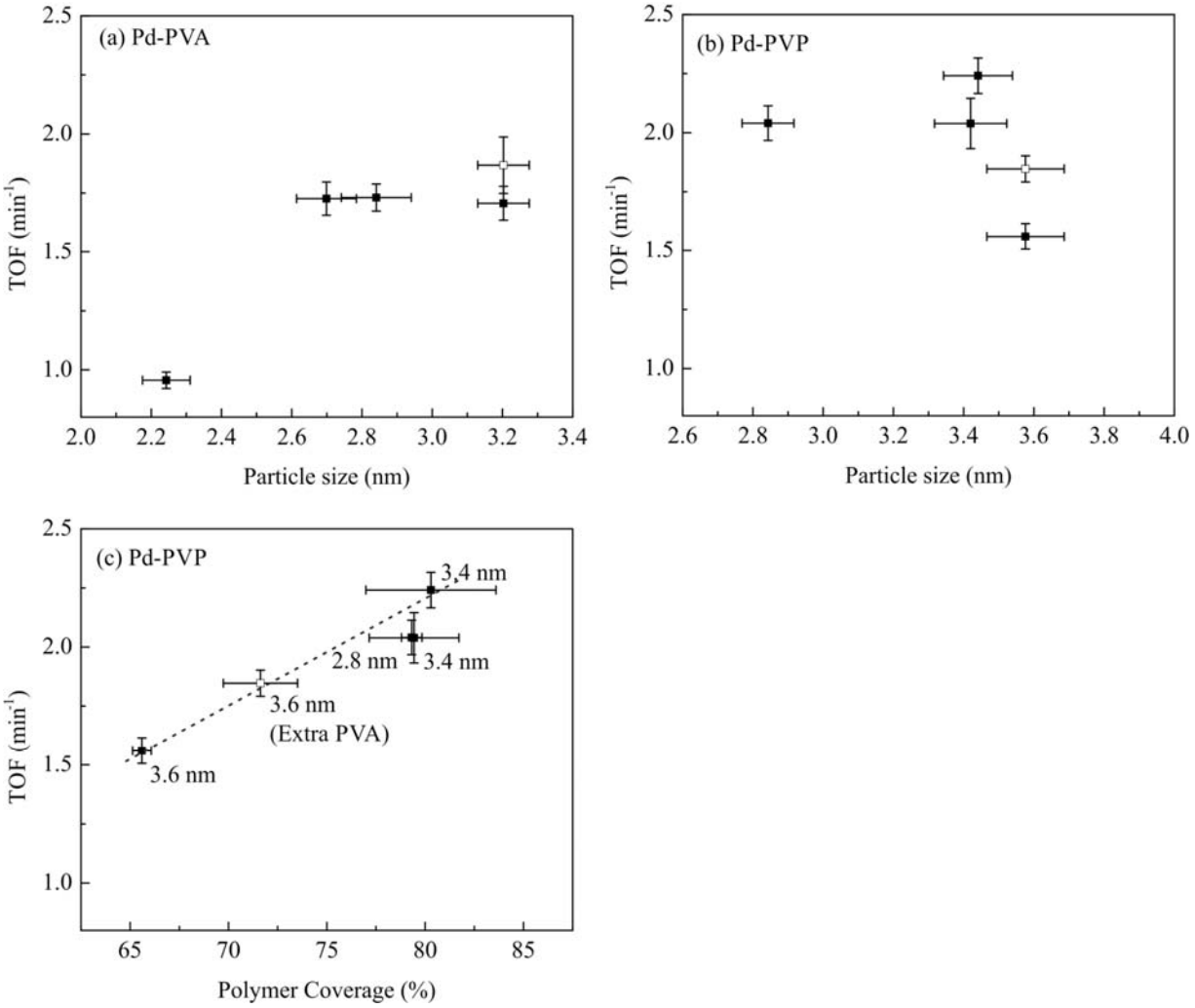

Figure 10. Initial activity per active site: TOF as function of particle sizes of (a) Pd-PVA and (b) Pd-PVP colloid; TOF as function of polymer coverage of Pd-PVP colloid. TOF was calculated based on number of active sites determined by CO chemisorption in aqueous phase. The error bars represent 95% confidential intervals.

In summary, the catalytic activity of Pd-PVA and Pd-PVP colloid for nitrite hydrogenation is determined by Pd particle size as well as polymer coverage on the Pd surface. In the case of PVA, Pd surface sites are simply blocked and the remaining sites reveal constant activity. In

contrast, PVP induces two competing effects: first, blocking of sites decreases the overall activity and second, the activity of the remaining sites increases with PVA coverage.

4.2. Selectivity to ammonium of Pd-PVA and Pd-PVP colloids for nitrite hydrogenation

As shown in Figure 8(c), ammonium selectivity at 50% nitrite conversion decreased with decreasing Pd-PVA particle size, remaining constant when extra PVA was added, clearly indicating that Pd particle size rather than polymer concentration determines the selectivity of Pd-PVA colloid. Thus selectivity to ammonium of Pd-PVA colloid is only dependent on Pd particle size and large particles are more favourable for ammonium formation than small particles.

This observation agrees with Mendez et al., reporting higher ammonium selectivity with large Pd NPs (10 nm) than with small Pd NPs (2 nm) supported on γ-Al_2O_3 in a batch experiment. [42] They suggested the small size of Pd NPs restricts formation of β-hydride suppressing nitrite deep hydrogenation to ammonium. This could also be the case in this study; however, it cannot be ruled out that particle size influences also the relative concentration of adsorbed species, as it has been reported that the ratio of adsorbed nitrogen-containing species (i.e. adsorbed nitrite as well as other reaction surface intermediates) and adsorbed hydrogen influences the ration of rate of formation of N_2 and NH_4^+. [39, 43, 44]

On the other hand, the opposite effect of Pd particle size on ammonium selectivity has been reported by Yoshinaga et al.; ammonium selectivity decreased with increasing Pd particle size on Pd/activated carbon in a trickle-bed experiment. [45] Also Shuai et al. also reported the same trend with Pd NPs supported on carbon nanofibers in a batch experiment. [38] In both

cases, the authors suggested that low coordination sites are responsible for deep hydrogenation to ammonium.

The confusion in the above observations can probably be explained as follows. First, both Mendez et al. and Yoshinaga et al. compared the ammonium selectivity at strongly varying conversion levels. Figure 8 clearly demonstrates that selectivity is strongly influenced by the conversion level, which is caused by the fact that the concentrations of nitrite, hydrogen and protons vary in time in a batch experiment, and along the reactor axis in a fixed bed reactor. [39, 46] Second, G-L mass transfer limitation was not excluded by both Mendez et al. and Yoshinaga et al., inducing further variation of the local concentrations of nitrite, hydrogen and protons, at the active sites. Therefore concentration gradients will influence the selectivity. On the other hand, internal mass transfer limitation is also likely to influence the performance of supported catalysts in case of large diffusion distances and in case of narrow pores. This might be especially relevant when depositing Pd NPs in the internal nano-pore in carbon nanofibers.

Interestingly, Shuai et al. recently reported that the influence of particle size of Pd-PVP on the TOF depends on the nitrite concentration [47] In other words, the structure-performance relationship depends on the nitrite concentration. The nitrite concentration in this study is right in between the concentration considered in [47]. Unfortunately, it is not known whether the relationship between particle size and selectivity depends on the nitrite concentration, and possibly this causes the discrepancy between our observation and the results of Shuai et al. [47].

The selectivity to ammonium for Pd-PVP colloid was lower as compared to Pd-PVA colloid in general, as shown in Figure 8, and adding extra PVP after colloid formation reduced the

formation of ammonium while no influence was observed when adding extra PVA. The effect of PVP on suppressing ammonium formation is in good agreement with observation reported by Hähnlein et al. [48]. In short, PVP not only influences the overall reaction rate per active site as discussed above, but also influences selectivity.

4.3 General discussion

The fact that PVA does not influence the TOF of the accessible sites, as well as the observation that additional PVA does not influence the selectivity, is in agreement with ATR-IR results. Figure 4(a) shows that the positions of the bands assigned to CO_L and CO_{B+H} do not shift when varying the polymer amount. Furthermore, CO_L/CO_{B+H} peak area ratios decreased with increasing Pd particle size as shown in Figure 5(a), similar to what is reported for supported Pd catalyst with clean Pd surface [34-37]. These observations indicate that PVA has no influence on adsorbed CO; therefore, it is reasonable to assume the same is true for adsorbed nitrite and other surface intermediates during nitrite hydrogenation.

In contrast, PVP is found to influence both the TOF as well as the selectivity as discussed above. ATR-IR studies of chemisorbed CO show in Figure 4 (b) that the position of the CO_{B+H} band shifted to a lower wavenumber when decreasing the $polymer_{mono}$/Pd ratio. Addition of extra PVP after colloid synthesis, causes the band to shift back to a higher wavenumber, confirming the shift is induced by the polymer rather than the size of the Pd particle. Apparently, PVP interacts with adsorbed CO, either directly or indirectly via the metal, influencing the C-O bond strength. This is further supported by the observation that the CO_L/CO_{B+H} peak area ratio remains constant for Pd-PVP with varying Pd particle size, as shown

in Figure 5(b), in contrast to what is observed for clean supported Pd particles as well as Pd-PVA, as discussed above. Therefore, this confirms that adsorbed CO is significantly influenced by PVP. It is plausible that a similar interaction with adsorbed reactants like nitrite or NO is responsible for the effect of PVP on the TOF and selectivity. Further investigation would be needed to decide whether this is due to a direct interaction of PVP with adsorbed CO, or to an effect of PVP on the metal particles, e.g. via the electronic structure [49] or via shielding of specific surface sites [47].

Finally, the charge of Pd-PVP colloids in reaction media is less negative as compared to that of Pd-PVA colloids with same $polymer_{mono}$/Pd mole ratio, as shown in Figure 3. This may also contribute to the suppression of the reaction to ammonium by increasing the local N/H ratio at the active sites because of less repulsing of the nitrite anion, favouring nitrite adsorption.

5. Conclusions

Pd colloid with different particle sizes have been prepared by varying the amount of PVA or PVP used as stabilizer. CO chemisorption reveals that the coverage of polymer on Pd surface is in the order of 80% in aqueous phase. The TOF for nitrite hydrogenation as well as the selectivity to ammonium is not influenced by PVA; however, ammonia selectivity increases with increasing Pd particle size. In contrast, increasing coverage with PVP increases the TOF and also reduces ammonium formation.

Acknowledgments

Y. Zhao gratefully acknowledges financial support from China Scholarship Council (File No.2009625054). J.A. Baeza, L. Calvo, and M.A. Gilarranz greatly appreciate financial support from the Spanish MINECO (CTQ2012-32821) and 435 Comunidad de Madrid (REMTAVARES S-2009/AMB-1588). J.A. Baeza thanks to the Spanish MINECO for research grant (BES-2010-030059). The authors are also grateful to M. Smithers for TEM, and B. Geerdink for technical support.

References

[1] K. An, G.A. Somorjai, Chemcatchem, 4 (2012) 1512-1524.

[2] N. Semagina, L. Kiwi-Minsker, Catal. Rev., 51 (2009) 147-217.

[3] A.V. Gaikwad, in: Faculty of Science, University of Amsterdam, Amsterdam, 2009.

[4] K.A. Guy, H. Xu, J.C. Yang, C.J. Werth, J.R. Shapley, J. Phys. Chem. C, 113 (2009) 8177-8185.

[5] S.C. Kim, S.C. Jung, Y.K. Park, H.G. Ahn, S.G. Seo, J. Nanosci. Nanotechnol., 13 (2013) 1961-1965.

[6] H. Hirai, N. Yakura, Polym Advan Technol, 12 (2001) 724-733.

[7] T. Teranishi, M. Miyake, Chem. Mater., 10 (1998) 594-600.

[8] L.S. Ott, R.G. Finke, Coord. Chem. Rev., 251 (2007) 1075-1100.

[9] H. Thiele, H.S. von Levern, Journal of Colloid Science, 20 (1965) 679-694.

[10] A. Villa, D. Wang, D.S. Su, L. Prati, Chemcatchem, 1 (2009) 510-514.

[11] A. Quintanilla, V.C.L. Butselaar-Orthlieb, C. Kwakernaak, W.G. Sloof, M.T. Kreutzer, F. Kapteijn, J. Catal., 271 (2010) 104-114.

[12] Y. Li, M.A. El-Sayed, J. Phys. Chem. B, 105 (2001) 8938-8943.

[13] C. Aliaga, J.Y. Park, Y. Yamada, H.S. Lee, C.-K. Tsung, P. Yang, G.A. Somorjai, J. Phys. Chem. C, 113 (2009) 6150-6155.

[14] E.G. Rodrigues, S.A.C. Carabineiro, J.J. Delgado, X. Chen, M.F.R. Pereira, J.J.M. Órfão, J. Catal., 285 (2012) 83-91.

[15] Y. Borodko, H.S. Lee, S.H. Joo, Y. Zhang, G. Somorjai, J. Phys. Chem. C, 114 (2009) 1117-1126.

[16] R.M. Rioux, H. Song, J.D. Hoefelmeyer, P. Yang, G.A. Somorjai, J. Phys. Chem. B, 109 (2004) 2192-2202.

[17] P. Dash, T. Bond, C. Fowler, W. Hou, N. Coombs, R.W.J. Scott, J. Phys. Chem. C, 113 (2009) 12719-12730.

[18] L.R. Baker, G. Kennedy, J. Krier, M. Spronsen, R. Onorato, G. Somorjai, Catal. Lett., 142 (2012) 1286-1294.

[19] Y. Zhao, L. Jia, J.A. Medrano, J.R.H. Ross, L. Lefferts, ACS Catal., 3 (2013) 2341-2352.

[20] J.A. Lopez-Sanchez, N. Dimitratos, C. Hammond, G.L. Brett, L. Kesavan, S. White, P. Miedziak, R. Tiruvalam, R.L. Jenkins, A.F. Carley, D. Knight, C.J. Kiely, G.J. Hutchings, Nat. Chem., 3 (2011) 551-556.

[21] C. Evangelisti, N. Panziera, A. D'Alessio, L. Bertinetti, M. Botavina, G. Vitulli, J. Catal., 272 (2010) 246-252.

[22] H. Tsunoyama, N. Ichikuni, H. Sakurai, T. Tsukuda, J Am Chem Soc, 131 (2009) 7086-7093.

[23] N.K. Chaki, H. Tsunoyama, Y. Negishi, H. Sakurai, T. Tsukuda, J. Phys. Chem. C, 111 (2007) 4885-4888.

[24] S.D. Ebbesen, B.L. Mojet, L. Lefferts, Langmuir, 22 (2005) 1079-1085.

[25] J.A. Baeza, L. Calvo, M.A. Gilarranz, A.F. Mohedano, J.A. Casas, J.J. Rodriguez, J. Catal., 293 (2012) 85-93.

[26] M. Králik, A. Biffis, J. Mol. Catal. A: Chem., 177 (2001) 113-138.

[27] T. Ashida, K. Miura, T. Nomoto, S. Yagi, H. Sumida, G. Kutluk, K. Soda, H. Namatame, M. Taniguchi, Surf. Sci., 601 (2007) 3898-3901.

[28] J.S. Bradley, E.W. Hill, S. Behal, C. Klein, A. Duteil, B. Chaudret, Chem. Mater., 4 (1992) 1234-1239.

[29] M.R. Mucalo, R.P. Cooney, Chem. Mater., 3 (1991) 1081-1087.

[30] M. Crespo-Quesada, J.-M. Andanson, A. Yarulin, B. Lim, Y. Xia, L. Kiwi-Minsker, Langmuir, 27 (2011) 7909-7916.

[31] S.D. Ebbesen, B.L. Mojet, L. Lefferts, Phys Chem Chem Phys, 11 (2009) 641-649.

[32] W. Juszczyk, Z. Karpiński, I. Ratajczykowa, Z. Stanasiuk, J. Zieliński, L.L. Sheu, W.M.H. Sachtler, J. Catal., 120 (1989) 68-77.

[33] L.F. Liotta, G.A. Martin, G. Deganello, J. Catal., 164 (1996) 322-333.

[34] G. Cabilla, A. Bonivardi, M. Baltanás, Catal. Lett., 55 (1998) 147-156.

[35] R.F. Hicks, A.T. Bell, J. Catal., 90 (1984) 205-220.

[36] L.R. Becerra, C.P. Slichter, J.H. Sinfelt, J. Phys. Chem., 97 (1993) 10-12.

[37] R. Van Hardeveld, F. Hartog, Surf. Sci., 15 (1969) 189-230.

[38] D. Shuai, J.K. Choe, J.R. Shapley, C.J. Werth, Environ Sci Technol, 46 (2012) 2847-2855.

[39] A. Pintar, G. Berčič, J. Levec, Aiche J., 44 (1998) 2280-2292.

[40] X. Wang, P. Sonström, D. Arndt, J. Stöver, V. Zielasek, H. Borchert, K. Thiel, K. Al-Shamery, M. Bäumer, J. Catal., 278 (2011) 143-152.

[41] J.K. Chinthaginjala, J.H. Bitter, L. Lefferts, Appl. Catal., A, 383 (2010) 24-32.

[42] C.M. Mendez, H. Olivero, D.E. Damiani, M.A. Volpe, Appl. Catal., B, 84 (2008) 156-161.

[43] S.D. Ebbesen, B.L. Mojet, L. Lefferts, J. Catal., 256 (2008) 15-23.

[44] J.K. Chinthaginjala, L. Lefferts, Appl. Catal., B, 101 (2010) 144-149.

[45] Y. Yoshinaga, T. Akita, I. Mikami, T. Okuhara, J. Catal., 207 (2002) 37-45.

[46] A. Pintar, J. Batista, J Hazard Mater, 149 (2007) 387-398.

[47] D. Shuai, D.C. McCalman, J.K. Choe, J.R. Shapley, W.F. Schneider, C.J. Werth, ACS Catal., 3 (2013) 453-463.

[48] M. Hähnlein, U. Prüße, J. Daum, V. Morawsky, M. Kröger, M. Schröder, M. Schnabel, K.D. Vorlop, Stud. Surf. Sci. Catal., 118 (1998) 99-107.

[49] Y. Borodko, S.M. Humphrey, T.D. Tilley, H. Frei, G.A. Somorjai, J. Phys. Chem. C, 111 (2007) 6288-6295.

Supporting Information

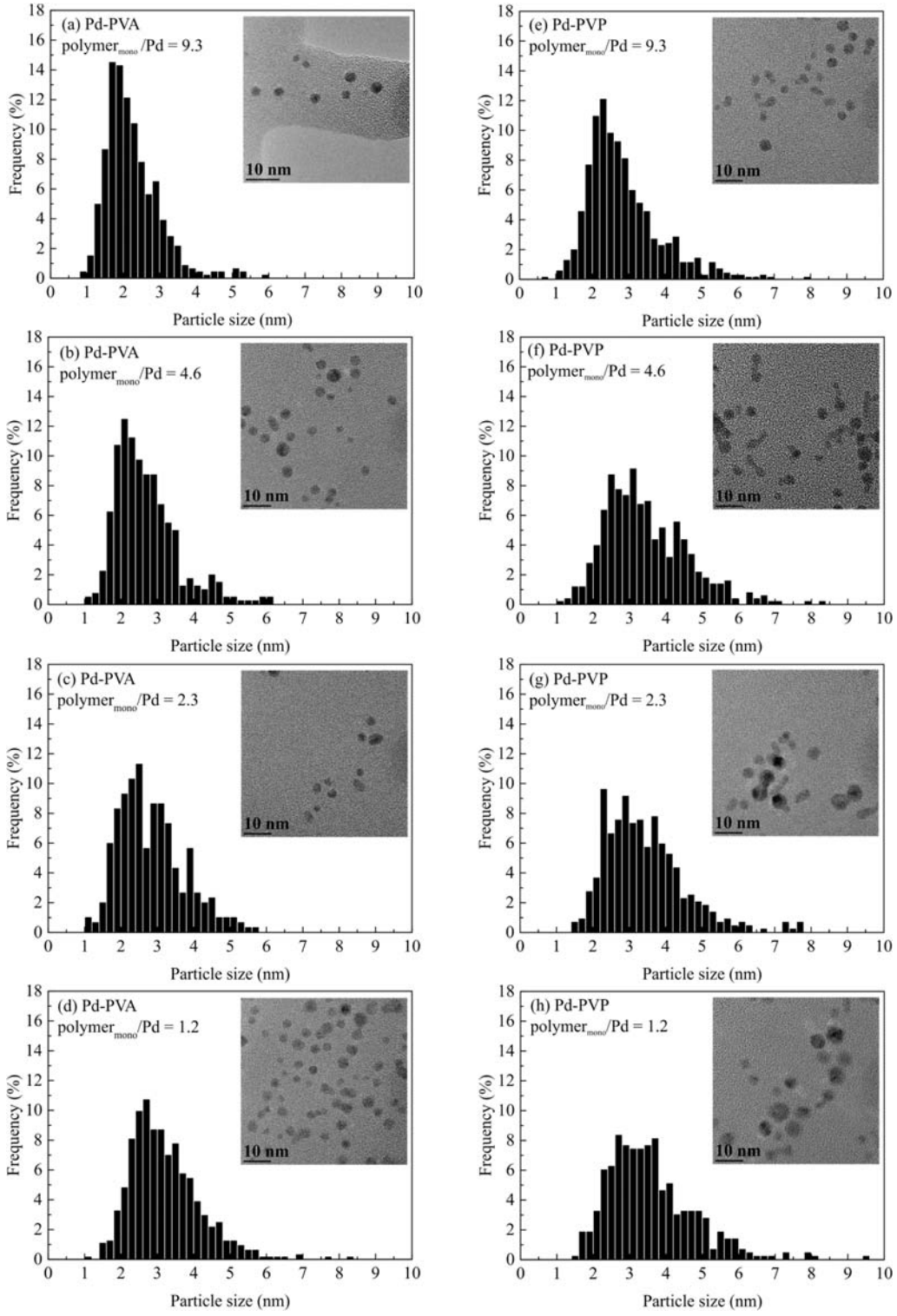

Fig. S-1. TEM and particle size distribution of (a) – (d) Pd-PVA and (f) – (h) Pd-PVP colloids.

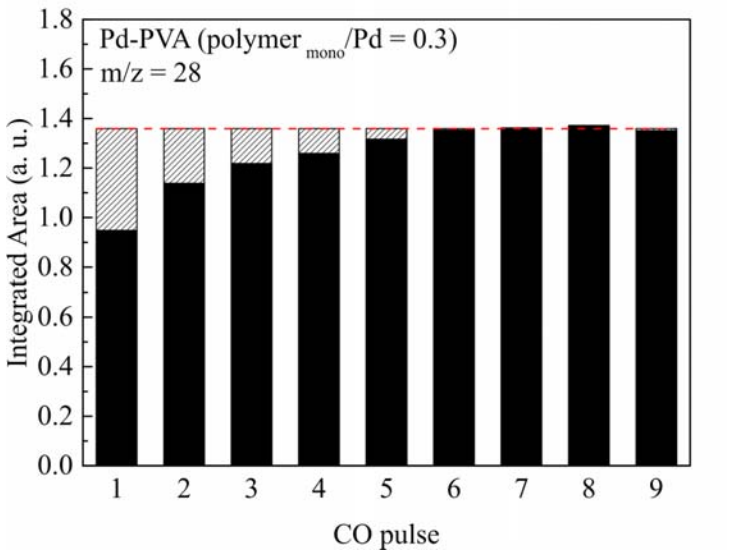

Fig. S-2. Integrated area of CO pulse peaks of typical mass spectrometry during CO chemisorption of Pd colloid in aqueous phase. The shallow bars represent amount of CO adsorbed by Pd colloid.

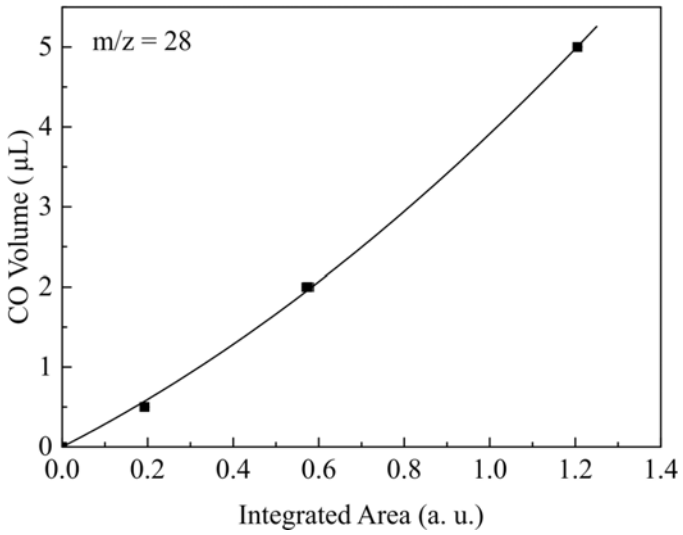

Fig. S-3. Volume of CO for one pulse as function of integrated area. The curve represents 2nd order fitting of the data points. (R^2 = 0.9997)

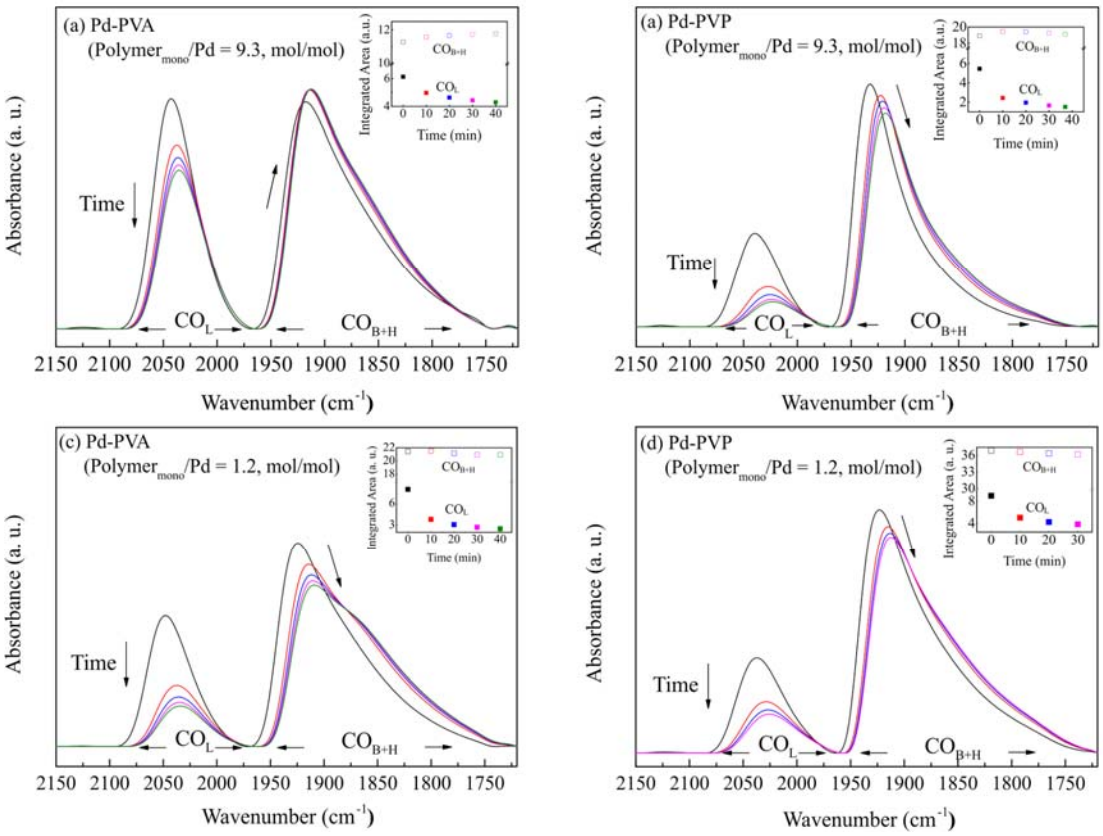

Fig.S-4. ATR-IR spectra of chemisorbed CO on Pd-PVA and Pd-PVP colloid in Ar atmosphere after CO chemisorption. The peaks showed red shift in Ar flow, while the integrated area of CO_L peaks decreased with slightly increasing of the integrated area of CO_{B+H} peaks with both Pd-PVA and Pd-PVP colloid. The CO_{B+H} peaks also became boarder in Ar flow as compared with in CO flow. These phenomena indicated (1) partly desorption of CO weakly adsorbed on Pd surface and (2) relocation of CO_L into bridge or hollow sites with decreasing CO partial pressure.

Nitrite Hydrogenation at pH = ~5.5. Typically, 70 mL colloidal suspension was added into 230 mL H_2O. The mixed suspension was then stirred vigorously in H_2/He/CO_2 atmosphere (H_2/He/CO_2 = 6/3/1 by volume flow rate, total flow rate = 100 mL min^{-1}, total pressure = 1 bar) for at least 1 h. CO_2 was used as a buffer according to reaction shown in Eq. (S-1) and (S-2) to supply the protons consumed by nitrite hydrogenation.

$$CO_2 + H_2O \longrightarrow HCO_3^- + H^+ \qquad \text{(S-1)}$$

$$HCO_3^- + H_2O \longrightarrow CO_3^{2-} + H^+ \qquad \text{(S-2)}$$

Then 3 mL 4.4 mmol L^{-1} $NaNO_2$ solution was introduced, from when the reaction started. 1 mL of reaction suspension was taken by syringe for each time of sampling, and then the sample was filtered through 40 mg of α-Al_2O_3 inside of the syringe and a syringe filter (PTFE, 0.2 μm) to remove Pd nanoparticles. The sample was then injected into IC to determine the content of nitrite and ammonium.

The absence of significant G-L mass transfer limitation was ensured experimentally by varying the catalyst concentration. The nitrite hydrogenation activity per mole total Pd remained constant at pH = 5.5±0.5 using CO_2 as buffer, as shown in Fig. S-5. All experiments in this study performed using a phosphate buffer (pH = 8.5 – 8.6) showed much lower reaction rates as compared with using CO_2 buffer. This is caused by the lower proton concentration at the higher pH, agreeing with the observations in many previous studies [1-4]. In any case, G-L mass transfer limitation can be excluded in this study.

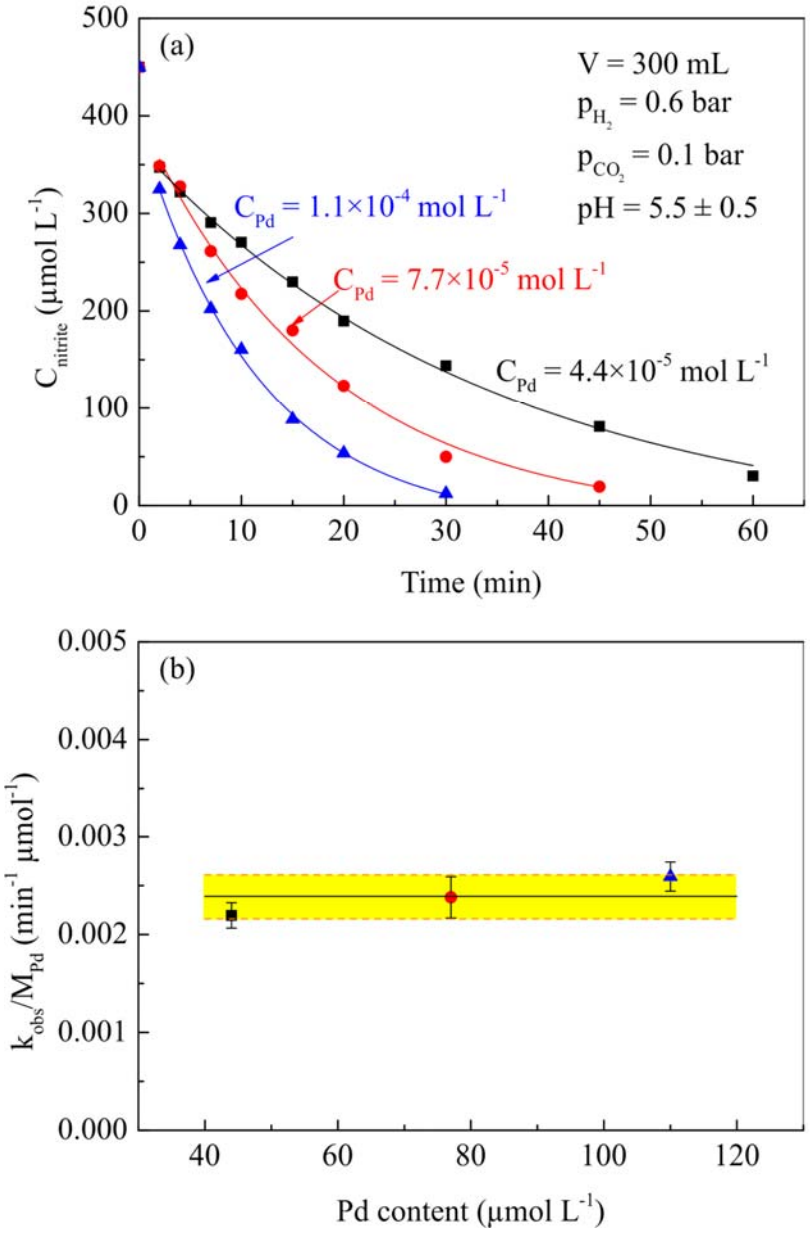

Fig. S-5. (a) Nitrite concentration vs. time using Pd-PVA colloid ($polymer_{mono}$/Pd = 2.4, mol/mol) as catalyst of different Pd concentration. CO_2 was used as a buffer (pH = 5.5). The lines are first-order fits to the data points. **(b)** The observed reaction rate constant calculated with first-order fits normalized by total amount of Pd. The yellow area with orange margins represents the 95% confidence interval of the average.

References

[1] A. Pintar, G. Berčič, J. Levec, Aiche J., 44 (1998) 2280-2292.

[2] I. Mikami, Y. Sakamoto, Y. Yoshinaga, T. Okuhara, Appl. Catal., B, 44 (2003) 79-86.

[3] K.A. Guy, H. Xu, J.C. Yang, C.J. Werth, J.R. Shapley, J. Phys. Chem. C, 113 (2009) 8177-8185.

[4] M. Al Bahri, L. Calvo, M.A. Gilarranz, J.J. Rodriguez, F. Epron, Appl. Catal., B, 138–139 (2013) 141-148.

CAPÍTULO VI /CHAPTER VI

Catalytic activity in 4-chlorophenol hydrodechlorination of catalysts based on nitrogen doped carbons obtained by pyrolysis of LDPE

Manuscript

Abstract

Nitrogen-doped carbons (NDCs) were prepared by co-pyrolysis of low density polyethylene (LDPE) with nitrogen precursors and tested in the aqueous phase catalytic hydrodechlorination (HDC) of 4-chlorophenol (4-CP). Ammonia, aniline, 1,10-phenanthroline and pyridine were used as nitrogen precursors. The NDCs appeared as clusters of spherical particles with carbon black-like structure. 1,10-phenanthroline and pyridine led to a significant content of nitrogen into the solid carbons (0.1-1.7%, w), with a preferential allocation of nitrogen at the outer regions of the carbons in the case of pyridine. Different pyrolysis conditions were tested to address their influence on the amount of nitrogen incorporeated to the carbon structure. The nitrogen incorporated showed different bonding configurations: pyridine-like, pyrrole-like, quaternary and nitrogen oxides. Those NDCs prepared with phenanthroline showed higher content of quaternary and lower of pyrrolic nitrogen in its structure. The NDCs exhibited some catalytic activity in HDC, showing their potential as metal free catalysts. The Pd/NDCs catalysts prepared yielded a much higher activity than Pd supported on non doped carbons used as blanks, thus suggesting a synergistic effect between NDCs and Pd. The Pd catalysts supported on NDCs prepared from 1,10-phenanthroline exhibited a remarkable activity of 55.6 $mmol \cdot g^{-1} \cdot min^{-1}$, which may be related to the higher amount of nitrogen of the support and a higher contribution of quaternary nitrogen species.

1. Introduction

Nitrogen-doped carbon materials (NDCs) have attracted attention in the last years due to the excellent properties that they exhibit for different applications such as energy storage, solar and fuel cells, batteries or catalysis. The NDCs have been showed to possess improved electrical, mechanical and structural characteristics in comparison to non-doped carbon materials [1]. The introduction of nitrogen in the carbon network modifies the carbon lattice, increasing the structure defectiveness. Likewise, the presence of nitrogen, as doping agent, lead to n-type structures with excess of electrons in the carbon network [2]. The final surface and electronic properties of NDCs depend on the sort of bonding established between nitrogen and carbon atoms [3,4]. In catalysis, NDCs used as catalysts supports showed an enhancement of the catalytic activity in several reactions such as hydrogenation, oxidation or photocatalysis, among others. This improvement in the activity has been related to several factors: the presence of nitrogen into the carbon network could favor a high dispersion of the metal on the support by driving the nucleation of the active phase to nitrogen-neighboring carbon atoms, thus controlling nanoparticle size [1, 5]; the higher conductivity of the support caused by the excess of electrons introduced by nitrogen in the carbon network could improve chemical reactivity for electron-transfer processes in the catalytic system [2, 5]; the insertion of nitrogen into the carbon network produces changes in the acid-base properties in the surface, since the excess of electrons increase surface basicity [5, 6]. Different methods have been used to

prepare NDCs, such as ammonia treatment of the carbon at high temperature [7], chemical vapor deposition on metal seeds [8] or solvothermal reduction of carbon and nitrogen precursors [1]. One of the most common methods used to obtain these carbons is the co-pyrolysis of the carbon precursor with nitrogen sources to obtain the NDCs. The variety of nitrogen sources is high, being ammonia, ethylenediamine, aniline, benzylamine and pyridine, among them [3, 9]. The carbon precursors are diverse, being ethanol, toluene, benzene, xylene, tiophene and ethylene the most common carbon sources employed [10, 11]. Nevertheless, other carbon sources have been less studied in spite of the fact that their use could generate environmental benefits such as the valorization of a waste, which could be the case of polyethylene. Plastic consumption worldwide has been drastically increasing since 1950 (1.7 million ton/y) up to 2011 (c.a. 280 million ton/y), where polyethylene represents 17 % of this consumption in Europe [12]. In the last years the dramatic consequences for the environment [13] of this huge production are increasing the concern on how to manage this sort of wastes.

In the current work, NDCs have been prepared by co-pyrolysis of low-density polyethylene (LDPE) with different nitrogen sources (ammonia, aniline, pyridine and phenanthroline). These carbons have been used as catalysts and as catalytic supports in the aqueous phase hydrodechlorination (HDC) of 4-chlorophenol (4-CP), which is a well-studied reaction, especially in our group [14-16]. The influence of pyrolysis conditions on nitrogen content and nitrogen species of the carbons has been evaluated in order to acquire an in-depth

knowledge on how the carbon structure influences on activity, which can contribute to future rational design of the catalysts.

2.Experimental

Synthesis of the NDCs. NDCs were synthesized by copyrolysis of LDPE, as main carbon source, supplied by Chemical Dow (150E) as virgin pellets, and ammonia (Panreac, 20%), aniline (Panreac, 99%), pyridine (Sigma-Aldrich, 99.8%) and 1,10-phenanthroline (Sigma-Aldrich, >99%), as nitrogen sources. LDPE virgin pellets were ground and sieved to obtain particles in size between 2.0 and 2.8 mm. The grinding was carried out in a blade mill (IKA Labortechnik) using liquid nitrogen as cooling agent. The LDPE was feed into a semi-continuous quartz reactor by means of a solid valve that varies the time between feeding pulses from 35 s to 109 s [17]. The pyrolysis temperatures ranged from 776 to 944 ^{o}C and the nitrogen flow rate was varied from 0 to 50 N mL·min^{-1}. Ammonia, aniline and pyridine were fed into the reactor by bubbling and saturation of nitrogen flow using as carried gas in the reaction zone. 1,10-phenanthroline was mixed with LDPE previous to introduction into the reactor.

Preparation of the Pd/NDCs catalysts. The impregnating solution for preparing the Pd-supported catalysts consisted on $PdCl_2$ dissolved in HCl 0.1N. All the catalysts were prepared with a palladium load of 0.5% (w). After the impregnation, the catalysts were dried overnight at 60 ^{o}C. Finally, the catalysts were calcined at 200 ^{o}C for 2 h and reduced with hydrogen at 100 ^{o}C for 1 h. Liquid phase catalytic 4-CP HDC experiments were carried out in a three-necked

jacketed glass reactor were H_2 was continuously fed at 50 N mL·min^{-1} flow rate under vigorous stirring (800 rpm) in order to facilitate hydrogen distribution through the 4-CP solution (150 mL) during 4 hours. The reaction temperature (30 ^{o}C) was controlled by a thermostatic bath. The system was equipped with a cold trap at the vent to check any possible stripping, but no significant stripping was detected. The initial concentration of 4-CP was 0.1g·L^{-1} and the catalyst concentration was 0.25-0.5 g·L^{-1}. A sampling system consisting on a thin tube connected to a syringe allowed taking liquid samples (1 mL), which were immediately filtered (PTFE filter, pore size 0.45 μm). The samples were analyzed by high performance liquid chromatography (Varian Prostar equipped with a UV-VIS detector) using a C_{18} column as stationary phase and a mixture of acetonitrile and water (1:1, v/v) as mobile phase. Cyclohexanone was analyzed by a GC/FID (GC 3900 Varian) using a 30 m long x 0.25 mm i.d. capillary column (CP-Wax 52 CB, Varian) and nitrogen as carrier gas. The quantification of chloride ion was performed by ion chromatography (Metrohm 790 Personal IC). The carbon and chlorine balances matched always above 90% and 95%, respectively.

Characterization of the NDCs and catalysts prepared. The solid carbon samples obtained were characterized by nitrogen adsorption-desorption isotherms at 77K (QuantachromeAutosorb I), elemental analysis (LECO CHNS-932), transmission (JEOL JEM 2000 FX) and scanning (Hitachi S 3000N) electron microscopy and XPS (K-Alpha – Thermo Scientific equipped with a AlKa X-ray excitation source, 1486.68 eV). Software 'XPS peak v4.1' was used for the deconvolution of the spectrograms in order to obtain the relative amounts of

the different nitrogen species. The analysis procedure involved smoothing, a Shirley background subtractionand mixed Gaussian–Lorentzian by a least-square method curve fitting. The width of the peaks was not fixed during the fitting process. C 1s peak (284.6 eV) was used as internal standard for binding energies corrections due to sample charging. Binding energies for N 1s for surface groups (pyridinic, pyrrolic, quaternary and nitrogen oxides) and Pd 3d for electrodeficient and zerovalent Pd species were taken from to literature [18,19].

Results and Discussion

Preparation and characterization of NDCs. The NDCs obtained by pyrolysis of LDPE as the only starting material are virtually free from nitrogen, therefore, the presence of nitrogen in the solid carbons obtained during the co-pyrolysis with nitrogen precursors can be interpreted as the result of doping. Table 1 shows the elemental analysis for selected samples prepared using four different nitrogen precursors. The NDCs obtained in the co-pyrolysis of LPDE with ammonia and aniline did not show significant nitrogen incorporation into the carbon network, on the contrary, those prepared with pyridine and 1,10-phenanthroline showed significant nitrogen doping. A number of works in literature have reported that ammonia is as an effective precursor for carbon doping. The poor results shown in the current work can be related to the lower temperature tested. In the case of aniline, primary pyrolysis leading to the removal of the amino group may result in a lower incorporation of nitrogen in the carbon structure.

Table 1. Elemental composition of representative solid carbons obtained by co-pyrolysis of LDPE and different nitrogen sources.*

Nitrogen source	C (%, w)	H (%, w)	N (%, w)
Ammonia	98.29	0.54	0.02
Aniline	97.88	0.24	0.01
Pyridine	94.80	0.34	0.13
1,10-phenanthroline	96.99	0.39	0.82

*Temperature: 860 ^{o}C, nitrogen flow rate: 25 N mL·min^{-1}, time between feeding pulses: 63 s

Figure 1 shows a homogeneous structure consisting of clusters of spherical particles, in a carbon black-like arrangement, for the NDCs obtained by co-pyrolysis of LDPE with pyridine and phenanthroline as nitrogen source. The LDPE fed into the reactor decompose into volatile products such as parafins (C_1-C_7) and olefins (C_2-C_7)[20], which can suffer secondary and tertiary reactions in the presence of nitrogen compound that lead to the formation of aromatic molecules that, finally, form solid carbons with nitrogen atoms inside the carbon network. Compared to the solid carbons obtained only from LDPE [17], the insertion of nitrogen atoms into the graphitic layers of the carbon does not affect to the morphology, although the size of the carbon spherules obtained seems to be dependent on the nitrogen source used, the carbon spherules obtained with pyridine (≈ 1.2 μm) being larger than those obtained with phenanthroline (≈ 0.7 μm). The NDCs exhibited a low porosity, with S_{BET} values lower than 50 m^2/g, similar to those obtained in the pyrolysis of LDPE alone [17].

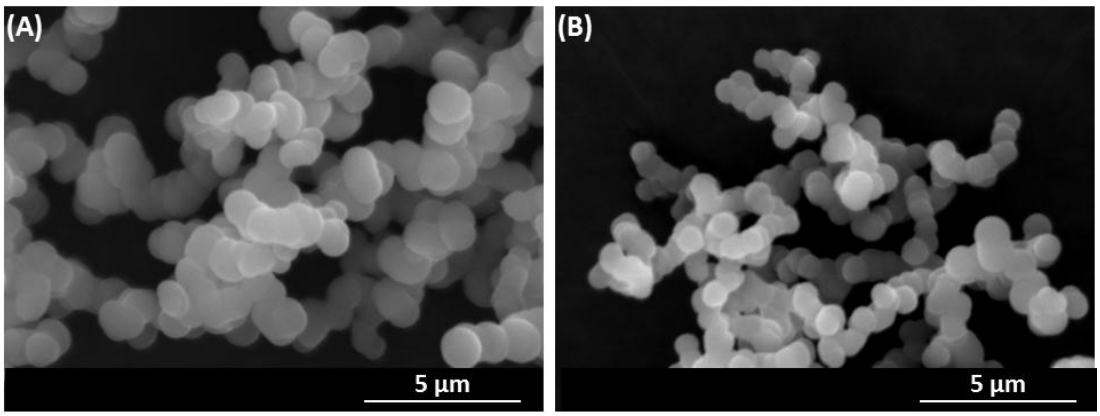

Figure 1. SEM images of NDCs obtained with (A) pyridine and (B) 1,10-phenanthroline (temperature: 860 ^oC, nitrogen flow rate: 25 N $mL \cdot min^{-1}$, time between feeding pulses: 63s).

The pyrolysis conditions used during the co-pyrolisis of LDPE with pyridine and 1,10-phenanthroline are shown in Table 2 together with the nitrogen content achieved, as determined by elemental analysis. A significantly higher nitrogen doping can be observed for the samples prepared using phenantroline as nitrogen source, which can be related to the preexisting bonds between nitrogen and the aromatic rings of the precursor. Data in Table 2 also show that the pyrolysis conditions have an important influence on the nitrogen content of the NDCs formed.

Table 2. Synthesis conditions and nitrogen content for NDCs samples prepared using pyridine and 1,10-phenanthroline as nitrogen source.

Nitrogen source	**Sample**	**T (°C)**	**Nitrogen Flow (N mL·min^{-1})**	**Time between Feeding Pulses (s)**	**N (%, w)**
Pyridine	PYR0.5	776	25	63	0.53
	PYR0.3	860	25	63	0.13
	PYR0.09	944	25	63	0.09
	PYR0.08	860	10	63	0.08
	PYR0.7	860	50	63	0.70
	PYR0.16	860	25	35	0.16
	PYR0.23	860	25	90	0.23
	PYR0.4	860	25	109	0.38
1,10-phenanthroline	PHE1.7	776	25	63	1.66
	PHE0.8	860	25	63	0.82
	PHE0.6	944	25	63	0.62
	PHE0.3	860	10	63	0.31
	PHE0.5	860	25	63	0.48
	PHE1.1	860	50	63	1.09

Thus, Figure 2 depicts nitrogen content of the carbon versus pyrolysis temperature. Decreasing pyrolysis temperatures led in the range studied (776-944 ^{o}C) to higher nitrogen contents of the carbons for both nitrogen sources used. The increase of pyrolysis temperature produces a more extensive cracking of LDPE generating a higher concentration of lighter hydrocarbons (e.g., CH_4, C_2H_6, and C_2H_4) in the gas phase [21, 22], which could lead to faster carbon condensation reactions [20, 23] thus reducing nitrogen bonding. This trend has been also observed by Yadav et al. [24] and Van Dommele et al. [25] in the synthesis of nitrogen doped carbon nanotubes. In addition to this, a higher temperature increases substantially the carbon yield [17] thus diluting nitrogen in the NDCs and can contribute to the evolution of the more labile nitrogen species formed during pyrolysis.

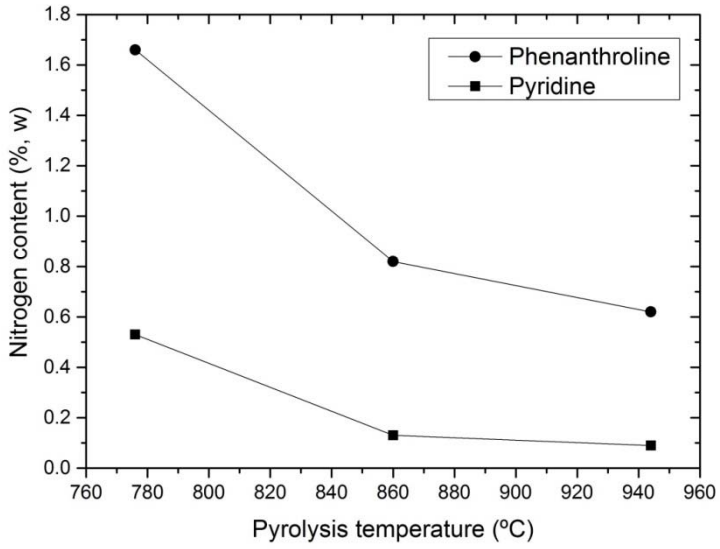

Figure 2. Nitrogen content of NDCs obtained with different pyrolysis temperatures and nitrogen sources.

Figure 3 depicts the nitrogen content of the NDCs versus the nitrogen flow rate used in the pyrolysis. Increasing nitrogen flow rate led to higher nitrogen percentage into the carbon network for both nitrogen sources employed. In the case of pyridine, where the nitrogen carries the nitrogen precursor at constant concentration, the results could be ascribed to a higher availability of nitrogen. However, the doping increases also in the case of phenantroline (solid nitrogen precursor). Again, the pyrolysis yield seems to play a role, since it has been shown [17] that a higher carbon yield is achieved at low nitrogen flow rates due to higher residence time of pyrolysis products, which promotes condensation reactions.

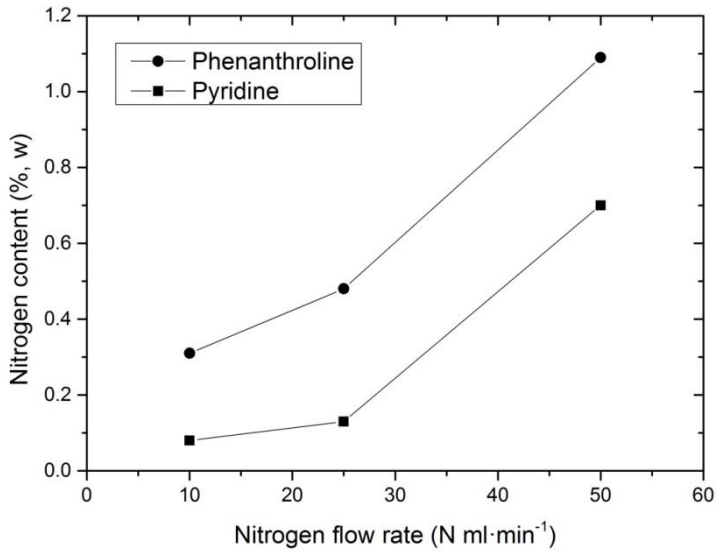

Figure 3. Nitrogen content of NDCs obtained with different nitrogen flow rates and nitrogen sources.

If the availability of nitrogen is high, as it is the case of the co-pyrolysis with pyridine, an increase of the residence time can also lead to higher nitrogen content of the NDCs. This effect can be observed in the experiments carried out at different time elapsing between feed pulses. As the time between feed pulses increases, a lower self displacement of the gas pyrolysis products takes place, thus increasing residence time, which has been found to be a major reason for carbon yield enhancement. In these conditions, the condensation reactions leading to the incorporation of nitrogen in the carbon structure are also promoted.

XPS analysis. Table 3 shows the deconvolved spectra for the samples PHE1.7 and PYR0.5 prepared under equivalent pyrolysis conditions using 1,10-phenanthroline and pyridine, respectively.The chemical composition determined by XPS showed that both NDCs showed equivalent surface nitrogen percentage (3.86 % and 3.65 %, respectively), but taking into account their different percentage of total nitrogen content (1.66 % and 0.53%, respectively), the ratio between surface nitrogen and total nitrogen is three times higher in the case of PYR0.5. Thus, NDCs obtained with 1,10-phenanthroline showed a more homogeneous nitrogen distribution into the carbon frame. However, during the synthesis of NDCs from LDPE and pyridine preferential allocation of the nitrogen at the most external part of the solid carbon takes places. This could indicate that in some extent doping takes place by deposition of nitrogen on already formed solid carbons.

Table 3. Binding energy of N 1s region for the surface functional groups and percentage of deconvolved curve areas assigned from XPS spectra for samples PHE1.7 and PYR0.5

Sample	Surface functional group	Binding energy (eV)	Area (%)
PHE1.7	Pyridinic	398.4	28.3
	Pyrrolic	400.1	2.8
	Quaternary	401.5	61.9
	Nitrogen oxides	403.2	7.0
PYR0.5	Pyridinic	398.8	26.2
	Pyrrolic	400.1	11.0
	Quaternary	401.1	52.9
	Nitrogen oxides	402.9	9.9

The nitrogen that was incorporated into the carbon structure from each nitrogen source showed different bonding configurations. Figure 4 shows the XPS deconvolved spectra for the N 1 s region of samples PHE1.7 and PYR0.5, form which four main bonding configurations can be observed, namely pyridine-like, pyrrole-like, quaternary and nitrogen oxides [3, 26]. As shown in Figure 4 and Table 3, in both cases, quaternary nitrogen is the predominant functional group, followed by pyridinic nitrogen, but in the case of PYR0.5 the relative amount of quaternary is lower and the pyrrolic is higher than for PHE1.7.

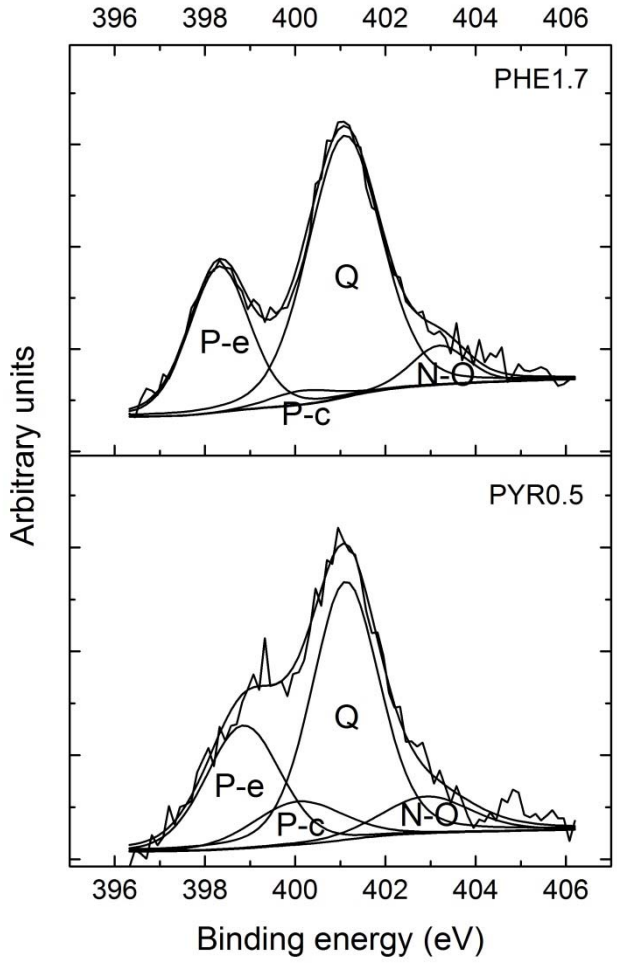

Figure 4. XPS spectra of N 1 s region for NDCs PHE1.7 and PYR0.5. ((Q) quaternary, (P-e) pyridinic, (P-c) pyrrolic and (N-O) nitrogen oxides)

Aqueous phase HDC of 4-CP. Four carbons were selected as supports for the study of the HDC of 4-CP: PHE1.7, which exhibited the highest amount of nitrogen inside the carbon network (1.66 %, w), PHE0.5 and PYR0.5, which were

synthesized from different nitrogen source and pyrolysis conditions but they showed equivalent amount of nitrogen (c.a. 0.5 %, w) and a solid carbon prepared by pyrolysis of only LDPE (Non-DC) using the same pyrolysis conditions as for sample PHE0.5. Besides, at shown above, samples PHE1.7 and PYR0.5 have equivalent concentration of nitrogen at the carbon surface. Figure 5 shows TEM images and size distributions of the catalysts obtained using the selected carbons as supports for the HDC study. As can be observed in Figure 5, the catalyst prepared with the non-doped carbon presented broad range of nanoparticle sizes, most of them between 2 and 10 nm and a most frequent value around 5 nm, but also with some presence of some large Pd nanoparticles with sizes between 50 and 85 nm. The presence of large nanoparticles was not observed in the case of the catalysts prepared on doped carbons. This observation is in agreement with works in literature indicating that the introduction of heteroatoms into the carbon network improves the control of the active phase size and size distribution [5]. However, in the current work the mean size distribution are higher and the size dispersion is broader for NDCs supported catalysts in the low size range (<15 nm), which is the most relevant with the view in the catalytic performance.

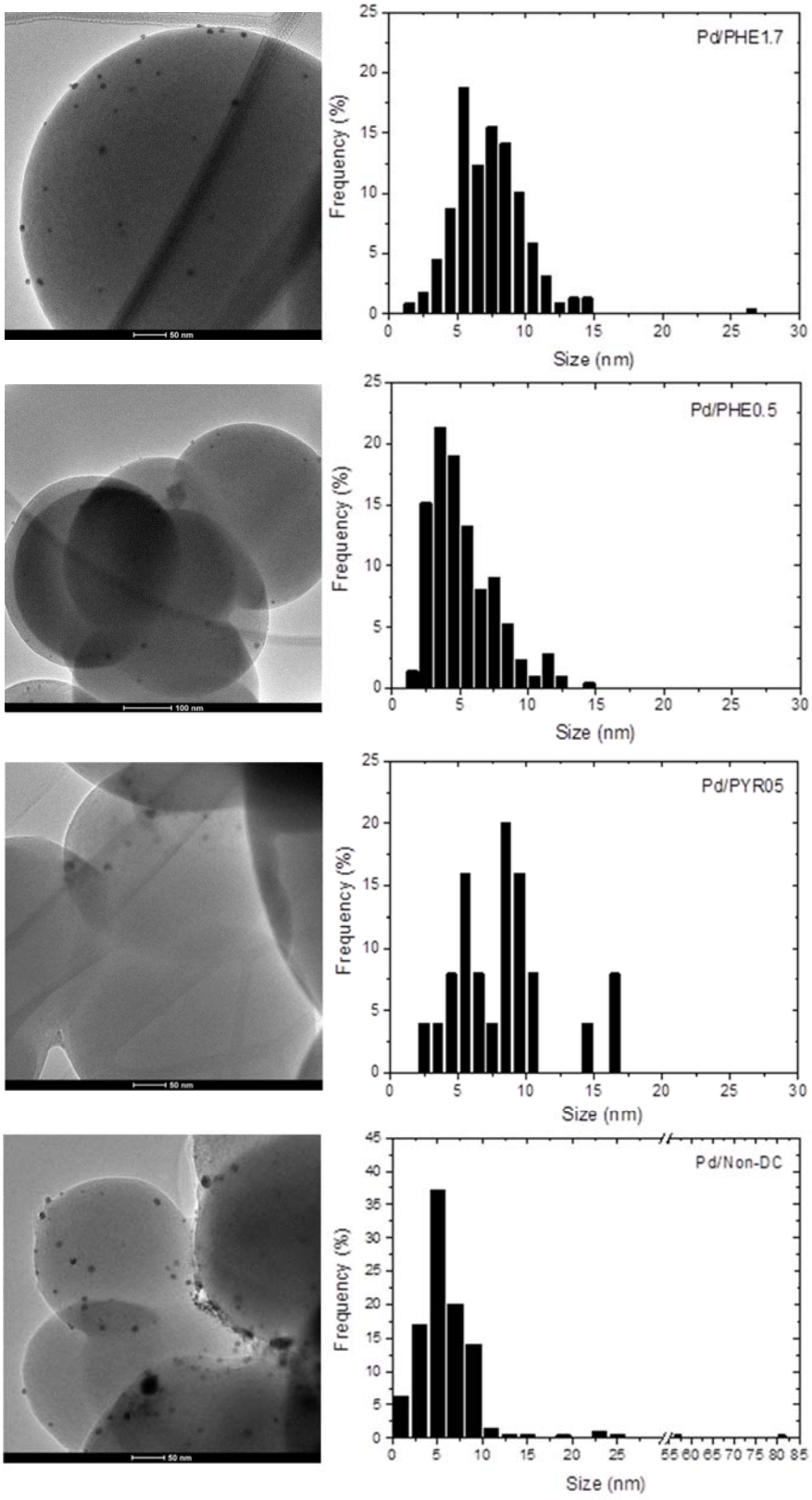

Figure 5. TEM images and size distributions of the catalysts prepared for the HDC of 4-CP study

Preliminary 4-CP HDC runs were carried out using the supports as catalyst without incorporation of Pd. In contrast to Non-DC, the three NDCs tested exhibited activity in the HDC reaction with 4-CP values between 5 and 6% and phenol as the only HDC product. Although these conversion data are low, the activity achieved is a remarkable result taking into account that the NDCs used have a very low surface area, most of it corresponding to micropores that have a very low contribution in liquid phase catalysis. Therefore, the application of NDCs as metal free catalysts has an interesting potential to be explored, as it has been reported for other water treatment reactions.

Figure 6 shows the conversion of 4-CP versus time for the PHE0.5 support and the different Pd/C catalysts prepared. The catalyst synthesized using the non-DC as support showed conversion slightly above 20% after 240 minutes reaction time. The activity in HDC of this catalyst is low when is compared to Pd catalysts supported on activated carbon [14], although again it can be considered as relevant taking into account that the non-DC obtained from LDPE pyrolysis has a very low porosity (S_{BET}< 50 $m^2 \cdot g^{-1}$). In addition to this, the mass of Pd in the form large size nanoparticles, that have a lower contribution in the reaction, is significant.

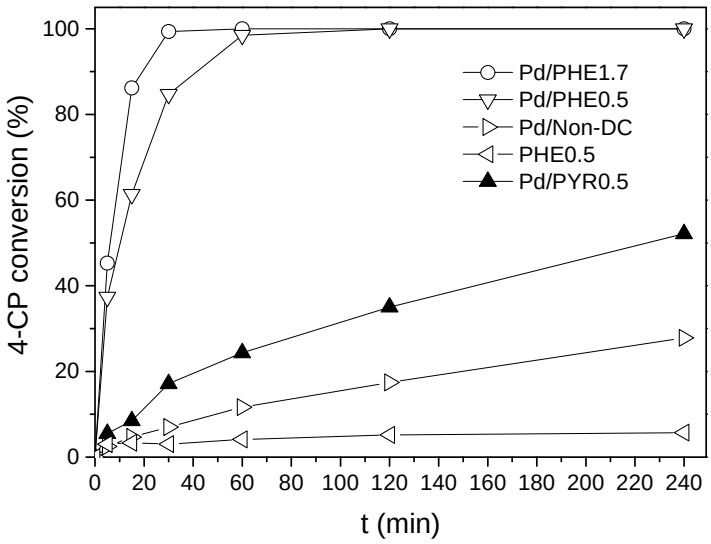

Figure 6. 4-CP conversion versus time for the Pd-based catalysts prepared.

The catalysts supported on NDCs showed a much higher activity than that supported on Non-DC. Likewise, those catalysts with supports prepared using phenanthroline as nitrogen source showed a very high activity in HDC of 4-CP. The catalyst Pd/PHE0.5 showed almost complete 4-CP conversion after 100 min reaction time, whereas the catalyst Pd/PHE1.7 showed outstanding performance with a total conversion of 4-CP for a reaction time of 30 min, which can be related to the higher nitrogen content of PHE1.7 support. Although the HDC activity values obtained were high, the ability to hydrogenate the resulting phenol to cyclonexanone and this last to cyclohexanol was poor in comparison with Pd catalysts supported on activated carbons [14], as can be seen from the selectivity data in table 4.

In order to quantify differences in activity a kinetic analysis was performed.. A simple pseudo-first order kinetic equation was used to describe the rate of 4-CP

disappearance. Since hydrogen is used in excess, its concentration was included into the pseudofirst-order rate constant (k_1):

$$(-r_{4-cp}) = \frac{-dC_{4-cp}}{dt} = k_1 \times C_{4-cp} \qquad [1]$$

$$t = 0; \quad C_{4-cp} = C_0$$

The activity data in Table 4 shows a very high activity value of 55.6 mmol·g^{-1}·min^{-1} for catalysts Pd/PHE1.7. The performance observe can be considered as remarkable taking into account the low surface area of the catalysts and that maximum activity values of 39.1 mmol·g^{-1}·min^{-1} were obtained in previous works using controlled-size unsupported Pd nanoparticles as catalyst model in HDC of 4-CP [15]. These results may indicate an important synergy between the nitrogen structures of NDCs and the metallic phase in HDC. Thus, the use of NDCs as supports can be an approach to the preparation of more active catalysts or catalyst that require lower metal load.

Table 4. Activity and selectivity to phenol (S_{ph}) and selectivity to cyclohexanone ($S_{c\text{-}one}$) for the catalysts tested.

Catalyst	Activity (mmol·g^{-1}·min^{-1})	S_{ph}* (%)	$S_{c\text{-}one}$* (%)
Pd/PHE1.7	55.6	94.9	5.1
Pd/PHE0.5	20.8	>99.9	traces
Pd/PYR0.5	0.9	100	n.d.
Pd/Non-DC	0.4	100	n.d.

*: after 240 min of reaction time ; n.d.: not detected

The catalyst prepared from the NDCs obtained using pyridine as nitrogen source also showed higher activity (0.9 mmol·g^{-1}·min-1) in HDC of 4-CP than that prepared from the non-doped carbon (0.4 mmol·g^{-1}·min^{-1}). In this case the increase in activity was less dramatic than for the NDCs obtained by using phenanthroline, which shows that the source of nitrogen employed in the synthesis of doped carbons has a crucial influence in the catalytic performance..

The results obtained in the present work are in good agreement with those reported in the literature on the enhancement of the activity in HDC and hydrogenation reactions due to catalysts with a nitrogen doped support. In these works, NDCs as supports are reported to have an impact on reactants adsorption, metal sintering and aggregation [27-29]. Moreover, it was reported that the presence of pyridinic nitrogen in the support favors the removal of HCl, by-product of HDC, from the active phase thus avoiding inhibition effect and also preventing nanoparticles aggregation [27]. On the other hand, the presence of large nanoparticles located next to quaternary nitrogen led to an electron-enriched carbon surface, offering higher reaction rates by weakening the C≡N group and favoring the hydrogenation [28]. However, in the current work the activity in the hydrogenation of the phenol produced by 4-CP HDC was very low.

Although the XPS data shown in Table 3 shows only slight differences between the NDCs prepared from phenantroline and pyridine, the results from HDC indicate that such differences in bonding configuration are relevant for the synergy with Pd in the HDC of 4-CP. Thus, the higher contribution of quaternary

nitrogen in the case of the NDCs obtained from phenantroline could be related to the higher catalytic activity.

Conclusions

NDCs have been synthesized by co-pyrolysis of low density polyethylene and different nitrogen sources. Among the nitrogen sources studied only pyridine and phenanthroline led to significant nitrogen content of carbons. NDCs prepared with phenanthroline showed higher nitrogen content and a more homogeneous distribution of nitrogen than those prepared with pyridine under equivalent conditions. In the range studied the nitrogen content of the carbons increased for low pyrolysis temperatures, high nitrogen flow in the pyrolysis reactor and long time between feeding pulses. The activity observed for the NDCs indicate some potential as metal free catalysts to be explored. The NDCs employed as supports showed an important synergy with Pd in the catalysis of the HDC of 4-CP, especially in the case of those carbons prepared with phenantroline as support. The higher contribution of quaternary nitrogen in such carbons could be related to the higher catalytic activity.

Acknowledgments.

The authors greatly appreciate financial support from the Spanish MINECO (CTQ2012-32821) and CAM (REMTAVARES S-2009/AMB-1588). J.A. Baeza thanks to the Spanish MICINN a research grant (BES-2010-030059).

References

[1] C.H. Choi, S.H. Park, M.W. Chung, S.I. Woo, Carbon 55 (2013) 98.

[2] Z.R. Ismagilov, A.E. Shalagina, O.Y. Podyacheva, A.V. Ischenko, L.S. Kibis, A.I. Boronin, Y.A. Chesalov, D.I. Kochubey, A.I. Romanenko, O.B. Anikeeva, T.I. Buryakov, E.N. Tkachev, Carbon 47 (2009) 1922.

[3] N.J.C. E.N. Nxumalo, Materials 3 (2010) 2141.

[4] Y. Shao, J. Sui, G. Yin, Y. Gao, Applied Catalysis B: Environmental 79 (2008) 89.

[5] A.B. Ayusheev, O.P. Taran, I.A. Seryak, O.Y. Podyacheva, C. Descorme, M. Besson, L.S. Kibis, A.I. Boronin, A.I. Romanenko, Z.R. Ismagilov, V. Parmon, Applied Catalysis B: Environmental 146 (2014) 177.

[6] R.P. Rocha, J. Restivo, J.P.S. Sousa, J.J.M. Órfão, M.F.R. Pereira, J.L. Figueiredo, Catalysis Today (2014) .

[7] X. Li, H. Wang, J.T. Robinson, H. Sanchez, G. Diankov, H. Dai, J. Am. Chem. Soc. 131 (2009) 15939.

[8] A.V. Okotrub, L.G. Bulusheva, A.G. Kudashov, V.V. Belavin, D.V. Vyalikh, S.L. Molodtsov, Applied Physics A 94 (2009) 437.

[9] E. Cruz-Silva, D.A. Cullen, L. Gu, J. Romo-Herrera, E. Muñoz-Sandoval, F. López-Urías, B.G. Sumpter, V. Meunier, J. Charlier, D.J. Smith, H. Terrones, M. Terrones, ACS Nano 2 (2008) 441.

[10] Y. Li, F. Hou, Z. Yang, J. Feng, X. Zhong, J. Li, Materials Science and Engineering: B 158 (2009) 69.

[11] A.A. Koós, M. Dowling, K. Jurkschat, A. Crossley, N. Grobert, Carbon 47 (2009) 30.

[12] Association of Plastics Manufacturers, Plastics – The Facts 2012, PlasticsEurope, Brussels, Belgium, 2012.

[13] G.A. Harse, UCLA Journal of Environmental Law and Policy 29 (2011) 331.

[14] L. Calvo, M.A. Gilarranz, J.A. Casas, A.F. Mohedano, J.J. Rodríguez, Applied Catalysis B: Environmental 67 (2006) 68.

[15] J.A. Baeza, L. Calvo, M.A. Gilarranz, A.F. Mohedano, J.A. Casas, J.J. Rodriguez, Journal of Catalysis 293 (2012) 85.

[16] J.A. Baeza, L. Calvo, M.A. Gilarranz, J.J. Rodriguez, Chem. Eng. J. 240 (2014) 271.

[17] N. Alonso-Morales, M.A. Gilarranz, F. Heras, S. Eser, J.J. Rodriguez, Energy & Fuels 23 (2009) 6102.

[18] F. Kapteijn, J.A. Moulijn, S. Matzner, H.-. Boehm, Carbon 37 (1999) 1143.

[19] http://srdata.nist.gov/xps/, .

[20] M.d.R. Hernández, A. Gómez, Á.N. García, J. Agulló, A. Marcilla, Applied Catalysis A: General 317 (2007) 183.

[21] J.A. Conesa, R. Font, A. Marcilla, A.N. Garcia, Energy Fuels 8 (1994) 1238.

[22] A.F. C.G. Jung, in: W.K. J. Scheirs (Ed.), Wiley, Chichester, U.K., 2006, p. 251.

[23] V. Cozzani, Ind Eng Chem Res 36 (1997) 5090.

[24] R. Yadav, P. Dobal, T. Shripathi, R.S. Katiyar, O.N. Srivastava, Nanoscale Research Letters 4 (2008) 197.

[25] S. van Dommele, A. Romero-Izquirdo, R. Brydson, K.P. de Jong, J.H. Bitter, Carbon 46 (2008) 138.

[26] J.L. Figueiredo, M.F.R. Pereira, Catalysis Today 150 (2010) 2.

[27] Q. Liu, Z. Cui, Z. Ma, S. Bian, W. Song, J. Phys. Chem. C 112 (2008) 1199.

[28] A. Nieto-Márquez, D. Toledano, P. Sánchez, A. Romero, J.L. Valverde, Journal of Catalysis 269 (2010) 242.

[29] K. Chizari, I. Janowska, M. Houllé, I. Florea, O. Ersen, T. Romero, P. Bernhardt, M.J. Ledoux, C. Pham-Huu, Applied Catalysis A: General 380 (2010) 72.

CONCLUSIONES PRINCIPALES /

MAIN CONCLUSIONS

Conclusiones principales

- ✓ La concentración de agente protector y el tipo y concentración de agente reductor afectan al tamaño de las nanopartículas de Pd obtenidas por síntesis coloidal. Los coloides de nanopartículas de Pd sintetizados no presentan capacidad de hidrogenar el fenol, al contrario de lo que sucede con catalizadores de Pd soportados recogidos en la bibliografía. La actividad por unidad de masa de catalizador aumenta cuando el tamaño de nanopartícula decrece, probablemente debido a una mayor superficie disponible. Sin embargo, la actividad por unidad de superficie es más alta para los tamaños de nanopartícula mayores, lo que quizá pueda relacionarse con el estado de oxidación de las nanopartículas y la coordinación de los átomos de Pd, que pudieran favorecer una menor energía de adsorción de reactivos y productos sobre ellos.

- ✓ La concentración de agente protector y de agente reductor afectan al tamaño y estado de oxidación de las nanopartículas de Rh obtenidas mediante síntesis coloidal. Las nanopartículas de Rh muestran valores de actividad equivalentes a los obtenidos con nanopartículas de Pd, a pesar de que los catalizadores de Rh soportados han sido generalmente considerados como menos activos que los de Pd. El tamaño y el estado de oxidación de las nanopartículas de Rh mostraron una influencia importante en la actividad. Ésta aumenta hasta un tamaño de partícula de 2.8 nm, a partir del cual disminuye drásticamente. Por otro lado, se observó que la actividad se encuentra favorecida por altas

cantidades relativas de Rh cerovalente en la fase metálica. Los modelos de regresión permitieron comprobar que el tamaño de nanopartícula y el estado de oxidación tienen influencia sobre la selectividad a ciclohexanona y ciclohexanol y que ambas variables tienen un efecto cruzado.

- ✓ El análisis cinético basado en los mecanismos de reacción en dos etapas y de Langmuir-Hinshelwood han sido aplicados para modelar la hidrodecloración de 4-clorofenol en fase acuosa usando nanopartículas de Rh sin soportar como catalizadores. La buena correspondencia entre las predicciones teóricas y los datos experimentales han permitido validar el modelo, mostrando que es aplicable a nanopartículas no soportadas y que el análisis cinético puede ser una buena estrategia a la hora de abordar el diseño de catalizadores. La información mecanística proporcionada por los modelos sugiere que la reacción de hidrodecloración de 4-clorofenol se ve favorecida en los átomos de las caras ("terraces") frente a los de los límites ("edges") de las nanopartículas.

- ✓ El método de síntesis (co-reducción y reducción sucesiva) y la relación molar Pd/Rh presentan una clara influencia sobre la estructura de las nanopartículas bimetálicas obtenidas, aunque no es posible establecer una relación entre el método de síntesis y el tipo de estructura de nanopartícula obtenida (core-shell/cluster-in-cluster). Por este motivo, el estudio de catalizadores bimetálicos de Pd/Rh en hidrodecloración debe realizarse teniendo en cuenta la estructura de las nanopartículas, dado que la disposición de los metales en la partícula puede conducir a efectos antagónicos o sinérgicos en la actividad o

selectividad de los catalizadores. Se ha constatado que un alto contenido de Pd en las nanopartículas conduce a una mayor actividad de las mismas, aunque sólo se produce una mejora significativa respecto a las mezclas de nanopartículas monometálicas de Pd y Rh cuando la relación molar Pd/Rh alcanza valores de 5. Las actividades más bajas se observaron en las muestras con mayor presencia de Rh en superficie, sin embargo, esta configuración condujo a una mayor hidrogenación de los productos, por lo que han de equilibrarse ambos efectos según los propósitos de la catálisis. A pesar del papel predominante del Rh en la capacidad de hidrogenación, la presencia de Pd en la estructura de las nanopartículas fue esencial para lograr altos valores de selectividad a productos de hidrogenación de fenol.

- ✓ El tipo de agente protector empleado en la síntesis de nanopartículas de Pd afecta al tamaño de partícula, siendo siempre menor el tamaño de partícula obtenido con PVA que con PVP cuando se emplean cantidades equivalentes. La quimisorción de CO en fase acuosa mostró que la cobertura de la superficie del Pd se encuentra en torno al 80 %. La PVA no afecta significativamente a las especies adsorbidas en la superficie del Pd, por lo que las propiedades catalíticas de los sitios catalíticos no se ven afectadas en términos de TOF y de selectividad. Por el contrario, la PVP afecta significativamente a las especies adsorbidas, aumentando el TOF y disminuyendo la selectividad a amonio a medida que aumenta la cobertura de la superficie por el PVP.

- ✓ Se ha realizado la síntesis de sólidos carbonosos dopados con nitrógeno mediante copirólisis de polietileno de baja densidad y 1,10-fenantrolina o piridina, alcanzándose incorporaciones significativas de nitrógeno en la matriz carbonosa. En las condiciones estudiadas el contenido de nitrógeno de los carbones aumentó para temperaturas bajas de pirólisis, caudal alto de nitrógeno y tiempos altos entre pulsos de alimentación de los precursores. La actividad en hidrodecloración observada, aunque discreta, indica un potencial a explorar de los sólidos carbonosos dopados con nitrógeno como catalizadores sin fase metálica. Los sólidos carbonosos dopados con nitrógeno utilizados como soporte muestran un claro efecto sinérgico con el Pd en la hidrodecloración de 4-CP, especialmente en el caso de aquellos preparados empleando 1,10-fenantrolina como precursor. La mayor contribución del nitrógeno cuaternario en este tipo de sólidos carbonosos podría estar relacionada con su mayor actividad catalítica.

Main Conclusions

- ✓ The concentration of protective agent and the type and concentration of reducing agent has influence in the size of the colloidal Pd nanoparticles obtained by chemical reduction. The colloids of Pd nanoparticles synthesized do not show activity in the hydrogenation of phenol, in contrast to what has been reported in literature for supported Pd catalysts. The activity per mass of catalyst increases when the nanoparticle size decreases, probably due to a higher availability of catalytic surface. However, the activity per unit of surface area is higher for larger nanoparticles. This may be related to the oxidation state of the nanoparticles and the coordination of Pd atoms, which may favor lower energy adsorption reactants and products on them.

- ✓ The concentration of protective agent and reducing agent used during the colloidal synthesis affects the size and state of oxidation of the Rh nanoparticles obtaind. Rh nanoparticles show activity values equivalent to those obtained with Pd nanoparticles in the hydrodechlorination of 4-chlorphenol, although the Rh supported catalysts have been usually considered to be less active than those based on Pd. The size and the oxidation state of Rh nanoparticles showed a significant influence in the activity. The activity increases up to a particle size of 2.8 nm, from which drops dramatically. Furthermore, it was observed that the activity is favored by a high relative amount of zerovalent Rh in the metal phase. Regression models showed that the selectivity to cyclohexanone and cyclohexanol is influenced by both the

nanoparticle size and the oxidation state, and that these two variables have a crossed effect.

- ✓ A kinetic analysis based on the two step reaction and Langmuir-Hinshelwood mechanisms has been applied to model the hydrodechlorination of 4-chlorophenol in aqueous phase using unsupported Rh nanoparticles as catalysts. The good agreement between theoretical predictions and experimental data showd the validity of the model, showing that it can be applied to unsupported nanoparticles and that the kinetic analysis can be a good tool for the design of catalysts. The mechanistic information provided by the models suggests that the reaction of 4-chlorophenol hydrodechlorination is favored in the atoms of the terraces rather than in the edges of the nanoparticles.

- ✓ The synthesis method (co-reduction and successive reduction) and the Pd/Rh molar ratio show a clear influence in the structure of the bimetallic nanoparticles obtained, although it is not possible to establish a relationship between the method of synthesis and the type of nanoparticle structure obtained (core-shell/cluster-in-cluster). Therefore, the study of bimetallic Pd/Rh catalysts in hydrodechlorination must take into account the structure of the nanoparticles, as the arrangement of the metals in the particles can lead to synergistic or antagonistic effects on the activity and selectivity of the catalysts. It has been found that a high content of Pd in the nanoparticles leads to a

higher activity, but significant improvement over mixtures of monometallic Pd and Rh nanoparticles is only observed when the Pd/Rh molar ratio reaches values of 5. The lowest activities were observed for nanoparticles with a higher presence of Rh at their surface, however, this configuration led to increased hydrogenation of the products. Therefore, both effects have to be balanced taking into account the purpose of catalysis. In spite of the predominant role of Rh in the hydrogenation ability of the nanoparticles, the presence of Pd in the structure was essential for achieving high values of selectivity to the hydrogenation products of phenol.

- ✓ The type of protective agent used in the synthesis of nanoparticles of Pd affects the particle size, being the size smaller for PVA than for PVP when equivalent amounts of protective agent are used. The chemisorption of CO in aqueous phase showed that the coverage of Pd surface is about 80%. The PVA does not significantly affect the species adsorbed on the surface of Pd, thus the catalytic properties of the catalytic sites are unaffected in terms of TOF and selectivity. However, PVP significantly affects the adsorbed species, increasing the TOF and decreasing ammonium selectivity as the coverage by the PVP increases.

- ✓ The synthesis of nitrogen doped carbon solids with a significant incorporation of nitrogen in the carbon matrix was achieved by copyrolysis of LDPE and 1,10-phenanthroline or pyridine. Under the conditions studied the nitrogen content of the solid carbons increased for low pyrolysis temperature, high nitrogen flow rate and long time between precursors feeding pulses. The doped solid carbons exhibited activity in hydrodechlorination, evidencing a potential as metal free

catalysts to be explored. The nitrogen doped carbon solids used as supports show a synergistic effect with the Pd metallic in the hydrodechlorination 4-CP, especially in the case of those prepared by using 1,10-phenanthroline as precursor. The higher contribution of the quaternary nitrogen in such carbon solids could be related to their higher catalytic activity.

TRABAJOS FUTUROS /
FUTURE WORKS

Trabajos Futuros

Los trabajos realizados en la presente tesis han permitido generar nuevo conocimiento de los factores que afectan a la actividad y/o selectividad de catalizadores en la hidrodecloración de 4-clorofenol y en la reducción de nitritos. Asimismo, se exploró la posibilidad de utilizar análisis cinéticos como posible estrategia de apoyo para el diseño racional de catalizadores, así como la introducción de heteroátomos en carbones preparados a partir de polietileno de baja densidad como estrategia para la futura ejecución de soportes de altas prestaciones.

De este modo, sobre la base del conocimiento generado, algunos de los trabajos de investigación posteriores podrían dirigirse hacia las siguientes líneas de investigación:

- Preparación de catalizadores soportados con control de tamaño de nanopartícula mediante métodos de síntesis in-situ y ex-situ. Influencia del soporte en la actividad y selectividad en hidrodecloración. Estudio de propiedades y estabilidad.
- Preparación de catalizadores no soportados de distintas morfología (tetraédrica, cúbica, etcétera). Estudio de la influencia de la forma. Preparación de catalizadores de partículas con distinta morfología soportados y estudio de su estabilidad en hidrodecloración.
- Preparación de soportes dopados con heteroátomos (P, B) y su evaluación como catalizadores libres de metal. Síntesis de catalizadores soportados en carbones dopados. Influencia en la actividad y selectividad en hidrodecloración.